

Plant controls on Late Quaternary whole ecosystem structure and function

Elizabeth S. Jeffers¹, Nicki J. Whitehouse², Adrian Lister³, Gill Plunkett⁴, Phil Barratt², Emma Smyth^{4,†}, Philip Lamb^{5,††}, Michael W. Dee⁶, Stephen J. Brooks⁷, Katherine J. Willis^{1,8}, Cynthia A. Froyd⁹, Jenny E. Watson⁴ and Michael B. Bonsall¹

¹ Department of Zoology, University of Oxford, Oxford OX1 3PS, UK, elizabeth.jeffers@zoo.ox.ac.uk, kathy.willis@zoo.ox.ac.uk, michael.bonsall@zoo.ox.ac.uk

² School of Geography, Earth & Environmental Sciences, University of Plymouth, Plymouth PL4 8AA, UK, nicola.whitehouse@plymouth.ac.uk, philip.barratt@plymouth.ac.uk

³ Department of Earth Sciences, Natural History Museum London, London SW7 5BD, UK, a.lister@nhm.ac.uk

⁴ School of Natural and Built Environment, Queen's University Belfast, Belfast BT7 1NN, UK, G.Plunkett@qub.ac.uk

⁵ School of Geography & the Environment, University of Oxford, Oxford OX1 3QY, UK,

⁶ Research Laboratory for Archaeology & the History of Art, University of Oxford OX1 3QY, UK

⁷ Department of Life Sciences, Natural History Museum London, London SW7 5BD, UK, S.Brooks@nhm.ac.uk

⁸ Royal Botanic Gardens, Kew, Richmond TW9 3AE, UK

⁹ Department of Biosciences, Swansea University, Swansea SA2 8PP, UK, c.froyd@swansea.ac.uk

[†] Current address: School of Geography and Environmental Sciences, University of Ulster, Coleraine BT52 1SA, UK, Smyth-E28@email.ulster.ac.uk

^{††} Current address: School of Biological Sciences, University of East Anglia, Norwich Research Park, Norwich, Norfolk, NR4 7TJ, UK, P.Lamb@uea.ac.uk

^{†††} Current address: Center for Isotope Research, Faculty of Science & Engineering, University of Groningen, Netherlands, m.w.dee@rug.nl

Short running title: Plant controls on Late Quaternary ecosystems

Keywords: megafauna extinction, nutrient cycling, plant community composition, climate change, plant-plant interactions, plant-soil interactions, landscape burning

Type of article: Letter

149 words in abstract, 4,982 words in main text, 61 references, 4 figures, 2 tables and supplementary information

Corresponding author: Elizabeth S. Jeffers Department of Zoology, University of Oxford, Oxford OX1 3PS, UK, elizabeth.jeffers@zoo.ox.ac.uk, (+44) 1865 271114

Statement of Authorship: E.S. J. and N.J.W. designed the study; E.S.J., G.P., C.A.F., E.S., P.L., J.E.W., S.J.B., A.L., P.B., M.W.D. collected and processed data. E.S.J. and M.B.B. analysed the data. E.S.J. wrote the paper with significant inputs from all authors. All authors discussed the results and provided comments on the manuscript.

Data Accessibility Statement: The data used in this study have been archived in Dryad: DOI: doi:10.5061/dryad.845n3f6.

ABSTRACT

Plants and animals influence biomass production and nutrient cycling in terrestrial ecosystems; however their relative importance remains unclear. We assessed the extent to which mega-herbivore species controlled plant community composition and nutrient cycling, relative to other factors during and after the Late Quaternary extinction event in Britain and Ireland, when two-thirds of the region's mega-herbivore species went extinct. Warmer temperatures, plant-soil and plant-plant interactions, and reduced burning contributed to the expansion of woody plants and declining nitrogen availability in our five study ecosystems. Shrub biomass in particular was consistently one of the strongest predictors of ecosystem change, equaling or exceeding the effects of other biotic and abiotic factors. In contrast, there was relatively little evidence for mega-herbivore control on plant community composition and nitrogen availability. The ability of plants to determine the fate of terrestrial ecosystems during periods of global environmental change may therefore be greater than previously thought.

INTRODUCTION

Which biotic factors are most important for determining the structure and function of terrestrial ecosystems? If animal consumers are a primary driver of ecosystem change, then the extinction of large-bodied herbivores could result in major upheaval in ecosystems worldwide (Dirzo *et al.* 2014). Alternatively, if primary producers control the fates of ecosystems, then ongoing climate change will likely be a more urgent threat, possibly via acceleration of the current extinction crisis (Cahill *et al.* 2013). Documented declines in consumer populations – including extinctions – provide an opportunity to test these alternatives. The fossil record provides key information about the structure and functioning of past ecological communities (Jeffers *et al.* 2015b) that can be used to infer the relative strength of these top-down versus bottom-up drivers of ecosystem change (Jeffers *et al.* 2012) during an extinction event.

The most recent major extinction event occurred toward the end of the last glacial period. Over half (55%) of the 42 mega-herbivore genera (defined here as herbivorous mammals weighing on

average ≥ 44 kg) extant in the northern hemisphere during the Late Pleistocene period are now globally extinct (est. from Koch & Barnosky 2006). A further seven of these (16%) are extinct on at least one continent. This extinction event offers an opportunity to study the impacts of concurrent changes in climate and ecological communities on ecosystem structure and function. The loss of mega-herbivore species was largely coincident with a reduction in plant species diversity across the Arctic (Willerslev *et al.* 2014), the encroachment of woody plants in northern ecosystems (Lister & Stuart 2008) and global declines in terrestrial nitrogen availability (McLauchlan *et al.* 2013). Early Holocene terrestrial ecosystems were therefore less open, less species diverse and less fertile than in the preceding glacial period. Were these changes a response to the Late Quaternary extinctions? In North America and Australia, palaeoecological research suggests that the mega-herbivore extinctions immediately preceded changes in plant communities and fire activity (Gill *et al.* 2009; Rule *et al.* 2012; Johnson *et al.* 2015). This has been interpreted as evidence that the Late Quaternary mega-herbivore extinctions caused the observed changes in ecosystem structure and function (Gill 2014; Bakker *et al.* 2016; Doughty *et al.* 2016). To understand the impacts of this extinction event, and – importantly – to be able to predict the consequences of future losses of large herbivores on ecosystem structure and function, it is essential to systematically disentangle the biotic and abiotic factors contributing to Late Quaternary ecosystem change.

Here we report palaeoecological proxy data that reflect concurrent changes in mega-herbivore biomass (Gill *et al.* 2013), nitrogen availability (McLauchlan *et al.* 2007), growing season temperatures (Brooks & Birks 2001; Heiri *et al.* 2011), fire activity (Tinner *et al.* 1998) and above-ground plant biomass of herbs, shrubs and trees (Seppä *et al.* 2009) spanning the full extinction event from the Late Pleistocene to the middle Holocene (ca. 16,000 to 4,800 years ago) in Britain and Ireland. Since trends in Late Quaternary ecosystem dynamics are often time-transgressive and tend to follow unique, context-specific successional trajectories, it is essential for any investigation of the ecological consequences of mega-herbivore declines to represent this temporal and ecological breadth. The British Isles provide an excellent model system with which to investigate the ecological context of Eurasian mega-herbivore extinctions in steppe-tundra ecosystems because

they offer many well-stratified localities that exemplify the variety of floral and faunal assemblages, and range of climatic conditions found across the Palearctic steppe-tundra biome over this period (Lowe & Walker 1997).

Our palaeoecological dataset contains 179 published radiocarbon dates from the nine mega-herbivore species extant in Britain and Ireland during the extinction event and 241 observations of fossil pollen, dung fungal spore and charcoal influx; 199 of these records also have corresponding stable nitrogen isotope and chironomid-based mean July air temperature data. This is – to our knowledge – the first such study to utilize independent lines of evidence of ecosystem *and* climate change measured concurrently through time at a number of study sites in order to assess the relative importance of plants, animals, burning and climate in determining the fate of terrestrial ecosystems at the Pleistocene – Holocene transition. Importantly, unlike related studies, we applied statistical modelling to these data in order to assess the evidence for each of the proposed drivers of ecosystem change during this extinction event.

MATERIALS AND METHODS

Study sites. Britain and Ireland represent the western front of the Eurasian Late Quaternary mega-fauna extinctions, many of which proceeded from west to east (Stuart & Lister 2012), tracking the retreat of continental conditions and open habitats (Allen *et al.* 2010). Our five sites (Fig. S1) span mire and heathland communities dominated by oceanic conditions in the northwest, to species-diverse grasslands with continental climates in the southeast (Appendix 1). The palaeoecological time-series data were derived from new and existing sedimentary sequences in England (Quidenham Mere 14,527 to 8,309 cal. yr. BP; Jeffers *et al.* 2011a), Scotland (Dubh-Lochan, 10,888 to 4,863 cal. yr. BP; Froyd 2005), and Ireland (Lough Nadourcan, 15,712 to 10,481 cal. yr. BP; Turney *et al.* 2006; Watson *et al.* 2010; Ballynahatty, 10,328 to 8,232 cal. yr. BP; Plunkett *et al.* 2008; and Long Lough, 13,939 to 9,837 cal. yr. BP; unpublished data collected by E.S. and G.P.). These sites contain plant (TableS2) and animal assemblages (Movie S3) that are representative of the Eurasian steppe-tundra.

Fossil pollen, spores and charcoal. We used fossil pollen influx as a proxy for above-ground plant biomass (Seppä *et al.* 2009). Influx data account for variation in sedimentation rates through time and provide independent measures of change. Fossil pollen grains were extracted from lake and bog sediments following standard chemical treatments (Bennett & Willis 2001) and identified to plant family or genus level. Pollen concentrations of each plant taxon were calculated relative to the quantities of exotic pollen of a known concentration, which were introduced during sediment preparation (Bennett & Willis 2001). Pollen influx was calculated by multiplying the concentration values by sediment accumulation rates estimated for each core (FigS4). Influx rates for each plant taxon were combined for all herbs, shrubs and trees (TableS2) in order to determine the factors affecting plant community structure across sites (see Appendix 1 for information on dynamics within each plant functional group).

Sporormiella is a dung-associated fungus and the influx of its spores into lake and bog sediments is indicative of mega-herbivore density (Gill *et al.* 2013) and biomass (Baker *et al.* 2016) in the landscape surrounding the basin. We counted individual spores of *Sporormiella* from pollen slides and calculated concentrations and influx in the same way as for pollen (Baker *et al.* 2013). The influx of micro-charcoal fragments reflects patterns of fire activity at the landscape to regional scale. Micro-charcoal fragments were counted from pollen slides (Tinner & Hu 2003) and converted into charcoal concentrations and then influx as above. Pollen, *Sporormiella* and charcoal influx data were obtained for all five of our study sites, resulting in a database of 241 concurrent observations of plant and mega-herbivore biomass and landscape burning spanning ca. 16,000 to 4,800 cal. yr BP (i.e. over the full extinction event), at an average temporal resolution of c. 90 years.

Stable isotopes of nitrogen. The stable nitrogen isotope composition of bulk lake sediments ($\delta^{15}\text{N}$) reflects broad trends in nitrogen availability to plants within the lake catchment (McLauchlan *et al.* 2007; see Appendix 2). Sedimentary $\delta^{15}\text{N}$ was measured from bulk lake sediments at the Godwin Laboratory for Palaeoclimate Research, University of Cambridge. One to two cubic centimetres of sediment were dried at 50°C and homogenized with a mortar and pestle then approximately 10 mg of sediment was placed in a tin capsule and sealed. Samples were analysed for $\delta^{15}\text{N}$ using a

Costech Elemental Analyzer attached to a Thermo MAT 253 mass spectrometer in continuous flow mode. Known reference standards from IAEA (USGS 40, $\bar{x} = -4.61\text{‰}$, $\sigma = 0.04$ and caffeine, $\bar{x} = 1.11\text{‰}$, $\sigma = 0.04$) were analyzed at various points throughout the run; these values were used to calibrate the sample results to the international standards. Results are reported relative to air (atmospheric N_2) with a value of 0‰. Standard deviations were determined from replicate analyses to be 0.08‰. Sedimentary $\delta^{15}\text{N}$ data were available for three of these sites: Lough Nadourcan, Ireland (Jeffers *et al.* 2012); Quidenham Mere, England (Jeffers *et al.* 2011a); and Dubh-Lochan, Scotland (Jeffers *et al.* 2015a).

Mean July air temperature. We reconstructed mean July air temperatures ($^{\circ}\text{C}$) with a chironomid-based transfer function (Brooks & Birks 2001; Heiri *et al.* 2011). Head capsules of larval chironomids were extracted from 0.5-3 g of bulk sediment and mounted on microscope slides for identification with a light microscope following Brooks *et al.* 2007. Chironomid assemblages were translated into mean July air temperatures with a three-component WA-PLS transfer function based on a 153-lake modern Norwegian chironomid training set (Brooks & Birks 2001; Heiri *et al.* 2011). Temperature reconstructions were available for Lough Nadourcan (Jeffers *et al.* 2012), Quidenham Mere (Jeffers *et al.* 2011a) and Dubh-Lochan (Jeffers *et al.* 2015a). Prediction errors for each site ranged between 1.05-1.55 $^{\circ}\text{C}$. In total, we had 199 records of sedimentary $\delta^{15}\text{N}$ and mean July air temperature that were concurrent with our pollen, charcoal and *Sporormiella* influx.

Sedimentary sequence chronology. Chronologies for each of the five sedimentary sequences were developed in OxCal (version 4.2.3) (Ramsey 1995) using existing radiocarbon dates as reported in the original publications for each site (TableS5). New dates were obtained for the Long Lough sequence at the ^{14}C HRONO Laboratory at Queen's University Belfast. All chronologies were built using a P-sequence model (Ramsey 2008), where depositional events are modelled using a Poisson process and deposit increments are controlled by a parameter, k , set by the user. A total of 52 accelerator mass spectroscopy (AMS) radiocarbon dates were used to build the chronologies for these five sites (OxCal model specifications available in FileS6).

Fossil bone chronology. Since large herbivore species vary in terms of their impact on ecosystem structure and function (Pastor *et al.* 2006), it is important to know the species assemblage dynamics across the study period. The dung fungus *Sporormiella* is able to sporulate on a variety of dung substrates (Baker *et al.* 2013); therefore the influx of these spores in lake sediments cannot be used to infer the ecological impacts of particular herbivore species. The only unequivocal evidence of herbivore species presence comes from AMS ^{14}C -dated fossil bone assemblages obtained from deposition sites within the region. We reconstructed mega-herbivore species assemblage dynamics through time by collating published records of directly-dated fossil bone specimens from each of the nine species that were extant in Britain and Ireland between 16,000 and 4,800 cal. yr BP: elk (*Alces alces*), aurochs (*Bos primigenius*), domestic cattle (*Bos taurus*), red deer (*Cervus elaphus*), wild horse (*Equus ferus*), woolly mammoth (*Mammuthus primigenius*), giant deer (*Megaloceros giganteus*), reindeer (*Rangifer tarandus*) and saiga antelope (*Saiga tatarica*). This resulted in a dataset of 205 AMS radiocarbon dates for these nine mega-herbivore species. Only directly-dated specimens with adequate taxonomic identification to species level for which AMS dates were obtained on purified collagen after 1980 (i.e. when sample pretreatment became widely used) were retained, following the methodology used in Stuart & Lister 2012 and Lister & Stuart 2013. After auditing, 179 samples from published records remained in our fossil bone database. The taxonomy of two *Bos taurus* specimens from Sutton Shell Midden in Ireland has recently come into question (Milner 2010); however we chose to retain the dates of these specimens in our database since their identification as cattle has not been convincingly discounted.

The fossil bone dates were combined for all species and modelled in OxCal (Ramsey 1995) using the Sum function to generate cumulative probability densities that represent the best estimate for the chronological distribution for each mega-herbivore species (OxCal model code available in FileS7). Specifically, all dates for each species were grouped by region and then modelled as independent, single Phases (i.e. groups of ^{14}C -dated bones that are assumed to co-occur within a relatively short period of time), delimited by start and end Boundaries that help constrain the width of the resulting probability density functions. A Sum command was placed inside each Phase to

calculate a cumulative probability density across all modelled dates. The cumulative probability densities reflect the best possible estimate of the true range of AMS ^{14}C dates collected per species.

Statistical modelling. The four response variables were sedimentary $\delta^{15}\text{N}$ (our proxy for nitrogen availability) and the influx of herb, shrub and tree pollen (all proxies for above-ground plant biomass). All influx data were log-transformed (FigS8) using the formula $\log_{10}(x+1)$ prior to analysis in order to minimize the impacts of extreme values (i.e. from periods of increased sediment accumulation, FigS4) on the model results and to correct for non-normal distributions in the response and explanatory variables (Birks *et al.* 2012). While log-transformation may not remove all effects of varying sedimentation from the influx variables, we found no consistent pattern of correlation between the influx variables or between these variables and time after log-transformation (TableS9).

Scatter plots of the log-transformed data indicated non-linear relationships between predictor and response variables (data not shown). We therefore chose to use generalized additive modelling (GAM) to interrogate our palaeoecological data. This local, non-parametric regression method provides a useful tool for modelling non-linear relationships between variables in time-series data (Birks *et al.* 2012). GAM smoothers are used to estimate the dependence of the mean response variable on one or more of the predictor terms (Hastie & Tibshirani 1990). Model-fitting was conducted in R version 3.4.3 (R Core Team, 2017), using the *mgcv* package version 1.8-22 (Wood 2006). The GAMs were estimated with cubic regression splines using generalised cross-validation to automatically determine the optimal level of smoothing for each term in the model and automatic term selection (see Appendix 3 for further details). The significance of each term in the model was determined using the summary function in *mgcv*, which applies a Wald test to approximate p-values for each smoother term (Wood 2006). The approximate p-values for individual smoother terms are known to underestimate the true p-value (Zuur 2009); therefore we focused primarily on the individual model terms with the highest level of significance ($p \leq 0.001$).

We applied a series of GAMs to the time series data and recorded model selection metrics for each iteration. We calculated Akaike Information Criterion (AIC) weights to identify the models that were best able to predict the observed changes in each of our four response variables. AIC weights are a normalized indicator of support for each model given the evidence within each dataset while penalizing more complex models (Burnham & Anderson 1998). We obtained AIC scores using the AIC function in R and calculated AIC weights relative to the model with the lowest AIC score. AIC values can only be compared across a common dataset, so we fitted the GAMs and calculated AIC weights separately for the three-site ($n=199$, i.e. including all available sedimentary $\delta^{15}\text{N}$ and temperature records) and five-site ($n=241$, i.e. containing all influx data without climate and nitrogen isotope records) datasets.

RESULTS

Ecosystem dynamics. Six of the mega-herbivore species that were extant in Britain, and three in Ireland, between 16,000 and 12,000 years ago (Fig. 1 and MovieS3) became regionally extinct by 10,000 calendar years before present (cal. yr BP): woolly mammoth (*Mammuthus primigenius*), wild horse (*Equus ferus*), saiga (*Saiga tatarica*), giant deer (*Megaloceros giganteus*), moose or elk (*Alces alces*) and reindeer (*Rangifer tarandus*). This represents a loss of more than two-thirds of the extant mega-herbivore species in the region. The only mega-herbivore species remaining in Britain after 10,000 cal. yr BP were red deer (*Cervus elaphus*) and aurochs (*Bos primigenius*), before the arrival of domestic cattle (*Bos taurus*).

There are far more AMS radiocarbon-dated mega-herbivore bone specimens (and greater species diversity) in England ($n=152$) than Ireland ($n=22$) or Scotland ($n=5$). The modelled dates are concentrated in time between 15,000 and 11,000 years ago (Fig. 1) and show good correspondence in time with our *Sporormiella* influx records of mega-herbivore biomass in England and Ireland (Fig. 2). Unfortunately, there were no modelled mega-herbivore dates in Scotland that overlapped with our sedimentary record from Dubh-Lochan; however the *Sporormiella* values suggest increasing large herbivore biomass from the start of the Holocene (Fig. 3).

Shrub and herb biomass increased during the Bølling warm period (ca. 14,500 to 14,000 cal. yr BP) and tree biomass was minimal when mega-herbivore species were relatively abundant (Fig. 2). Both plant and mega-herbivore biomass declined during the Younger Dryas cold period until 11,000 cal. yr BP, when shrub and then tree biomass increased coincident with rising mean July air temperature (Fig. 2). While mega-herbivore biomass increased slightly around this time, it did not recover to peak (late-glacial) levels and the timing of these changes varied by site.

Sedimentary $\delta^{15}\text{N}$, our proxy for terrestrial nitrogen availability, declined from ca 15,000 to 13,500 cal. yr BP coincident with rising plant and mega-herbivore biomass, recovered during the Younger Dryas cold period and declined again around the start of the Holocene epoch (ca 11,000 cal. yr BP) concurrently with increasing shrub and tree biomass and growing season temperatures (Fig. 2). These trends are consistent with broad global patterns of declining nitrogen availability from 15,000 to 7,500 cal yr. BP, as terrestrial ecosystems accumulated carbon (McLauchlan *et al.* 2013).

Generalised Additive Modelling. Did the loss of mega-herbivore species cause the expansion of woody plants and declines in nitrogen availability? In order to answer that question, we applied a series of GAMs to our palaeoecological time-series data and used AIC weights to identify the best-fitting model(s) for predicting observed changes in nitrogen availability and herb, shrub and tree biomass.

To explain changes in sedimentary $\delta^{15}\text{N}$ we began with a model whereby only *Sporormiella* influx (our proxy for mega-herbivore biomass) was used as a predictor variable. We compared the goodness of fit of this model to an alternative where the effects of *Sporormiella* influx on sedimentary $\delta^{15}\text{N}$ were site-specific. The AIC scores for these models show that the site-specific model (AIC = 499.0207) offered a better prediction of nitrogen dynamics than the model specified by a constant effect of mega-herbivores across all sites (AIC = 513.918, Table 1). Then, to investigate the influence of mega-herbivore biomass on nitrogen availability relative to changes in plant biomass, growing season temperature and fire activity, we added the following terms to the basic model: pollen influx for each of the three plant growth types at each site, mean July air temperature

and charcoal influx. Each term was added incrementally to the original model and model selection metrics were recorded at each step (Table 1). The AIC weights (w_i) show that the best-fitting model (AIC = 407.8037, w_i = 100%) for explaining the dynamics of sedimentary $\delta^{15}\text{N}$ included site-specific effects of *Sporormiella* and pollen influx combined with changes in mean July air temperature and charcoal influx (Table 1). Model validation analyses show that the results do not violate the model assumptions of homogeneity or normally distributed errors (Fig. 3; see Appendix 3 for more model validation analysis and details of alternative model configurations and results).

Model statistics for individual smoother terms indicate the strength and form of impacts on the dependent variables by each predictor term. Fire, mean July air temperature and woody plants (shrubs at Dubh Lochan, and trees at Lough Nadourcan) had the highest significance levels for explaining changes in nitrogen availability (Fig. 4A, see TableS10 for additional parameter statistics). In general, higher woody plant biomass, increasing growing season temperatures and declining fire activity were predicted to result in reduced nitrogen availability (Fig. 4A). Mega-herbivore biomass was a moderately significant factor for determining changes in nitrogen availability at Quidenham Mere, although it was less significant than burning and growing season temperatures (Fig. 4A). At the other sites, mega-herbivore biomass had only a low significance (Dubh-Lochan) or was excluded from the model due to lack of support (Lough Nadourcan).

We then applied the same series of models to explain changes in the pollen influx from herbs, shrubs and trees. As with sedimentary $\delta^{15}\text{N}$, the full model including mean July air temperature, charcoal influx and site-specific effects of pollen and *Sporormiella* influx provided the best explanation for changes in the pollen influx of all three plant growth types (Table 1) when applied to the three-site dataset ($n=199$). Since there were no mean July air temperature records for Ballynahatty or Long Lough, we re-applied the same set of models to the full dataset ($n=241$) and obtained independent model-selection metrics using the summary function as above (Table 2). Again, the full model with charcoal influx and site-specific effects of the biotic factors (*Sporormiella* and herb, shrub and/or tree pollen influx) provided the best fit to this five-site dataset (Table 2).

Shrub biomass was the most significant biotic factor for predicting changes in herb biomass at the majority of sites. At Long Lough shrubs were only moderately significant (Fig. 4B and see FigS11 for results using 3-site dataset only; additional parameter statistics are available in TableS12 and TableS13). At Quidenham Mere, mega-herbivore biomass was slightly more significant than shrubs. The smoothers for Dubh-Lochan had very wide confidence intervals, particularly at lower values. This is likely due to the relatively few observations for this site ($n=19$). At all sites, burning was the most significant term ($p=1.62e^{-33}$) overall for predicting changes in herb biomass. Increased burning was predicted to result in higher levels of herbaceous plant biomass (Fig. 4B).

At all but one site, herbs or trees were the most significant factors for predicting changes in shrub biomass, exceeding the effect of mega-herbivores, growing season temperature and – to a lesser extent – burning (Fig. 4C). Dubh-Lochan was the exception in that no biotic factors were predicted to have a significant effect on shrub biomass. Contrary to expectations, mega-herbivore biomass was not a highly significant factor for predicting shrub biomass at any study site (Fig. 4C).

Shrub biomass was the most significant term for predicting changes in tree biomass at all but one site and the shrub smoother terms show a predominantly positive effect of shrubs on tree biomass (Fig. 4D). Again Dubh-Lochan was the exception; trees dominated the landscape at that site from the beginning of the sequence (Fig. 2) and herb biomass was the most significant term ($p=1.22e^{-20}$) for predicting changes in tree biomass. Mega-herbivore biomass was a highly significant term for predicting tree dynamics at Lough Nadourcan ($p=1.44e^{-06}$) only, although shrubs were slightly more significant at that site ($p=1.91e^{-14}$). Growing season temperature was found to be highly significant for predicting tree biomass and rising temperatures were predicted to have a positive but saturating effect on tree biomass (Fig. 4D); however, biotic factors were more significant for predicting tree dynamics at all sites.

DISCUSSION

We presented palaeoecological evidence from ecosystems within Britain and Ireland spanning the full period of Late Quaternary megafauna change and extinction in northern Europe when two-thirds

of the extant mega-herbivores went extinct. This is, to our knowledge, the highest density of sites, number of palaeoecological proxies and observations used to assess the ecological consequences of the Late Quaternary extinctions. Extinction chronologies built on fossil bone records and modelled vegetation dynamics have previously demonstrated that several Eurasian mega-herbivores persisted during the productive Bølling warm period when herbaceous biomass increased relative to the preceding glacial period but then went extinct with the subsequent expansion of trees (Huntley *et al.* 2013). High temporal correspondence between the abundance of large herbivores and the extent of open landscapes in Great Britain during the Holocene has also been suggested by fossil beetle data (Sandom *et al.*, 2014). In the ecosystems we studied, we see a similar pattern where the loss of mega-herbivore species (Fig. 1) and declines in herbivore biomass (Fig. 2), were coincident with or preceded an increase in both shrub and tree biomass, although the timing of these changes varied by site. Yet, chronologies alone are not adequate for investigating the relative importance of contributing factors to long-term ecosystem changes.

Here, we used statistical analysis to infer the relative importance of biotic and abiotic factors in driving changes in plant community composition and nitrogen availability across the Late Quaternary extinction event from our palaeoecological data. Our results indicate support for a more holistic model of ecosystem change than has previously been proposed from qualitative interpretation of comparable datasets from other regions (Rule *et al.* 2012; Gill 2014; Johnson *et al.* 2016).

Firstly, our model-selection results show that mega-herbivores alone cannot explain the observed changes in nitrogen availability and plant community composition as the *Sporormiella*-only model had the least evidence for explaining changes in these variables (Tables 1, 2). Model fit, as indicated by lower AIC scores which penalizes against models with more terms, improved when we allowed for site-specific effects of mega-herbivores. Including the effects of fire and mean July air temperatures further improved the model fit; however, the inclusion of plant growth forms as a predictor variable provided the greatest improvement in model fit (i.e. largest reduction in AIC scores). All of the evidence in the data (as indicated by AIC weights) points to the model with site-

specific effects of mega-herbivores and plant growth forms operating alongside changes in the abiotic environment from fire and mean July air temperatures to drive shifts in nitrogen availability and plant community composition across the extinction event.

Secondly, the significance level for each predictor term within the model provides insights into the relative strength of each factor in determining long-term changes in nitrogen availability and plant biomass. Multiple factors were often found to be highly significant (i.e. $p\text{-value} \leq 0.001$) and the significance of each biotic term tended to vary between sites. Yet despite this complexity, a pattern emerged that indicates an important role for woody plants in determining long-term changes in nitrogen availability and plant community composition.

The expansion of shrubs and trees had an equally significant effect on nitrogen availability as landscape burning and changing growing season temperatures (Fig. 4A). Woody plants sequester nitrogen in long-term pools; therefore increasing woody biomass results in less nitrogen available for recycling, leading to long-term declines in nitrogen availability (McLauchlan *et al.* 2013), as predicted by the progressive nitrogen limitation hypothesis (Luo *et al.* 2004).

Fire and growing season temperature alter nitrogen availability directly by driving gaseous losses of nitrogen from soils (Morris *et al.* 2015) and indirectly through gains and losses in plant biomass (Craine *et al.* 2015). Declining fire activity in the early Holocene (Fig. 2) would have further limited the release of nutrients from long-term plant and soil pools (Dunnette *et al.* 2014), thus accelerating reductions in fertility at the ecosystem-scale.

Shrubs were the most significant biotic factor in determining changes in both herb and tree biomass at most sites; their impact was often comparable to changes in landscape burning and exceeded the effects of rising growing season temperatures (Figs. 4B and 4D). There was only one site, Dubh-Lochan, where trees were dominant in the landscape for the entire Holocene series (Fig. 2), where this pattern did not hold; yet even there the most significant factor for predicting changes in tree biomass was herb biomass, not burning or changing temperatures (Fig. 4D). These results

support the important role of plant-plant interactions in determining changes in plant community composition (Jeffers *et al.* 2015a).

Could shrubs have facilitated tree expansion in the early Holocene period? We see here that shrub expansion typically preceded the establishment and expansion of trees (Fig. 2) and our modelling results indicate a strongly positive effect of shrubs on tree biomass (Fig. 4D). Shrubs act as nurse plants for tree seedlings in stress-prone environments and thus have a net positive effect on tree recruitment, particularly in water-limited conditions (Gómez-Aparicio *et al.* 2004; Gómez-Aparicio *et al.* 2008) and grazed ecosystems (Vera 2006). Taken together, we argue that this is good evidence that shrubs played a key role in the postglacial expansion of trees in northwestern Europe. As described above, increasing woody plant biomass in turn had a significantly negative effect on nitrogen availability, contributing directly and indirectly to declining nitrogen availability in these terrestrial ecosystems. Our results implicate shrub encroachment as a key trigger for long-term changes in terrestrial ecosystem structure and function in this region during the Late Quaternary, just as it is in modern Arctic tundra (Myers-Smith *et al.* 2011) and grassland ecosystems worldwide (Bond 2016).

In conclusion, our results do not support the prevailing notion that the loss of mega-herbivore species caused the expansion of woody plants (Zimov *et al.* 2012; Bakker *et al.* 2016) and declining ecosystem fertility (Doughty *et al.* 2016) in terrestrial ecosystems at the end of the last glacial period. Instead, our findings indicate a relatively high level of plant control on ecosystem structure and function, an effect which has heretofore been largely overlooked as a direct driver of Late Quaternary ecosystem change (Willis *et al.* 1997; Jeffers *et al.* 2011b; Jeffers *et al.* 2015a). We suggest that interactions among plant growth forms and plant-soil feedbacks may have been more important than trophic interactions in determining changes in terrestrial nitrogen availability and above-ground plant biomass in northern European ecosystems as the Earth transitioned out of the last glacial period.

Overall, our results indicate that the mega-herbivores remaining in these ecosystems were not able to stem the expansion of woody plants at the onset of postglacial warming. Instead, it appears likely that plants strongly influenced the fate of the once extensive steppe-tundra biome in northwestern Europe. Whether or not these ecological changes contributed to the extinction of the Late Quaternary mega-herbivores in this region remains to be determined; however, our results are consistent with suggestions (Guthrie 1984; Stuart & Lister 2012; Willerslev *et al.* 2014) that ecological mechanisms may have played an important role in the extinction process. In a bottom-up world, where plants engineer the structure and function of terrestrial ecosystems, survival of even the largest consumers could chiefly depend on the fate of primary producers, and how they respond to changing climate and interactions with other plant growth forms.

ACKNOWLEDGEMENTS We thank David Benz for help with creating the study site map, and Kendra K. McLauchlan and Jack Williams for helpful comments on previous versions of the manuscript. The ¹⁴Chrono Centre at Queen's University Belfast kindly provided additional dates for the Long Lough sequence.

DATA ACCESSIBILITY STATEMENT Data used in the analysis are available from Dryad: DOI: doi:10.5061/dryad.845n3f6

REFERENCES

- Allen J.R.M., Hickler T., Singarayer J.S., Sykes M.T., Valdes P.J. & Huntley B. (2010). Last glacial vegetation of northern Eurasia. *Quaternary Science Reviews*, 29, 2604-2618.
- Baker A.G., Bhagwat S.A. & Willis K.J. (2013). Do dung fungal spores make a good proxy for past distribution of large herbivores? *Quaternary Science Reviews*, 62, 21-31.
- Baker A.G., Cornelissen P., Bhagwat S.A., Vera F.W.M. & Willis K.J. (2016). Quantification of population sizes of large herbivores and their long-term functional role in ecosystems using dung fungal spores. *Methods in Ecology and Evolution*, 1273-1281.
- Bakker E.S., Gill J.L., Johnson C.N., Vera F.W.M., Sandom C.J., Asner G.P. & Svenning J.C. (2016). Combining paleo-data and modern exclosure experiments to assess the impact of

- megafauna extinctions on woody vegetation. *Proceedings of the National Academy of Sciences*, 113, 847-855.
- Bennett K.D. & Willis K.J. (2001). Pollen. In: *Tracking Environmental Change Using Lake Sediments* (eds. Smol JP, Birks HJB & Last WM). Kluwer Academic Publishers Dordrecht, pp. 5-32.
- Birks H.J.B., Lotter A.F., Juggins S., Smol J.P. & Ebook Library. (2012). Data Handling and Numerical Techniques In: *Tracking Environmental Change Using Lake Sediments Vol 5*. Springer Netherlands Dordrecht.
- Bond W.J. (2016). Ancient grasslands at risk. *Science*, 351, 120-122.
- Brooks S.J. & Birks H.J.B. (2001). Chironomid-inferred air temperatures from Lateglacial and Holocene sites in north-west Europe: Progress and problems. *Quaternary Science Reviews*, 20, 1723-1741.
- Brooks S.J., Langdon P.G. & Heiri O. (2007). *The identification and use of palaeoecological Chironomidae larvae in palaeoecology*. Quaternary Research Association, London.
- Burnham K.P. & Anderson D.R. (1998). *Model selection and inference: a practical information-theoretic approach*. Springer, New York ; London.
- Cahill A.E., Aiello-Lammens M.E., Fisher-Reid M.C., Hua X., Karanewsky C.J., Yeong Ryu H., Sbeglia G.C., Spagnolo F., Waldron J.B., Warsi O. & Wiens J.J. (2013). How does climate change cause extinction? *Proceedings of the Royal Society of London B: Biological Sciences*, 280, 20121890.
- Craine J.M., Elmore A.J., Wang L., Augusto L., Baisden W.T., Brookshire E.N.J., Cramer M.D., Hasselquist N.J., Hobbie E.A., Kahmen A., Koba K., Kranabetter J.M., Mack M.C., Marin-Spiotta E., Mayor J.R., McLauchlan K.K., Michelsen A., Nardoto G.B., Oliveira R.S., Perakis S.S., Peri P.L., Quesada C.A., Richter A., Schipper L.A., Stevenson B.A., Turner B.L., Viani R.A.G., Wanek W. & Zeller B. (2015). Convergence of soil nitrogen isotopes across global climate gradients. *Sci. Rep.*, 5, 8280.
- Dirzo R., Young H.S., Galetti M., Ceballos G., Isaac N.J.B. & Collen B. (2014). Defaunation in the Anthropocene. *Science*, 345, 401-406.

- Doughty C.E., Roman J., Faurby S., Wolf A., Haque A., Bakker E.S., Malhi Y., Dunning J.B. & Svenning J.-C. (2016). Global nutrient transport in a world of giants. *Proceedings of the National Academy of Sciences*, 113, 868-873.
- Dunnette P.V., Higuera P.E., McLauchlan K.K., Derr K.M., Briles C.E. & Keefe M.H. (2014). Biogeochemical impacts of wildfires over four millennia in a Rocky Mountain subalpine watershed. *New Phytologist*, 203, 900-912.
- Froyd C.A. (2005). Fossil stomata reveal early pine presence in Scotland: Implications for postglacial colonization analyses. *Ecology*, 86, 579-586.
- Gill J.L. (2014). Ecological impacts of the late Quaternary megaherbivore extinctions. *New Phytologist*, 201, 1163-1169.
- Gill J.L., McLauchlan K.K., Skibbe A.M., Goring S., Zirbel C.R. & Williams J.W. (2013). Linking abundances of the dung fungus *Sporormiella* to the density of bison: Implications for assessing grazing by megaherbivores in palaeorecords. *J. Ecol.*, 101, 1125-1136.
- Gill J.L., Williams J.W., Jackson S.T., Lininger K.B. & Robinson G.S. (2009). Pleistocene megafaunal collapse, novel plant communities, and enhanced fire regimes in North America. *Science*, 326, 1100-1103.
- Gómez-Aparicio L., Zamora R., Castro J. & Hódar J.A. (2008). Facilitation of tree saplings by nurse plants: Microhabitat amelioration or protection against herbivores? *Journal of Vegetation Science*, 19, 161-172.
- Gómez-Aparicio L., Zamora R., Gómez J.M., Hódar J.A., Castro J. & Baraza E. (2004). Applying plant facilitation to forest restoration: a meta-analysis of the use of shrubs as nurse plants. *Ecological Applications*, 14, 1128-1138.
- Guthrie R.D. (1984). Mosaics, allelochemicals and nutrients: an ecological theory of Late Pleistocene megafaunal extinctions. In: *Quaternary Extinctions: a Prehistoric Revolution* (eds. Martin PS & Klein RD). University of Arizona Press Tuscon, pp. 259-298.
- Hastie T. & Tibshirani R. (1990). *Generalized additive models*. Chapman and Hall, London.

- Heiri O., Brooks S.J., Birks H.J.B. & Lotter A.F. (2011). A 274-lake calibration data-set and inference model for chironomid-based summer air temperature reconstruction in Europe. *Quaternary Science Reviews*, 30, 3445-3456.
- Huntley B., Allen J.R.M., Collingham Y.C., Hickler T., Lister A.M., Singarayer J., Stuart A.J., Sykes M.T. & Valdes P.J. (2013). Millennial climatic fluctuations are key to the structure of Last Glacial ecosystems. *Plos One*, 8, e61963.
- Jeffers E.S., Bonsall M.B., Brooks S.J. & Willis K.J. (2011a). Abrupt environmental changes drive shifts in tree-grass interaction outcomes. *J. Ecol.*, 99, 1063-1070.
- Jeffers E.S., Bonsall M.B., Froyd C.A., Brooks S.J. & Willis K.J. (2015a). The relative importance of biotic and abiotic processes for structuring plant communities through time. *J. Ecol.*, 103, 459-472.
- Jeffers E.S., Bonsall M.B., Watson J.E. & Willis K.J. (2012). Climate change impacts on ecosystem functioning: Evidence from an *Empetrum* heathland. *New Phytologist*, 193, 150-164.
- Jeffers E.S., Bonsall M.B. & Willis K.J. (2011b). Stability in ecosystem functioning across a climatic threshold and contrasting forest regimes. *Plos One*, 6, e16134.
- Jeffers E.S., Nogu   S. & Willis K.J. (2015b). The role of palaeoecological records in assessing ecosystem services. *Quaternary Science Reviews*, 112, 17-32.
- Johnson C.N., Rule S., Haberle S.G., Turney C.S.M., Kershaw A.P. & Brook B.W. (2015). Using dung fungi to interpret decline and extinction of megaherbivores: Problems and solutions. *Quaternary Science Reviews*, 110, 107-113.
- Johnson C.N., Rule S., Haberle S.G., Kershaw A.P., McKenzie G.M. & Brook B.W. (2016). Geographic variation in the ecological effects of extinction of Australia's Pleistocene megafauna. *Ecography*, 39, 109-116.
- Koch P.L. & Barnosky A.D. (2006). Late Quaternary extinctions: State of the debate. *Annual Review of Ecology, Evolution, and Systematics*, 37, 215-250.
- Lister A.M. & Stuart A.J. (2008). The impact of climate change on large mammal distribution and extinction: Evidence from the last glacial/interglacial transition. *C. R. Geosci.*, 340, 615-620.

- Lister A.M. & Stuart A.J. (2013). Extinction chronology of the woolly rhinoceros *Coelodonta antiquitatis*: reply to Kuzmin. *Quaternary Science Reviews*, 62, 144-146.
- Lowe J.J. & Walker M.J.C. (1997). *Reconstructing quaternary environments*. 2nd edn. Longman, Harlow.
- Luo Y., Su B., Currie W.S., Dukes J.S., Finzi A.C., Hartwig U., Hungate B., McMurtrie R.E., Oren R., Parton W.J., Pataki D.E., Shaw M.R., Zak D.R. & Field C.B. (2004). Progressive nitrogen limitation of ecosystem responses to rising atmospheric carbon dioxide. *Bioscience*, 54, 731-739.
- McLauchlan K.K., Craine J.M., Oswald W.W., Leavitt P.R. & Likens G.E. (2007). Changes in nitrogen cycling during the past century in a northern hardwood forest. *Proceedings of the National Academy of Sciences of the United States of America*, 104, 7466-7470.
- McLauchlan K.K., Williams J.J., Craine J.M. & Jeffers E.S. (2013). Changes in global nitrogen cycling during the Holocene epoch. *Nature*, 495, 352-355.
- Milner, N. (2010) Subsistence at 4000-3700 cal BC: landscapes of change or continuity? In: Filnaysen, B. & Warren, G (eds) *Landscapes in Transition*, Oxbow Books, Oxford, 46-54.
- Morris J.L., McLauchlan K.K. & Higuera P.E. (2015). Sensitivity and complacency of sedimentary biogeochemical records to climate-mediated forest disturbances. *Earth-Sci. Rev.*, 148, 121-133.
- Myers-Smith I.H., Forbes B.C., Wilmking M., Hallinger M., Lantz T., Blok D., Tape K.D., Macias-Fauria M., Sass-Klaassen U., Lévesque E., Boudreau S., Ropars P., Hermanutz L., Trant A., Collier L.S., Weijers S., Rozema J., Rayback S.A., Schmidt N.M., Schaepman-Strub G., Wipf S., Rixen C., Ménard C.B., Venn S., Goetz S., Andreu-Hayles L., Elmendorf S., Ravolainen V., Welker J., Grogan P., Epstein H.E. & Hik D.S. (2011). Shrub expansion in tundra ecosystems: Dynamics, impacts and research priorities. *Environmental Research Letters*, 6, 045509.
- Pastor J., Cohen Y. & Hobbs N.T. (2006). The roles of large herbivores in ecosystem nutrient cycles. In: *Large herbivore ecology, ecosystem dynamics and conservation* (eds. Danell K, Bergstrom R, Duncan P & Pastor J). Cambridge University Press Cambridge, pp. 289-325.

- Plunkett G., Carroll F., Hartwell B., Whitehouse N.J. & Reimer P.J. (2008). Vegetation history at the multi-period prehistoric complex at Ballynahatty, Co. Down, Northern Ireland. *Journal of Archaeological Science*, 35, 181-190.
- R Core Team (2017). R: A language and environment for statistical computing. R Foundation for Statistical Computing Vienna, Austria. URL <https://www.R-project.org/>.
- Ramsey B. (1995). Radiocarbon calibration and analysis of stratigraphy: The OxCal program. *Radiocarbon*, 37, 425-430.
- Ramsey C.B. (2008). Deposition models for chronological records. *Quaternary Science Reviews*, 27, 42-60.
- Rule S., Brook B.W., Haberle S.G., Turney C.S.M., Kershaw A.P. & Johnson C.N. (2012). The aftermath of megafaunal extinction: Ecosystem transformation in Pleistocene Australia. *Science*, 335, 1483-1486.
- Sandom C.J., Ejrnæs R., Hansen M.D.D. & Svenning J.C. (2014). High herbivore density associated with vegetation diversity in interglacial ecosystems. *Proceedings of the National Academy of Sciences*, 111, 4162-4167.
- Seppä H., Alenius T., Muukkonen P., Giesecke T., Miller P.A. & Ojala A.E.K. (2009). Calibrated pollen accumulation rates as a basis for quantitative tree biomass reconstructions. *The Holocene*, 19, 209-220.
- Stuart A.J. & Lister A.M. (2012). Extinction chronology of the woolly rhinoceros *Coelodonta antiquitatis* in the context of late Quaternary megafaunal extinctions in northern Eurasia. *Quaternary Science Reviews*, 51, 1-17.
- Tinner W., Conedera M., Amman B., Gaggeler H.W., Gedye S., Jones R. & Sagesser B. (1998). Pollen and charcoal in lake sediments compared with historically documented forest fires in southern Switzerland since AD 1920. *Holocene*, 8, 31-42.
- Tinner W. & Hu F.S. (2003). Size parameters, size-class distribution and area-number relationship of microscopic charcoal: Relevance for fire reconstruction. *Holocene*, 13, 499-505.
- Turney C.S.M., Van den Burg K., Wastegard S., Davies S.M., Whitehouse N.J., Pilcher J.R. & Callaghan C. (2006). North European last glacial-interglacial transition (LGIT; 15-9 ka)

tephrochronology: Extended limits and new events. *Journal of Quaternary Science*, 21, 335-345.

Vera F.W.M. (2006). Large herbivores: partners of trees and shrubs. In: *Large herbivore ecology, ecosystem dynamics and conservation* (eds. Danell K, Bergstrom R, Duncan P & Pastor J). Cambridge University Press Cambridge, pp. 203-231.

Watson J.E., Brooks S.J., Whitehouse N.J., Reimer P.J., Birks H.J.B. & Turney C. (2010). Chironomid-inferred late-glacial summer air temperatures from Lough Nadourcan, Co. Donegal, Ireland. *Journal of Quaternary Science*, 25, 1200-1210.

Willerslev E., Davison J., Moora M., Zobel M., Coissac E., Edwards M.E., Lorenzen E.D., Vestergard M., Gussarova G., Haile J., Craine J., Gielly L., Boessenkool S., Epp L.S., Pearman P.B., Cheddadi R., Murray D., Brathen K.A., Yoccoz N., Binney H., Cruaud C., Wincker P., Goslar T., Alsos I.G., Bellemain E., Brysting A.K., Elven R., Sonstebo J.H., Murton J., Sher A., Rasmussen M., Ronn R., Mourier T., Cooper A., Austin J., Moller P., Froese D., Zazula G., Pompanon F., Rioux D., Niderkorn V., Tikhonov A., Savvinov G., Roberts R.G., MacPhee R.D.E., Gilbert M.T.P., Kjaer K.H., Orlando L., Brochmann C. & Taberlet P. (2014). Fifty thousand years of Arctic vegetation and megafaunal diet. *Nature*, 506, 47-51.

Willis K.J., Braun M., Sumegi P. & Toth A. (1997). Does soil change cause vegetation change or vice versa? A temporal perspective from Hungary. *Ecology*, 78, 740-750.

Wood S.N. (2006). *Generalized Additive Models: An Introduction with R*. Chapman and Hall/CRC, Boca Raton Florida.

Zimov S.A., Zimov N.S., Tikhonov A.N. & Chapin F.S. (2012). Mammoth steppe: a high-productivity phenomenon. *Quaternary Science Reviews*, 57, 26-45.

Zuur A.F. (2009). *Mixed effects models and extensions in ecology with R*. Springer, New York; London.

FIGURE LEGENDS

Fig. 1. Mega- herbivore species assemblage dynamics. Cumulative probability densities for mega-herbivore species extant in Ireland, England and Scotland during the study period. The outputs shown were obtained by summing the selected radiocarbon dates for each species within bounded phases in OxCal, which defines periods of expected co-occurrence of individuals of the same species in time. The area circumscribed by the probability densities is proportional to the number of dated specimens. Note that the y-axes on the plots are shown on different scales due to large differences in the number of records available across the regions.

Fig. 2. Time-series of ecosystem dynamics. Pollen influx of herbs, shrubs and trees is used as a proxy for above-ground plant biomass at each of our five study sites ($n=241$). The influx of *Sporormiella*, a dung fungus, provides a proxy for mega-herbivore biomass in the surrounding landscape. Charcoal influx, shown with y-axes along the right hand side in the combined plots, reflects fire activity in the landscape and wider region. Nitrogen availability within the catchment is inferred from sedimentary $\delta^{15}\text{N}$ ($n=199$). Mean July air temperatures were reconstructed from chironomid assemblage data using a WA-PLS transfer function ($n=199$). All data were measured at concurrent levels across each sediment core.

Fig. 3. Model validation. Scatter plots of the response variables used in generalized additive models over time by site (A). Histogram plots of model residuals and scatter plots of residuals versus fitted values (B) for generalized additive models built using the 3-site data set (for predicting sedimentary $\delta^{15}\text{N}$) and the full 5-site data set (for predicting the three pollen influx variables).

Fig. 4. Modelled effects of biotic and abiotic factors on nitrogen availability and plant biomass. Plots of GAM smooth functions from the best-fitting model for describing changes in sedimentary $\delta^{15}\text{N}$ (A) at Dubh Lochan, Quidenham Mere and Lough Nadourcan, and pollen influx of herbs (B), shrubs (C) and trees (D) at all five sites. Nitrogen availability was modelled using data from the three sites for which these data are available ($n=199$) whereas plant biomass was modelled using data from all five sites ($n=241$) except for the climate term, which was modelled using only the 3-site dataset (see

FigS11 for all GAM smoother plots for the 3-site dataset). Asterisks indicate significance levels: * = $p\text{-value} \leq 0.05$; ** = $p\text{-value} \leq 0.01$; *** = $p\text{-value} \leq 0.001$. Gray areas represent two standard errors around the estimated effect. Tick marks along the x-axis indicate data points. The model included site-specific effects of the biotic factors on each response variable. Models were fit using the *mgcv* package in R with generalized cross-validation and automatic term selection. Flat lines indicate where a term has been dropped from the model. Note that some y-axes are shown on a different scale due to wide confidence intervals.

Supplementary Information

FigS1. Map of the five sedimentary sequences and fossil bone assemblages used in this study

TableS2. Plant taxa within each functional group present at each study site

MovieS3. Spatio-temporal probability densities for large herbivore species in Britain and Ireland

FigS4. Sediment accumulation rates by site

Appendix 1. Further information on study sites

Appendix 2. Sedimentary $\delta^{15}\text{N}$ as a proxy for nitrogen availability

TableS5. Age determinations of sedimentary sequences

FileS6. OxCal model specification for sedimentary sequence chronologies

FileS7. OxCal model specification for fossil bone chronologies

FigS8. Log-transformed time series data used in statistical modelling

TableS9. Correlation coefficients for the 3-site and 5-site datasets

Appendix 3. Statistical modeling

TableS10. Model statistics for individual smooth terms describing changes in sedimentary $\delta^{15}\text{N}$ at Dubh-Lochan, Quidenham Mere and Lough Nadourcan

FigS11. Modelled effects of biotic and abiotic factors on plant biomass using 3-site dataset

TableS12. Model statistics for individual smooth terms describing changes in pollen influx using 3-site dataset

TableS13. Model statistics for individual smooth terms describing changes in pollen influx using 5-site dataset

Table 1. Goodness of fit of each generalised additive model to the sedimentary $\delta^{15}\text{N}$ and pollen influx data from Dubh-Lochan, Quidenham Mere and Lough Nadourcan (3-site dataset). Model selection metrics were obtained using the *summary* function in the *mgcv* package in R. AIC weights (w_i) indicate the relative support for each model given the evidence in the data.

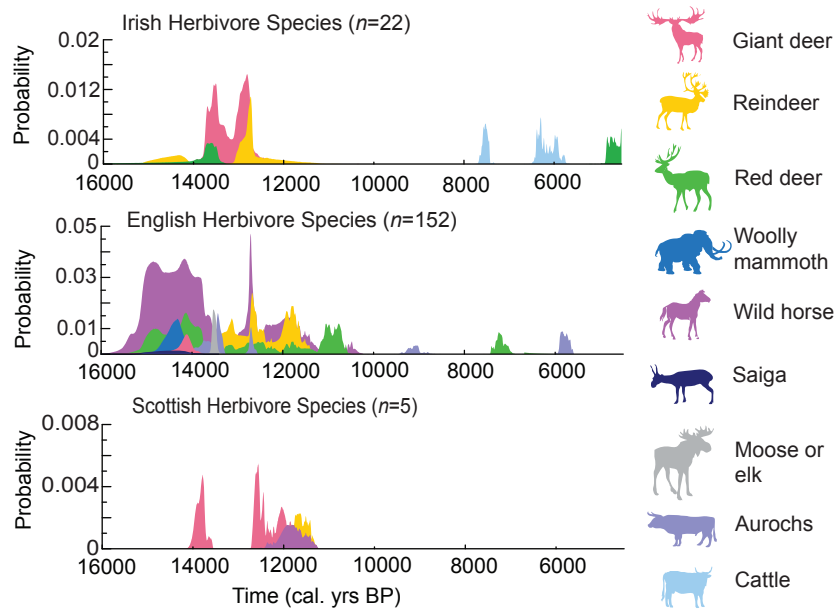
Models predicting Sedimentary $\delta^{15}\text{N}$				
Model	Dev. Exp.	Adj. R^2	AIC	w_i
$\delta^{15}\text{N} \sim \log(\text{Dung spores})$	9.42%	0.0699	513.918	0.00%
$\delta^{15}\text{N} \sim \log(\text{Dung spores}_{i, \text{ for all sites } i})$	22.90%	0.171	499.0207	0.00%
$\delta^{15}\text{N} \sim \log(\text{Dung spores}) + \text{Temp.}$	20.8	0.182	489.614	0.00%
$\delta^{15}\text{N} \sim \log(\text{Dung spores}_{i, \text{ for all sites } i}) + \text{Temp.}$	32.50%	0.282	468.513	0.00%
$\delta^{15}\text{N} \sim \log(\text{Dung spores}) + \log(\text{Charcoal})$	26.80%	0.228	481.5945	0.00%
$\delta^{15}\text{N} \sim \log(\text{Dung spores}_{i, \text{ for all sites } i}) + \log(\text{Charcoal})$	36.80%	0.309	465.6523	0.00%
$\delta^{15}\text{N} \sim \log(\text{Dung spores}) + \text{Temp.} + \log(\text{Charcoal})$	37.50%	0.336	453.0914	0.00%
$\delta^{15}\text{N} \sim \log(\text{Dung spores}_{i, \text{ for all sites } i}) + \text{Temp.} + \log(\text{Charcoal})$	45.20%	0.398	439.3393	0.00%
$\delta^{15}\text{N} \sim \log(\text{Dung spores}) + \text{Temp.} + \log(\text{Charcoal}) + \log(\text{Herb pollen}) + \log(\text{Shrub pollen}) + \log(\text{Tree pollen})$	43.90%	0.39	439.9324	0.00%
$\delta^{15}\text{N} \sim \log(\text{Dung spores}_{i, \text{ for all sites } i}) + \text{Temp.} + \log(\text{Charcoal}) + \log(\text{Herb pollen}_{i, \text{ for all sites } i}) + \log(\text{Shrub pollen}_{i, \text{ for all sites } i}) + \log(\text{Tree pollen}_{i, \text{ for all sites } i})$	57.20%	0.505	407.8037	100.00%
Models predicting Herb Pollen Influx				
Model	Dev. Exp.	Adj. R^2	AIC	w_i
$\log(\text{Herb pollen}) \sim \log(\text{Dung spores})$	42.10%	0.406	320.6112	0.00%
$\log(\text{Herb pollen}) \sim \log(\text{Dung spores}_{i, \text{ for all sites } i})$	69.10%	0.679	201.0699	0.00%
$\log(\text{Herb pollen}) \sim \log(\text{Dung spores}) + \text{Temp.}$	52.20%	0.486	300.0072	0.00%
$\log(\text{Herb pollen}) \sim \log(\text{Dung spores}_{i, \text{ for all sites } i}) + \text{Temp.}$	71.80%	0.702	188.3001	0.00%
$\log(\text{Herb pollen}) \sim \log(\text{Dung spores}) + \log(\text{Charcoal})$	65.40%	0.644	219.2119	0.00%
$\log(\text{Herb pollen}) \sim \log(\text{Dung spores}_{i, \text{ for all sites } i}) + \log(\text{Charcoal})$	78.40%	0.775	129.4189	0.00%
$\log(\text{Herb pollen}) \sim \log(\text{Dung spores}) + \text{Temp.} + \log(\text{Charcoal})$	70.30%	0.676	210.8094	0.00%
$\log(\text{Herb pollen}) \sim \log(\text{Dung spores}_{i, \text{ for all sites } i}) + \text{Temp.} + \log(\text{Charcoal})$	81%	0.798	111.8856	0.00%
$\log(\text{Herb pollen}) \sim \log(\text{Dung spores}_{i, \text{ for all sites } i}) + \log(\text{Charcoal}) + \log(\text{Shrub pollen}_{i, \text{ for all sites } i}) + \log(\text{Tree pollen}_{i, \text{ for all sites } i})$	91.40%	0.891	15.98281	100.00%
Models Predicting Shrub Pollen Influx				
Model	Dev. Exp.	Adj. R^2	AIC	w_i
$\log(\text{Shrub pollen}) \sim \log(\text{Dung spores})$	26.10%	0.244	288.6781	0.00%
$\log(\text{Shrub pollen}) \sim \log(\text{Dung spores}_{i, \text{ for all sites } i})$	39.40%	0.364	259.004	0.00%
$\log(\text{Shrub pollen}) \sim \log(\text{Dung spores}) + \text{Temp.}$	26.10%	0.241	290.6055	0.00%
$\log(\text{Shrub pollen}) \sim \log(\text{Dung spores}_{i, \text{ for all sites } i}) + \text{Temp.}$	43.10%	0.400	248.5863	0.00%
$\log(\text{Shrub pollen}) \sim \log(\text{Dung spores}) + \log(\text{Charcoal})$	36.70%	0.338	266.794	0.00%
$\log(\text{Shrub pollen}) \sim \log(\text{Dung spores}_{i, \text{ for all sites } i}) + \log(\text{Charcoal})$	48.80%	0.461	227.0712	0.00%
$\log(\text{Shrub pollen}) \sim \log(\text{Dung spores}) + \text{Temp.} + \log(\text{Charcoal})$	36.70%	0.338	266.794	0.00%
$\log(\text{Shrub pollen}) \sim \log(\text{Dung spores}_{i, \text{ for all sites } i}) + \text{Temp.} + \log(\text{Charcoal})$	51.80%	0.485	220.1156	0.00%
$\log(\text{Shrub pollen}) \sim \log(\text{Dung spores}_{i, \text{ for all sites } i}) + \log(\text{Charcoal}) + \log(\text{Herb pollen}_{i, \text{ for all sites } i}) + \log(\text{Tree pollen}_{i, \text{ for all sites } i})$	85.10%	0.818	33.31709	100.00%
Models Predicting Tree Pollen Influx				
Model	Dev. Exp.	Adj. R^2	AIC	w_i
$\log(\text{Tree pollen}) \sim \log(\text{Dung spores})$	24.60%	0.234	333.4624	0.00%
$\log(\text{Tree pollen}) \sim \log(\text{Dung spores}_{i, \text{ for all sites } i})$	53.50%	0.51	251.1887	0.00%
$\log(\text{Tree pollen}) \sim \log(\text{Dung spores}) + \text{Temp.}$	39%	0.363	302.1733	0.00%
$\log(\text{Tree pollen}) \sim \log(\text{Dung spores}_{i, \text{ for all sites } i}) + \text{Temp.}$	56.20%	0.524	251.1237	0.00%
$\log(\text{Tree pollen}) \sim \log(\text{Dung spores}) + \log(\text{Charcoal})$	48.10%	0.446	278.13	0.00%
$\log(\text{Tree pollen}) \sim \log(\text{Dung spores}_{i, \text{ for all sites } i}) + \log(\text{Charcoal})$	58.10%	0.546	241.1491	0.00%
$\log(\text{Tree pollen}) \sim \log(\text{Dung spores}) + \text{temp.} + \log(\text{Charcoal})$	54.20%	0.497	263.4908	0.00%
$\log(\text{Tree pollen}) \sim \log(\text{Dung spores}_{i, \text{ for all sites } i}) + \text{Temp.} + \log(\text{Charcoal})$	61.50%	0.572	233.38	0.00%
$\log(\text{Tree pollen}) \sim \log(\text{Dung spores}_{i, \text{ for all sites } i}) + \log(\text{Charcoal}) + \log(\text{Herb pollen}_{i, \text{ for all sites } i}) + \log(\text{Shrub pollen}_{i, \text{ for all sites } i})$	78.60%	0.757	124.1384	100.00%

Note: 'Pollen' refers to the pollen accumulation rate or influx, 'dung spores' are the influx of *Sporormiella* (the dung fungus), 'charcoal' refers to charcoal influx and the subscript i indicates terms with site-specific effects on the response variable, where i represents Dubh-Lochan, Quidenham Mere and Lough Nadourcan.

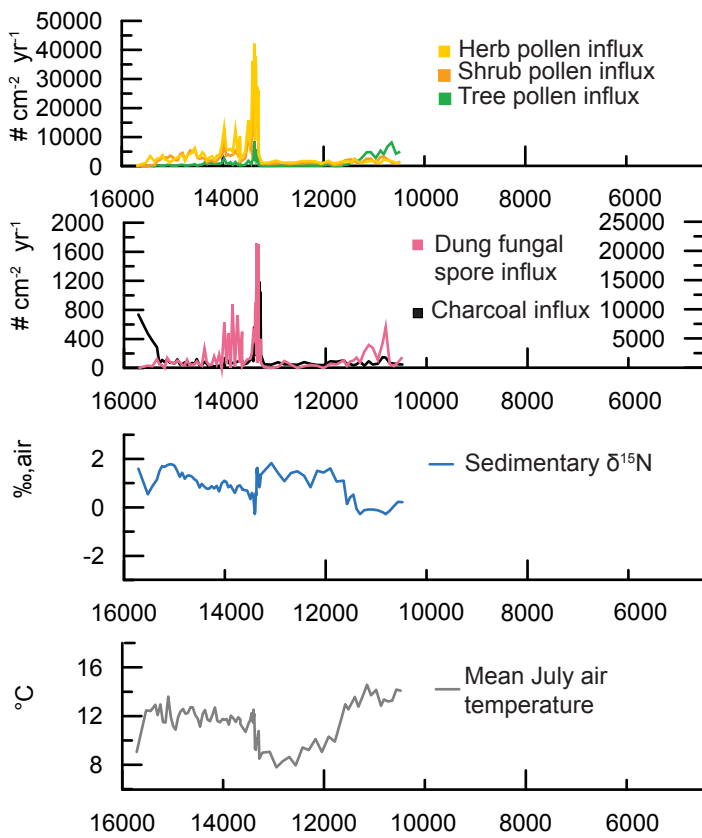
Table 2. Goodness of fit of each generalised additive model to the pollen influx data from all five study sites (5-site dataset). Model selection metrics were obtained using the *summary* function in the *mgcv* package in R. AIC weights (w_i) indicate the relative support for each model given the evidence in the data.

Models predicting Herb Pollen Influx				
Model	Dev. Exp.	Adj. R ²	AIC	w_i
log(Herb pollen) ~ log(Dung spores)	37%	0.354	397.6484	0.00%
log(Herb pollen) ~ log(Dung spores _{<i>i</i>} , for all sites <i>i</i>)	67.10%	0.651	257.6245	0.00%
log(Herb pollen) ~ log(Dung spores) + log(Charcoal)	53.80%	0.524	325.6721	0.00%
log(Herb pollen) ~ log(Dung spores _{<i>i</i>} , for all sites <i>i</i>) + log(Charcoal)	76.90%	0.75	181.599	0.00%
log(Herb pollen) ~ log(Dung spores _{<i>i</i>} , for all sites <i>i</i>) + log(Charcoal) + log(Shrub pollen _{<i>i</i>} , for all sites <i>i</i>) + log(Tree pollen _{<i>i</i>} , for all sites <i>i</i>)	91.70%	0.886	28.8873	100.00%
Models Predicting Shrub Pollen Influx				
Model	Dev. Exp.	Adj. R ²	AIC	w_i
log(Shrub pollen) ~ log(Dung spores)	17.50%	0.159	456.269	0.00%
log(Shrub pollen) ~ log(Dung spores _{<i>i</i>} , for all sites <i>i</i>)	56.40%	0.524	334.299	0.00%
log(Shrub pollen) ~ log(Dung spores) + log(Charcoal)	33.30%	0.308	413.4638	0.00%
log(Shrub pollen) ~ log(Dung spores _{<i>i</i>} , for all sites <i>i</i>) + log(Charcoal)	61.40%	0.58	303.6918	0.00%
log(Shrub pollen) ~ log(Dung spores _{<i>i</i>} , for all sites <i>i</i>) + log(Charcoal) + log(Herb pollen _{<i>i</i>} , for all sites <i>i</i>) + log(Tree pollen _{<i>i</i>} , for all sites <i>i</i>)	89.60%	0.871	44.73457	100.00%
Models Predicting Tree Pollen Influx				
Model	Dev. Exp.	Adj. R ²	AIC	w_i
log(Tree pollen) ~ log(Dung spores)	21.10%	0.198	456.6042	0.00%
log(Tree pollen) ~ log(Dung spores _{<i>i</i>} , for all sites <i>i</i>)	61.60%	0.591	305.3566	0.00%
log(Tree pollen) ~ log(Dung spores) + log(Charcoal)	39.70%	0.376	400.7345	0.00%
log(Tree pollen) ~ log(Dung spores _{<i>i</i>} , for all sites <i>i</i>) + log(Charcoal)	65.90%	0.626	289.6825	0.00%
log(Tree pollen) ~ log(Dung spores _{<i>i</i>} , for all sites <i>i</i>) + log(Charcoal) + log(Herb pollen _{<i>i</i>} , for all sites <i>i</i>) + log(Shrub pollen _{<i>i</i>} , for all sites <i>i</i>)	82.40%	0.802	143.24	100.00%

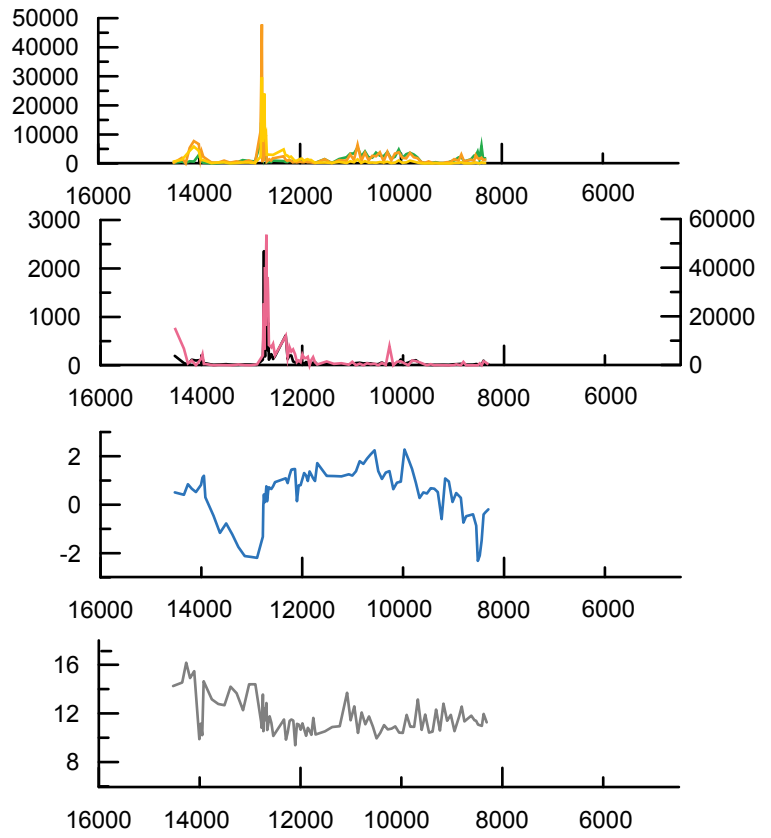
Note: 'Pollen' refers to the pollen accumulation rate or influx, 'dung spores' are the influx of *Sporormiella* (the dung fungus), 'charcoal' refers to charcoal influx and the subscript *i* indicates terms with site-specific effects on the response variable, where *i* represents Dubh-Lochan, Quidenham Mere, Lough Nadourcan, Ballynahatty and Long Lough.



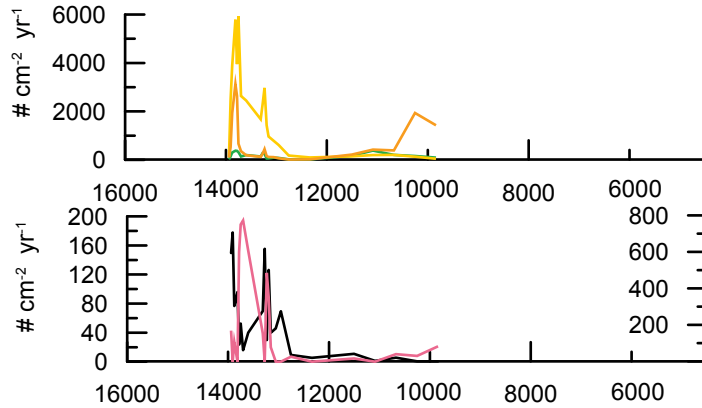
Lough Nadourcan, Ireland ($n=87$)



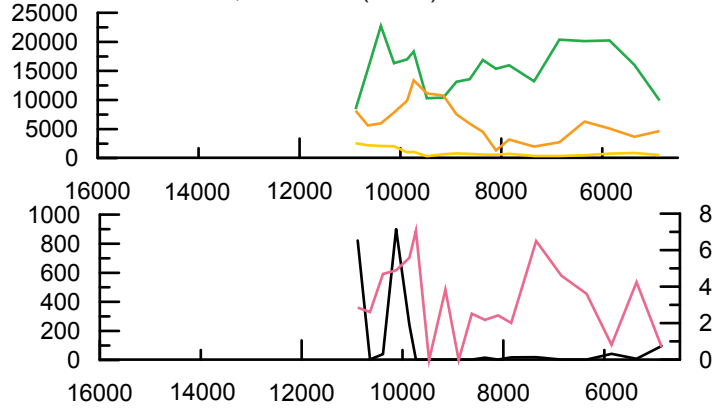
Quidenham Mere, England ($n=93$)



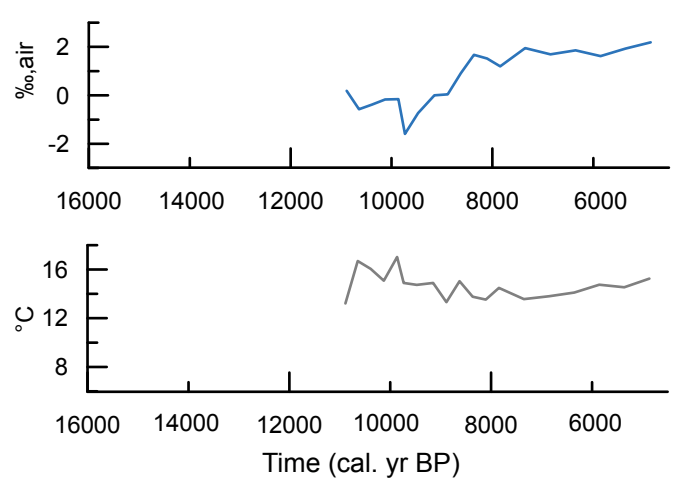
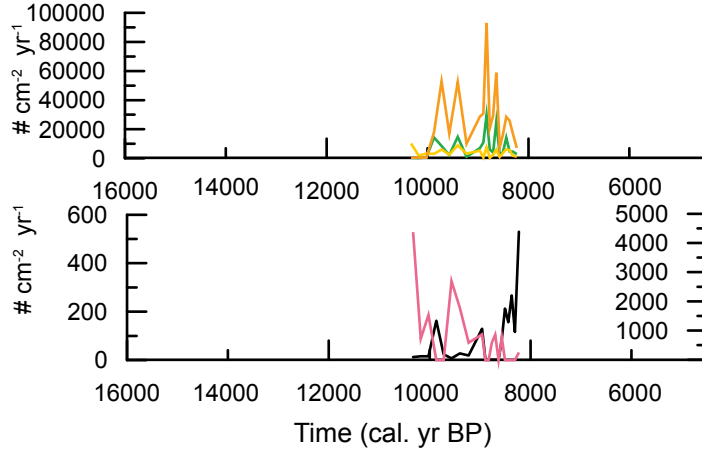
Long Lough, Ireland ($n=22$)

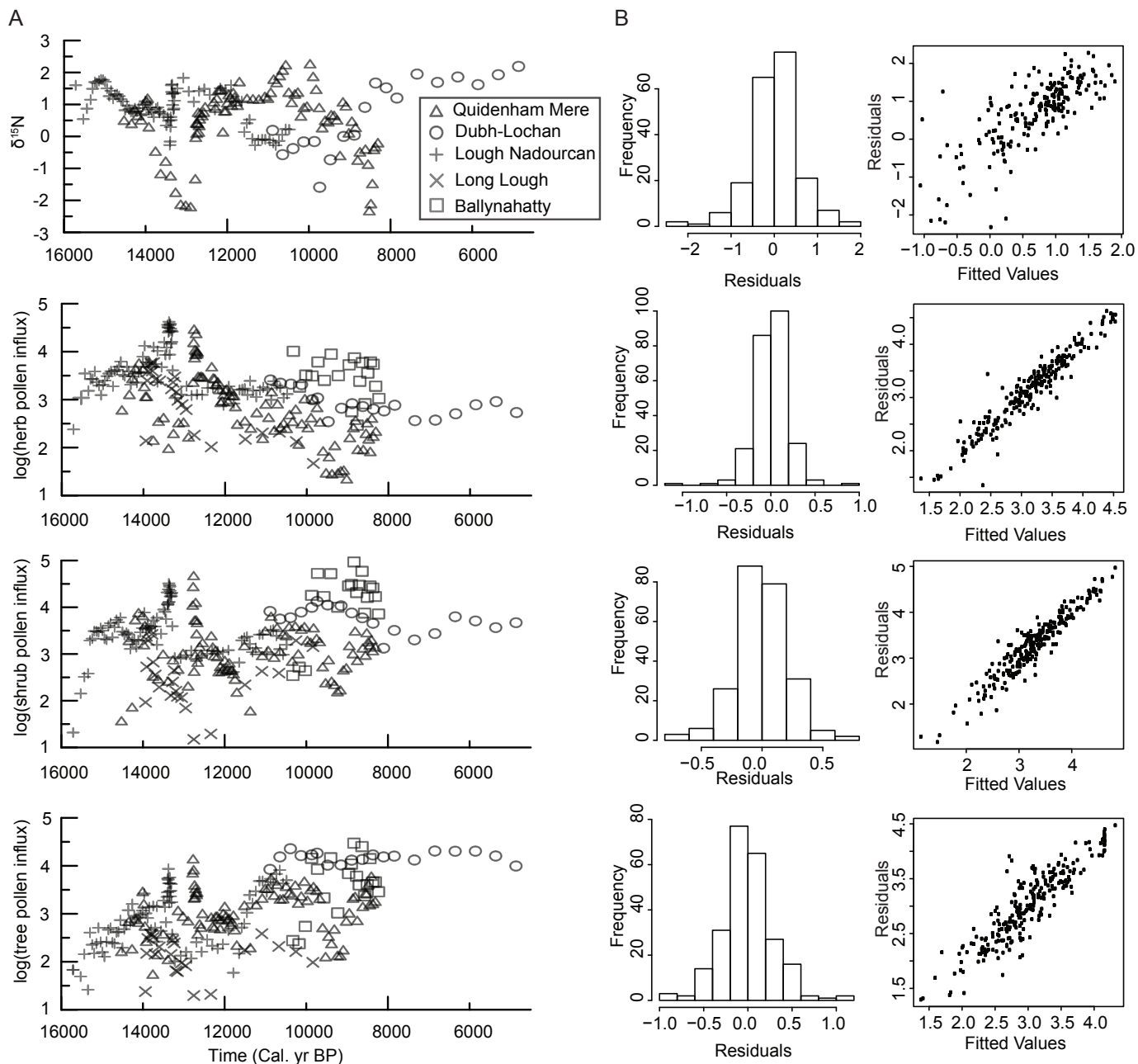


Dubh-Lochan, Scotland ($n=19$)

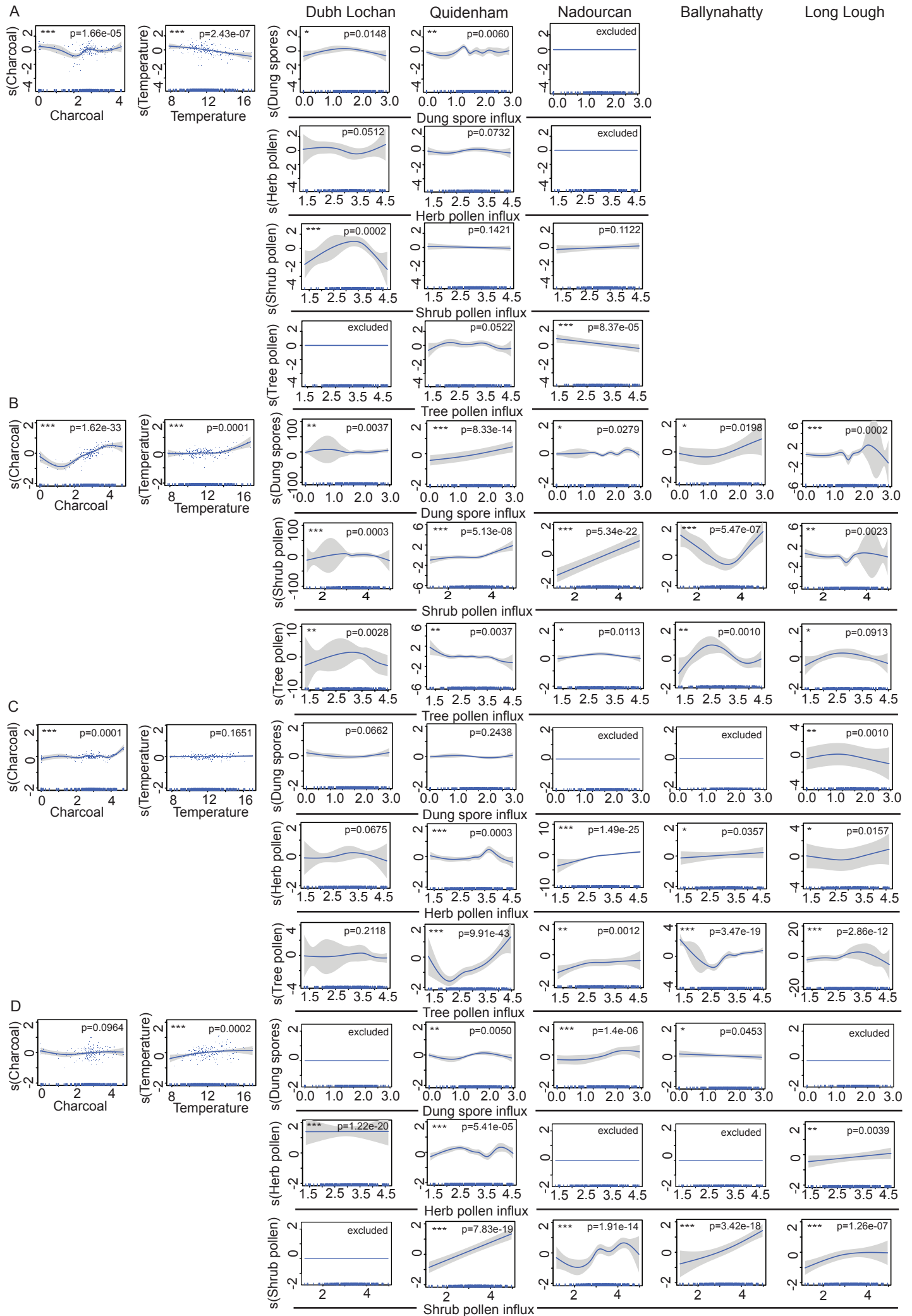


Ballynahatty, Ireland ($n=20$)





Biotic Factors - by Site



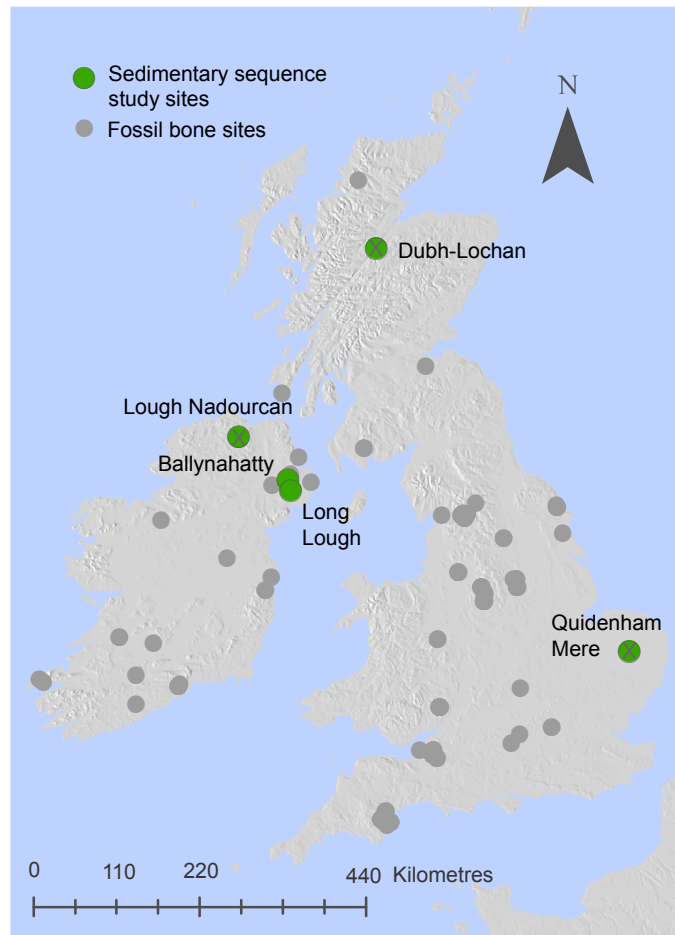
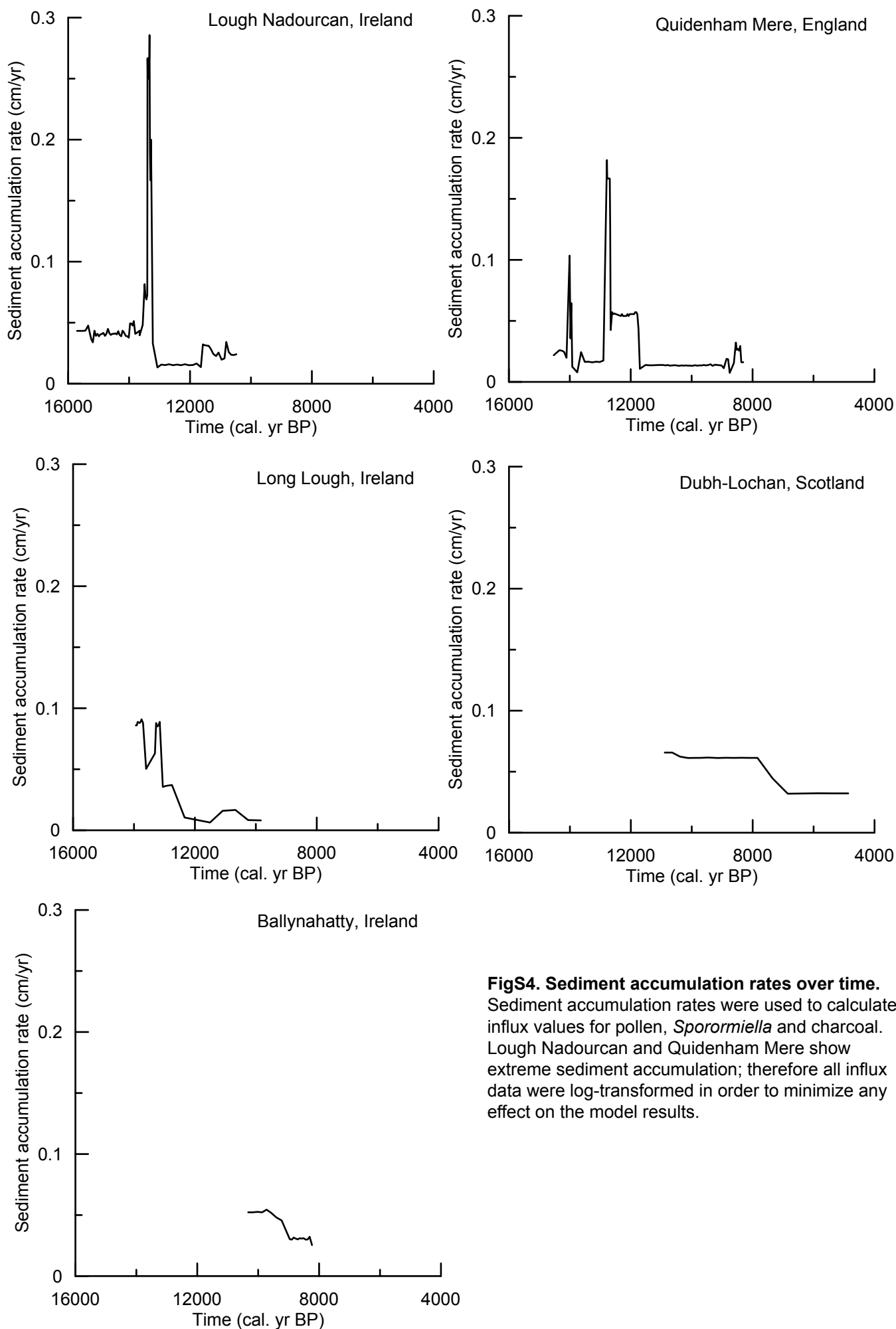


Fig. S1. Locations of the five sedimentary sequences and fossil bone assemblages used in this study. Palaeoecological proxy data for above-ground plant biomass, mega-herbivore biomass and fire activity are available at all five study sites. Proxy data for nitrogen availability and mean July air temperature are available at the three sites marked with an X.

TableS2. Plant taxa within each of the three functional groups and their presence at each study site.

Herbs	Site					Herbs (continued)	Site				
	D	Q	N	B	L		D	Q	N	B	L
Amaranthaceae (Chenopodiaceae)					X	Scrophulariaceae	X				
<i>Anemone</i>		X				<i>Solanum</i>					X
Apiaceae	X	X	X		X	<i>Stachys</i> t.					X
<i>Arctium</i>			X			<i>Succisa</i>	X				X
<i>Armeria</i>		X	X		X	<i>Thalictrum</i>	X	X	X		X
<i>Artemisia</i>	X	X	X		X	<i>Urtica</i>	X	X	X		
Brassicaceae	X	X	X		X	<i>Valeriana</i>		X	X		
<i>Caltha</i>	X	X	X			<i>Veronica</i>					X
<i>Campanula</i>		X				Shrubs					
Caprifoliaceae					X	<i>Buxus</i>		X			
Caryophyllaceae		X	X	X	X	<i>Calluna</i>	X	X	X	X	X
<i>Centaurea</i>			X			<i>Corylus avellana</i>	X	X	X	X	X
<i>Chamaenerium</i>				X	X	<i>Empetrum</i>	X	X	X	X	X
<i>Chenopodium</i>		X	X			<i>Ephedra</i>		X	X		
<i>Circaea</i>					X	Ericaceae	X	X			X
<i>Cirsium</i>		X	X			<i>Hedera</i>	X	X		X	X
Compositae	X	X	X	X	X	<i>Hippophae</i>			X		
Cyperaceae	X	X	X	X	X	<i>Ilex</i>	X	X			
<i>Drosera</i>		X				<i>Juniperus</i>	X	X	X	X	X
<i>Dryas</i>		X	X			<i>Lonicera</i>	X				
<i>Epilobium</i>		X	X			<i>Myrica</i>	X		X		
<i>Filipendula</i>	X	X	X	X	X	<i>Olea</i>		X			
<i>Galium</i>					X	<i>Salix</i>	X	X	X	X	X
<i>Gentiana</i>					X	<i>Sambucus nigra</i>		X			
<i>Geum</i>		X	X			<i>Vaccinium</i> group					X
<i>Helianthemum</i>		X	X			<i>Viburnum opulus</i>	X	X	X		
Lamiaceae		X	X		X	<i>Viscum album</i>		X			
Leguminosae	X				X	Trees					
<i>Limonium</i>				X		<i>Abies</i>			X		
<i>Linum</i>		X	X			<i>Acer</i>		X			
<i>Ludwigia palustris</i>		X				<i>Alnus</i>	X	X	X	X	X
<i>Matricaria</i>		X				<i>Betula</i>	X	X	X	X	X
<i>Melampyrum</i>		X	X		X	<i>Carpinus</i>		X	X		
<i>Mentha</i>		X				<i>Fagus</i>			X		
<i>Mercurialis</i>		X				<i>Fraxinus</i>	X			X	
<i>Ononis</i>		X	X			<i>Juglans</i>		X			
Papaveraceae					X	<i>Larix</i>		X			
<i>Plantago</i>	X	X	X	X		<i>Picea</i>		X			
Poaceae	X	X	X	X	X	<i>Pinus</i>	X	X	X	X	X
<i>Polemonium</i>		X				<i>Populus</i>	X	X	X	X	X
Polygonaceae		X			X	<i>Quercus</i>	X	X	X	X	X
<i>Potentilla</i>	X	X	X			<i>Sorbus</i>	X				
<i>Prunella</i> type		X				<i>Taxus</i>		X			X
Ranunculaceae	X	X	X	X	X	<i>Tilia</i>	X	X			
Rosaceae.	X	X	X	X	X	<i>Ulmus</i>	X	X	X	X	X
Rubiaceae		X									
<i>Rumex</i>	X	X	X		X						
Saxifragaceae		X	X		X						

Site names are denoted by D for Dubh-Lochan, Q for Quidenham Mere, N for Lough Nadourcan, B for Ballynahatty and L for Long Lough.



FigS4. Sediment accumulation rates over time. Sediment accumulation rates were used to calculate influx values for pollen, *Sporormiella* and charcoal. Lough Nadourcan and Quidenham Mere show extreme sediment accumulation; therefore all influx data were log-transformed in order to minimize any effect on the model results.

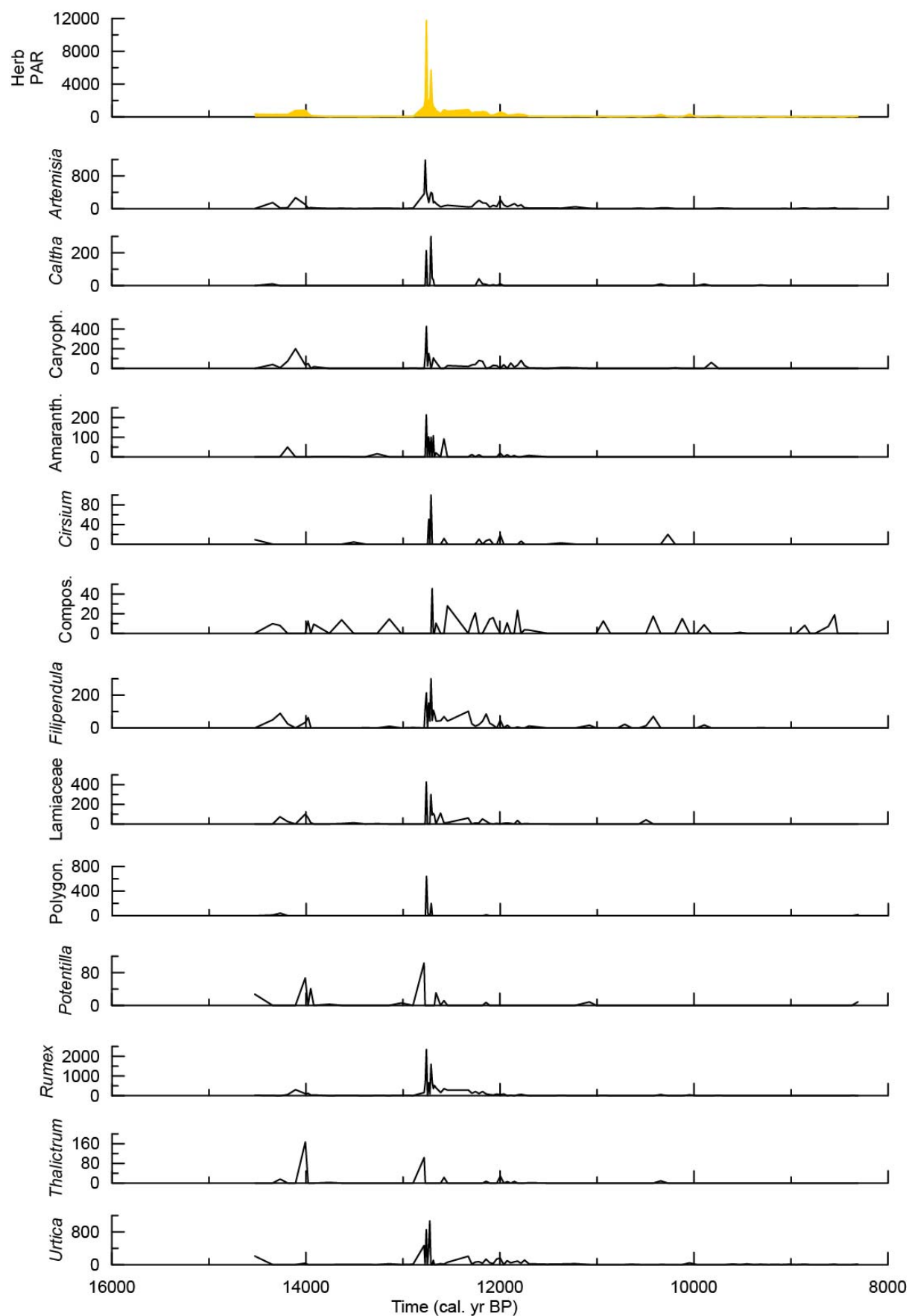
SUPPLEMENTARY INFORMATION

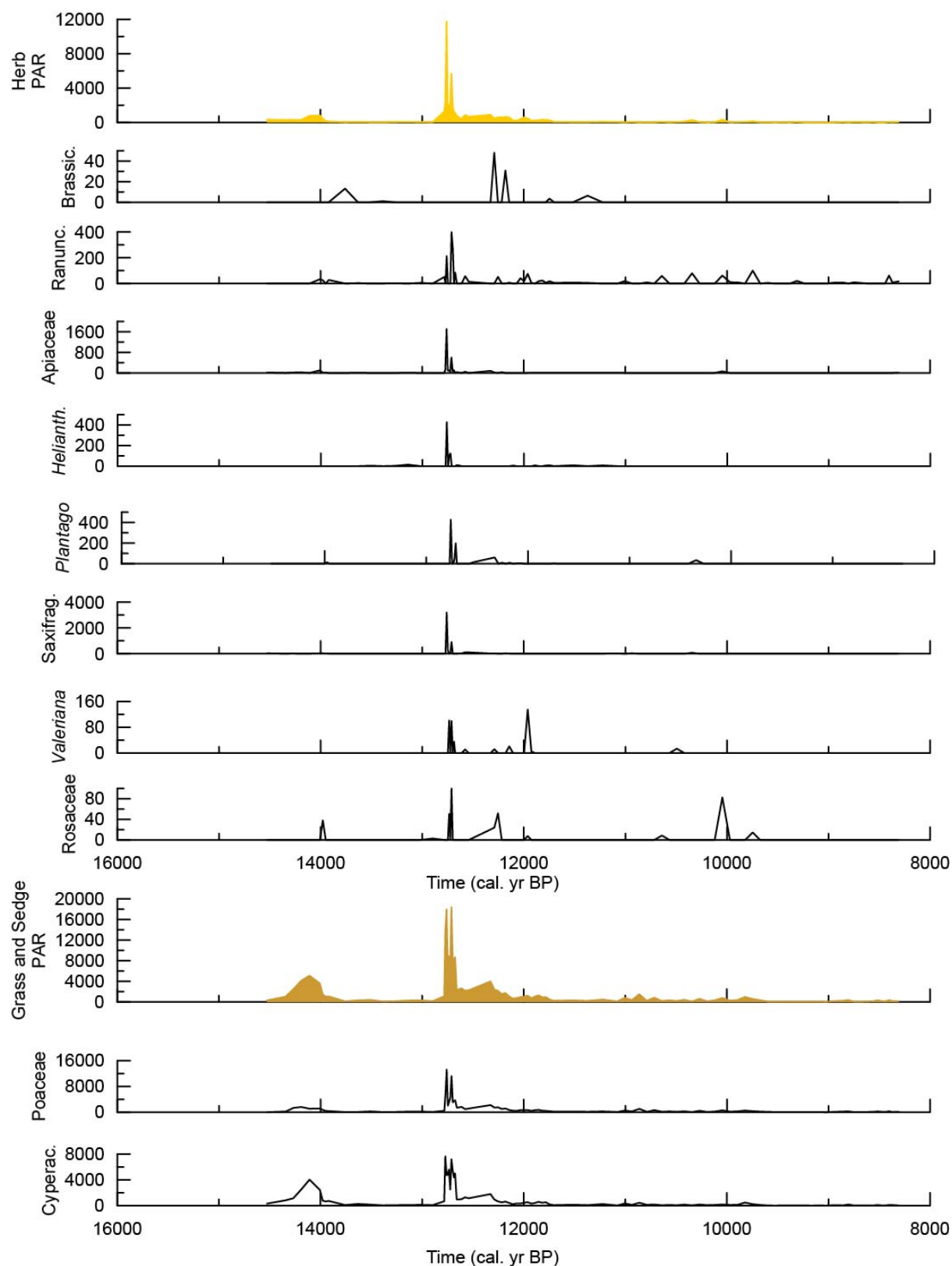
Plant controls on Late Quaternary whole ecosystem structure and function

E.S. Jeffers, N.J. Whitehouse, A. Lister, G. Plunkett, P. Barratt, E. Smyth, P. Lamb, M.W. Dee, S.J. Brooks, K.J. Willis, C.A. Froyd, J.E. Watson, M.B. Bonsall

Appendix 1 Study Sites

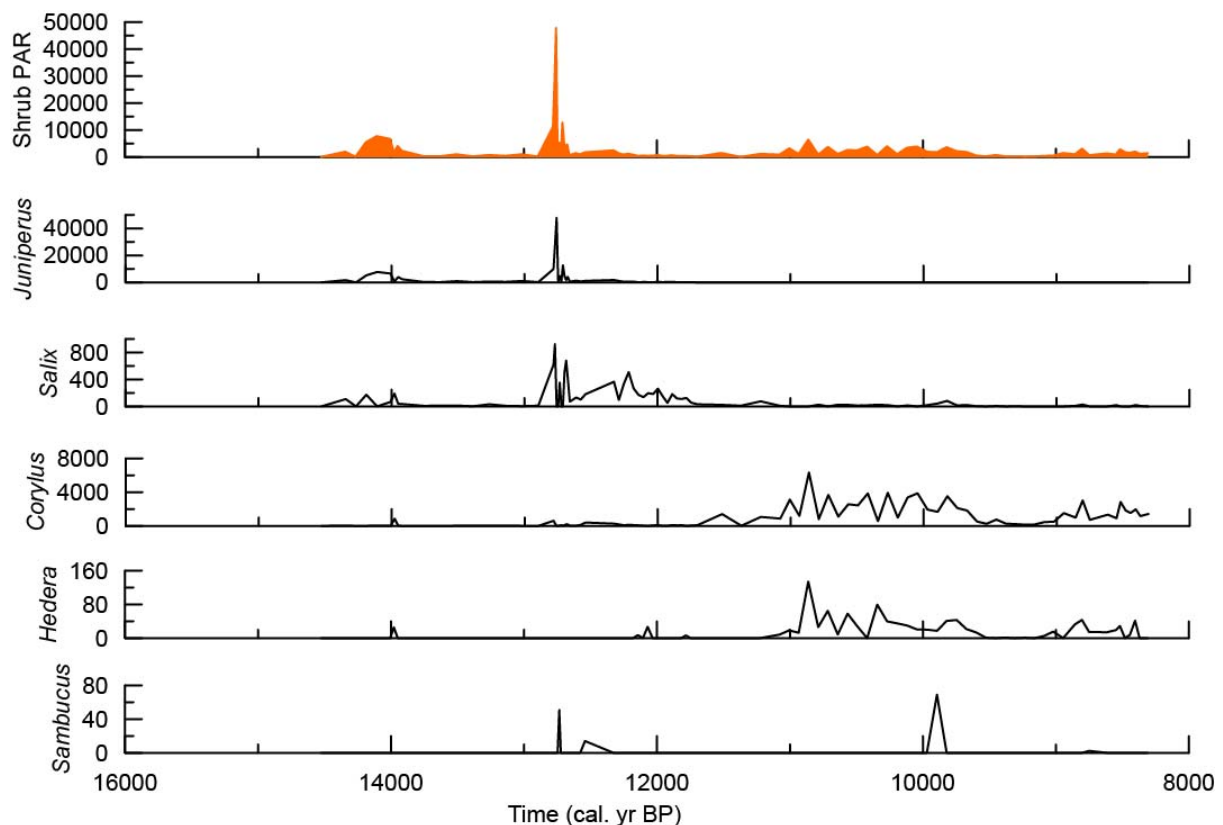
Quidenham Mere. Quidenham Mere, in the southeast of England, was surrounded by a chalk grassland at the end of the glacial period (Jeffers *et al.* 2011). Summer temperatures at Quidenham Mere during the Pleistocene – Holocene transition were more akin to those in continental Europe than the rest of the British Isles (Brooks & Langdon 2014). Thirty-nine herb plant taxa are represented at Quidenham Mere (Appendix Fig1) and their dynamics are largely consistent with the grasses (Poaceae) and sedges (Cyperaceae). Eighteen taxa were included in the summary herb pollen accumulation rate values but not shown here because their values were less than 1% of the total amount. Those not shown include: *Anemone*, *Armeria*, *Campanula*, *Drosera*, *Dryas*, *Epilobium*, *Geum*, *Helianthemum*, *Linum*, *Ludwigia*, *Matricaria*, *Melampyrum*, *Mentha*, *Mercurialis*, *Ononis*, *Polemonium*, *Prunella*, and Rubiaceae. The initial rise in herb biomass included at least 15 taxa, while the peak included at least six more.





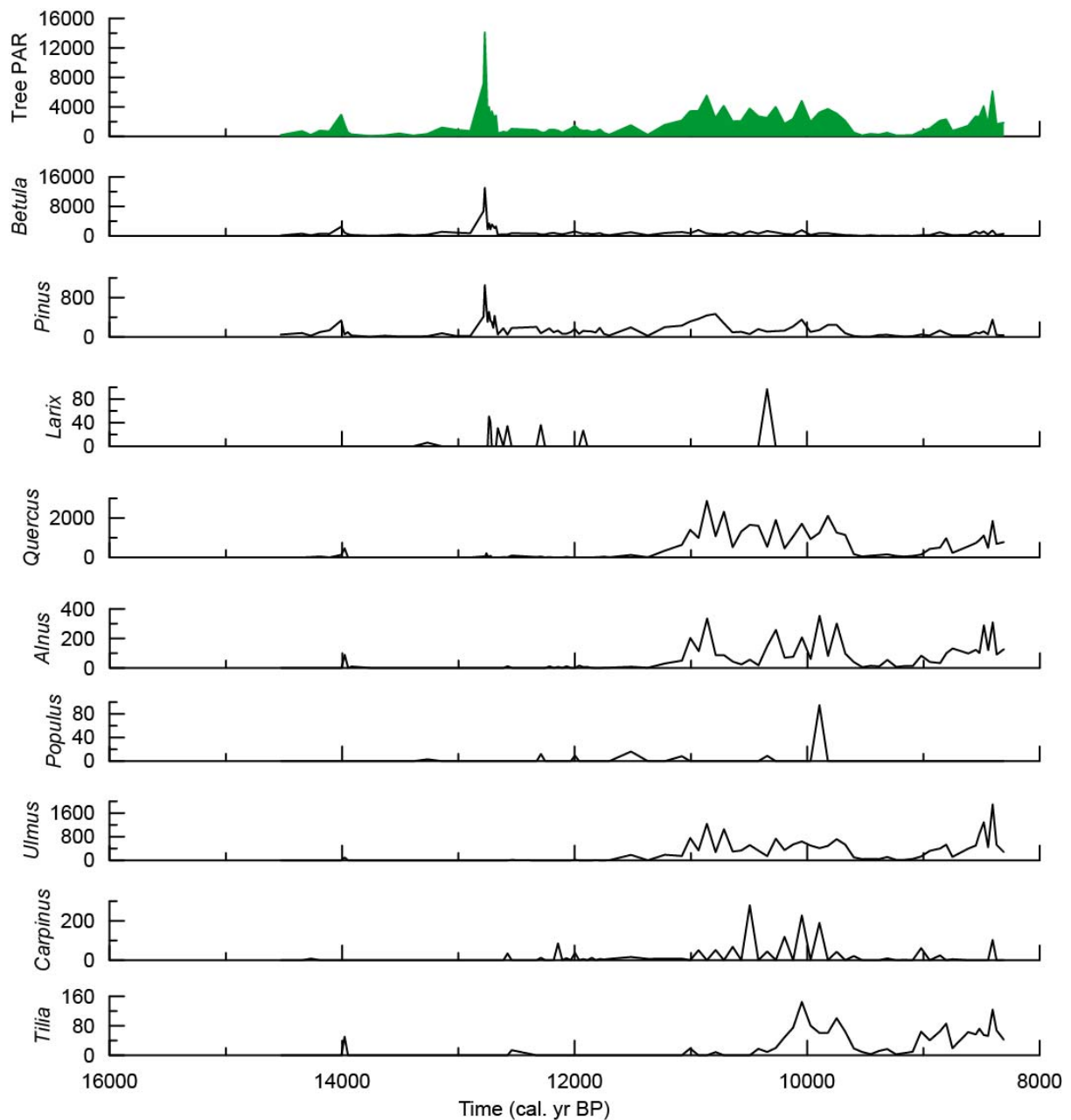
Appendix Fig. 1. Herb and grass pollen accumulation rates (grains cm⁻² yr⁻¹) at Quidenham Mere. The summary data for each growth form are presented in colour while the data for the component taxa within the group are presented in black. Note that the y-axis values vary between graphs.

There were 14 shrub taxa at Quidenham Mere (Appendix Fig2) although nine of these were at insufficient quantities for plotting (i.e. pollen accumulation rates were less than 1% of the summary value of the plant functional type). Those not shown include: *Buxus*, *Calluna*, Ericaceae, *Empetrum*, *Ephedra*, *Ilex*, *Olea*, *Viburnum*, and *Viscum*. While *Salix* was present throughout the record, there was a distinct shift from *Juniperus* to *Corylus* as the dominant shrub in the plant community at the start of the postglacial period.



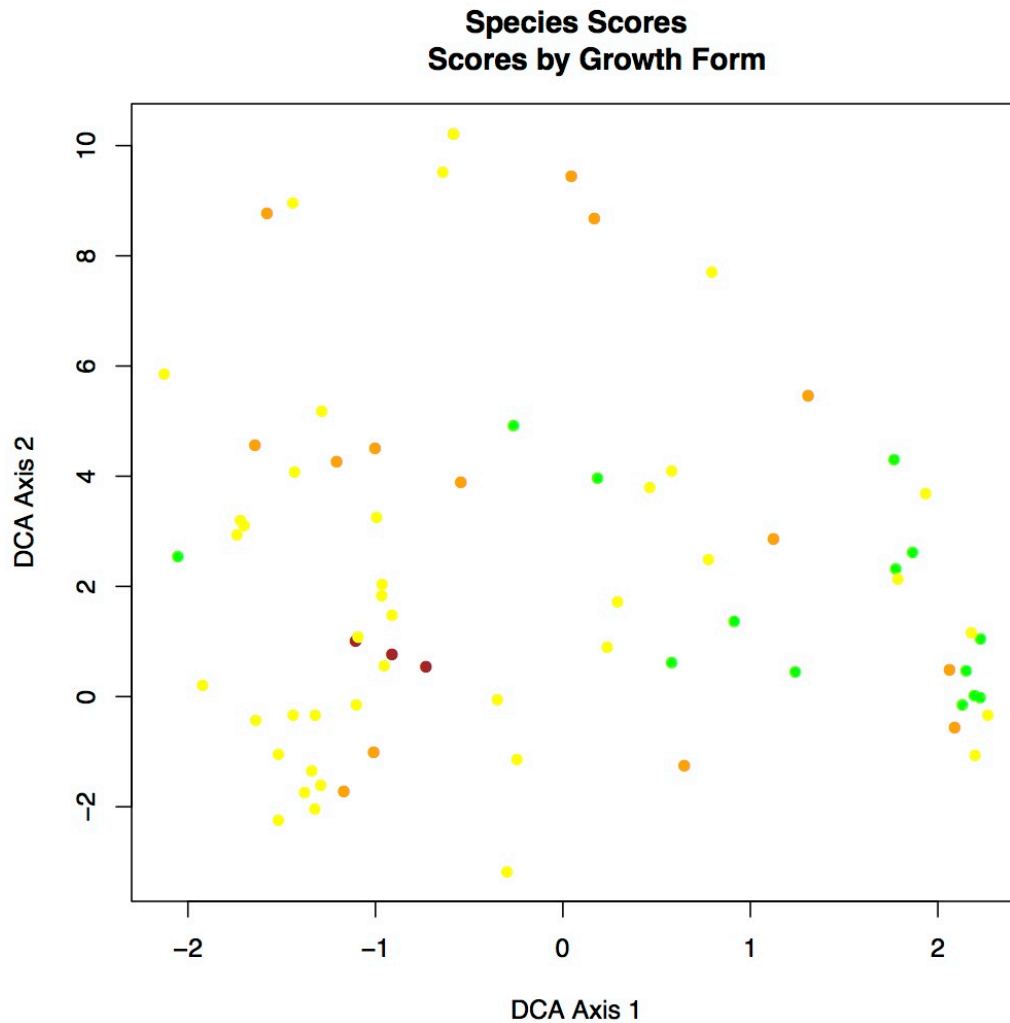
Appendix Fig2. Shrub pollen accumulation rates (grains cm⁻² yr⁻¹) at Quidenham Mere. The summary data for each growth form are presented in colour while the data for the component taxa within the group are presented in black. Note that the y-axis values vary between graphs.

There were 13 genera of trees at Quidenham Mere and these were predominantly broadleaved (Appendix Fig3). Four genera, *Acer*, *Juglans*, *Picea*, and *Taxus* were not included in the graph due to insufficient quantities. The initial woodland included *Betula* and *Pinus*, while later woodland development was dominated by *Quercus* and *Ulmus*.



Appendix Fig3. Tree pollen accumulation rates (grains cm⁻² yr⁻¹) at Quidenham Mere. The summary data for each growth form are presented in colour while the data for the component taxa within the group are presented in black. Note that the y-axis values vary between graphs.

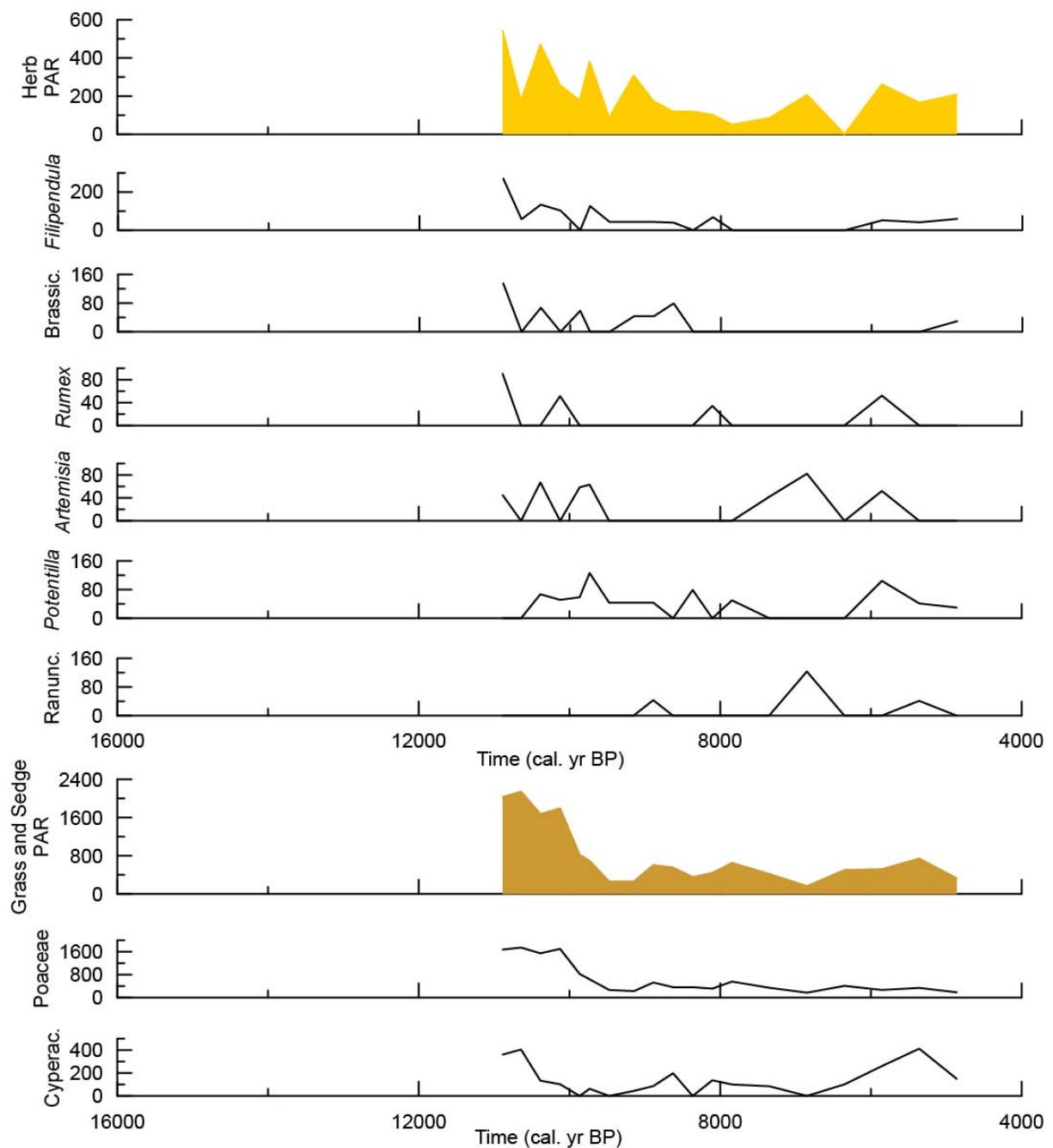
Detrended correspondence analysis (conducted with the *decorana* function in the *vegan* package version 2.4-5 in R) of the individual plant taxa records at Quidenham Mere show that herb and shrub pollen influx span the breadth of the two primary axes of variation, while tree pollen influx shows relatively more consistent variation within the functional type (Appendix Fig4).



Appendix Fig4. Plot of species scores from detrended correspondence analysis of pollen accumulation rates for herbs (yellow), grass (brown), shrubs (orange) and trees (green) at Quidenham Mere.

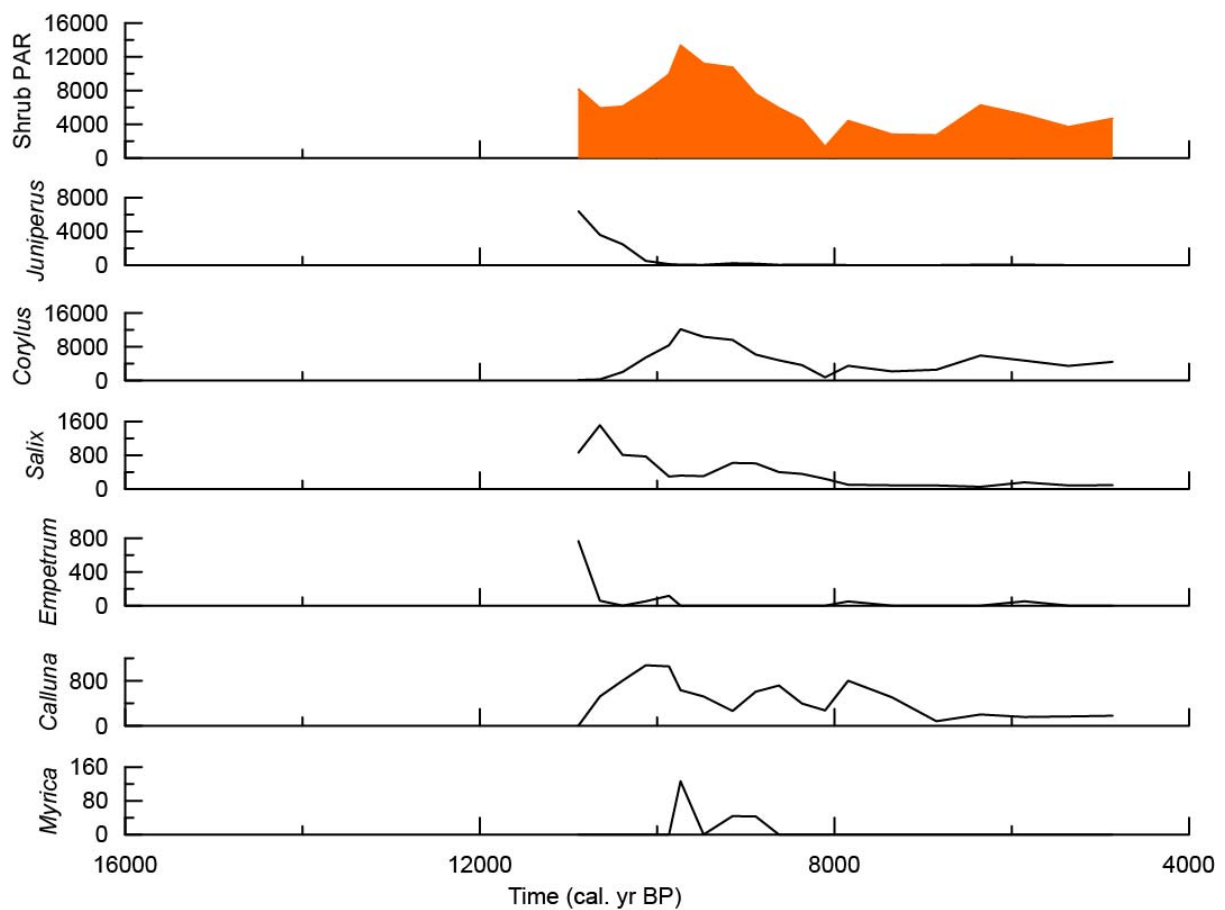
Dubh-Lochan. Dubh-Lochan is located in the Scottish Highlands and throughout the analysis period supports plant assemblages dominated by a mix of coniferous and deciduous tree species (Froyd 2006). The site is occupied by a *Juniperus* scrub community in the early Holocene, followed by *Betula-Corylus* woodland from ~10,400 – 9000 cal. yrs BP. *Pinus sylvestris* is dominant at the site from 9000 – 7200 cal. yrs BP, after which a mixed woodland consisting of *Pinus sylvestris*, *Betula*, *Corylus avellana*, *Alnus glutinosa* and *Quercus* develops. Total pollen percentage for grasses and other herbaceous species ranges between 2 – 11 % (Froyd 2002).

Mean July air temperatures around Dubh-Lochan were relatively stable during the early Holocene and were higher than those reported for Quidenham Mere for the same time periods (Jeffers *et al.* 2015). Sixteen herb plant taxa are represented at Dubh-Lochan (Appendix Fig5) and their dynamics are consistent with the grasses and sedges. Ten taxa were included in the summary herb pollen accumulation rate values but not shown here: *Apiaceae*, *Caltha*, *Compositae*, *Fabaceae*, *Plantago*, *Rosaceae*, *Scrophularia*, *Succisa*, *Thalictrum*, and *Urtica*. All but *Ranunculaceae* were present throughout the record.



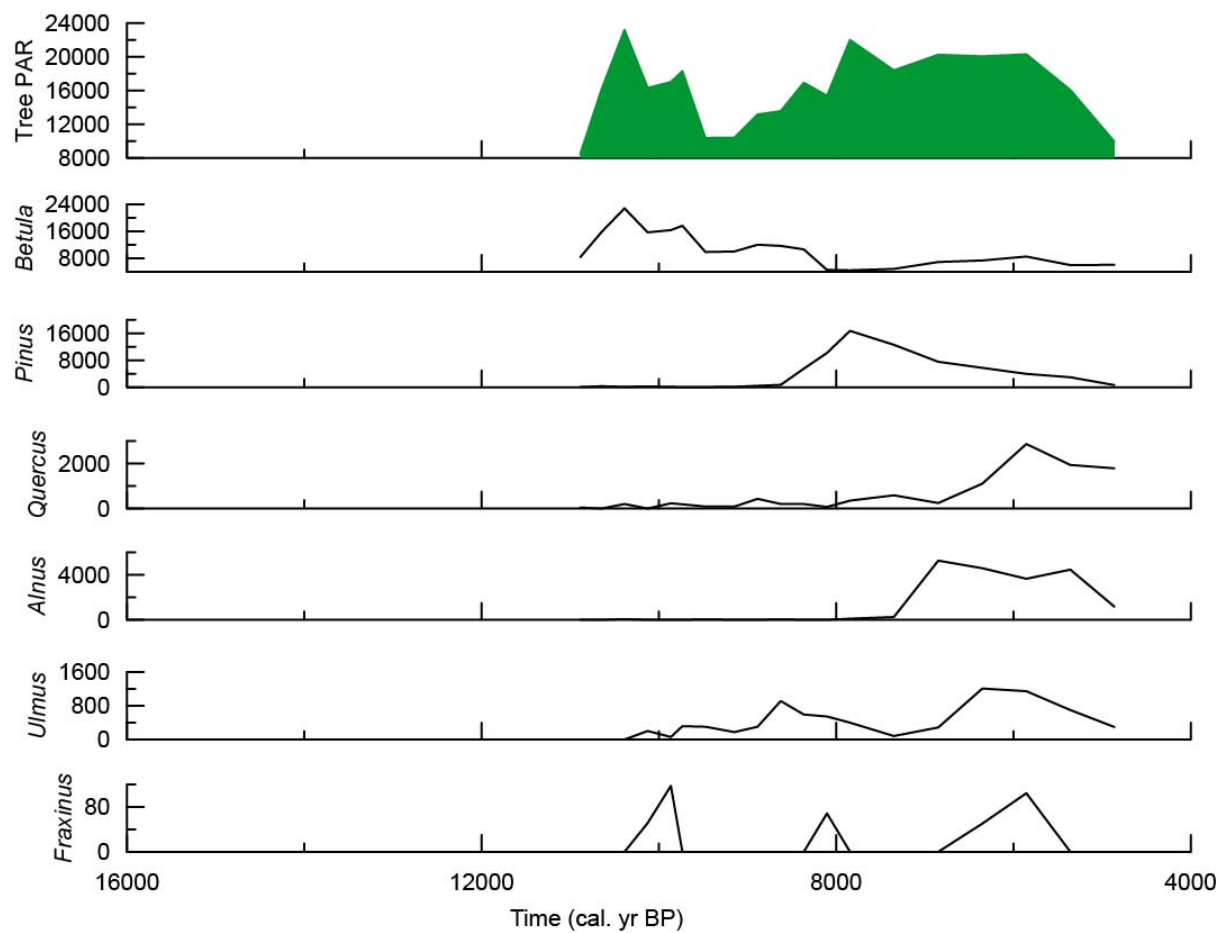
Appendix Fig5. Herb pollen accumulation rates (grains cm⁻² yr⁻¹) at Dubh-Lochan. The summary data for each growth form are presented in colour while the data for the component taxa within the group are presented in black. Note that the y-axis values vary between graphs.

There were 11 shrub taxa at Dubh-Lochan (Appendix Fig6) although five of these were at insufficient quantities for plotting. Those not shown include: *Ericaceae*, *Hedera*, *Ilex*, *Lonicera*, and *Viburnum*. *Juniperus* and *Empetrum* declined abruptly near the start of the record and were replaced by *Corylus* and *Calluna* (albeit at much lower densities than *Corylus*).



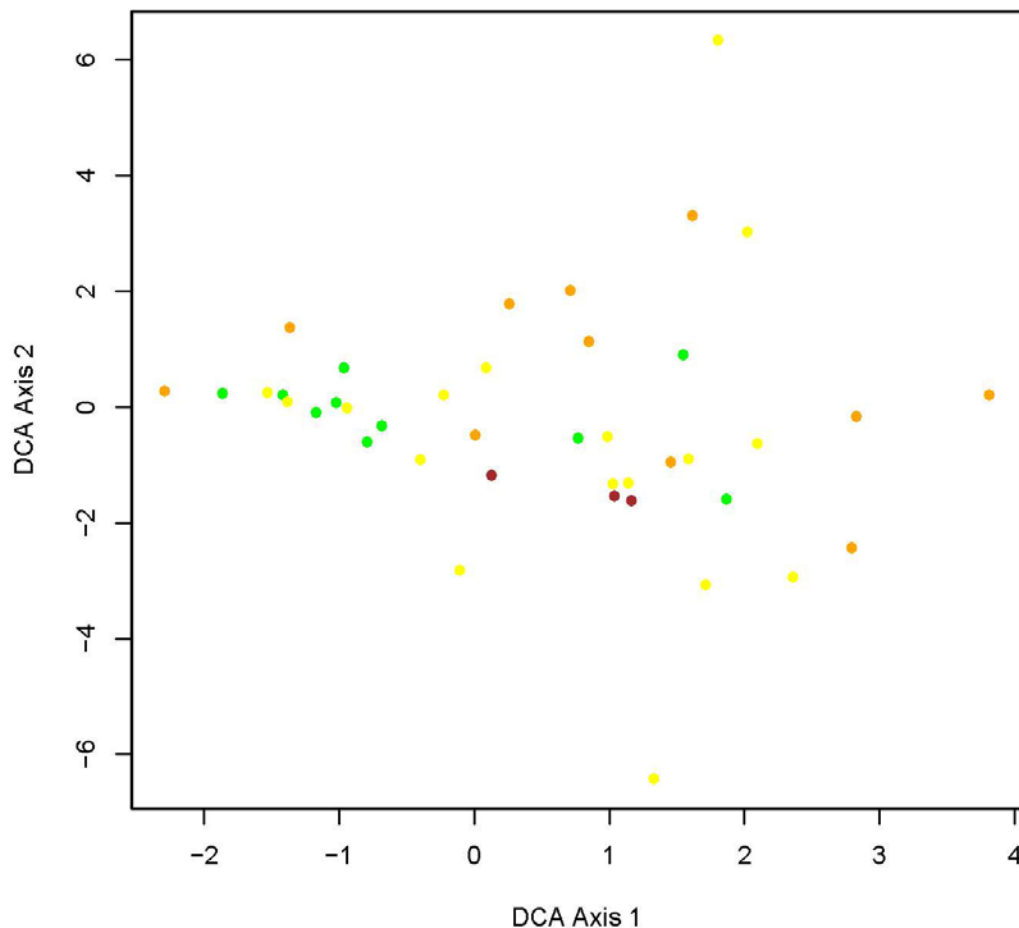
Appendix Fig6. Shrub pollen accumulation rates (grains cm⁻² yr⁻¹) at Dubh-Lochan. The summary data for each growth form are presented in colour while the data for the component taxa within the group are presented in black. Note that the y-axis values vary between graphs.

There were nine genera of trees at Dubh-Lochan (Appendix Fig7) although three genera - *Populus*, *Sorbus*, and *Tilia* - were not included in the graph due to insufficient quantities. The initial woodland was dominated by *Betula* and *Pinus*, as at Quidenham Mere. These populations were largely replaced by *Alnus* and *Quercus* around the mid-Holocene (~7,300 cal. yrs BP).



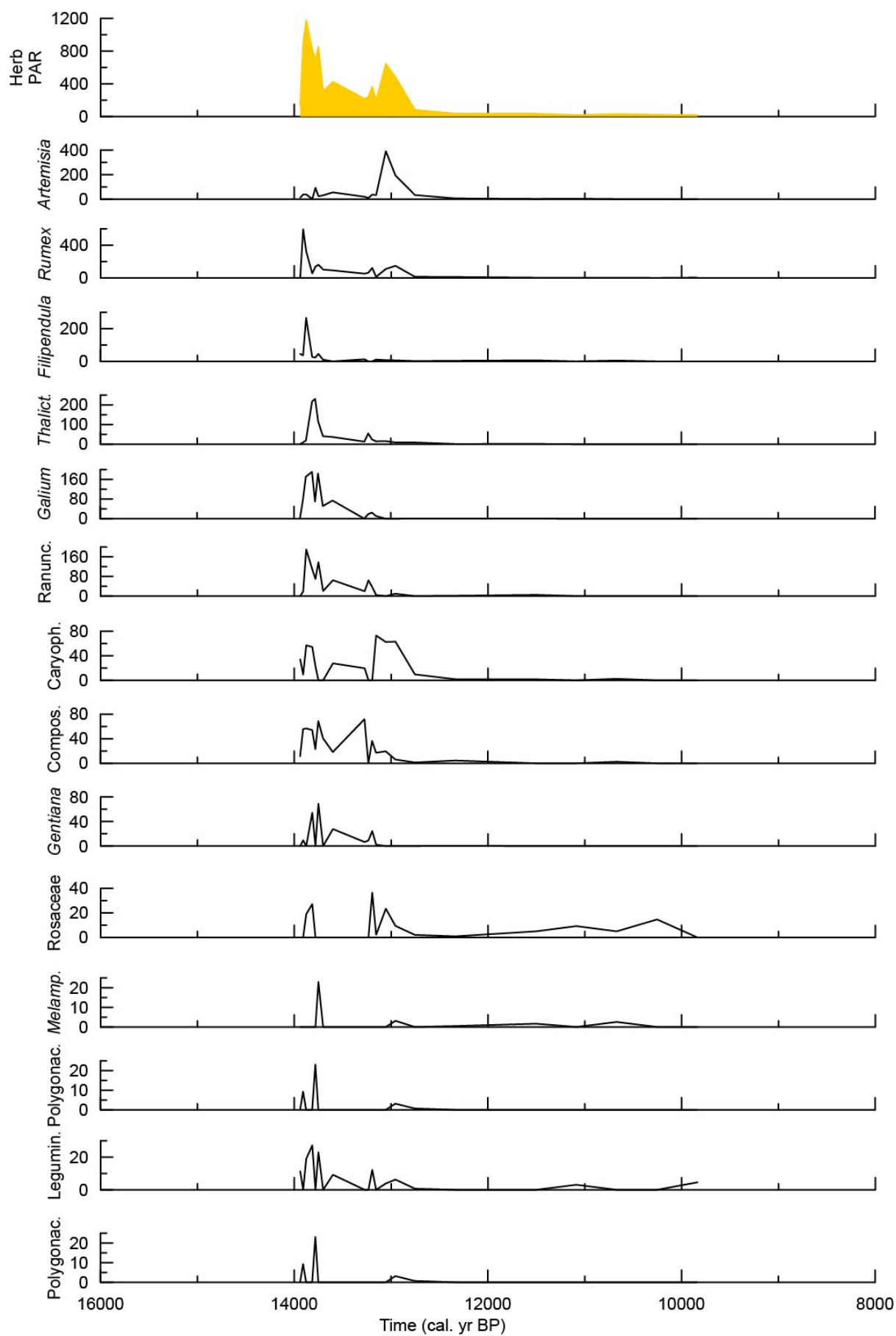
Appendix Fig 7. Tree pollen accumulation rates (grains cm⁻² yr⁻¹) at Dubh-Lochan. The summary data for each growth form are presented in colour while the data for the component taxa within the group are presented in black. Note that the y-axis values vary between graphs.

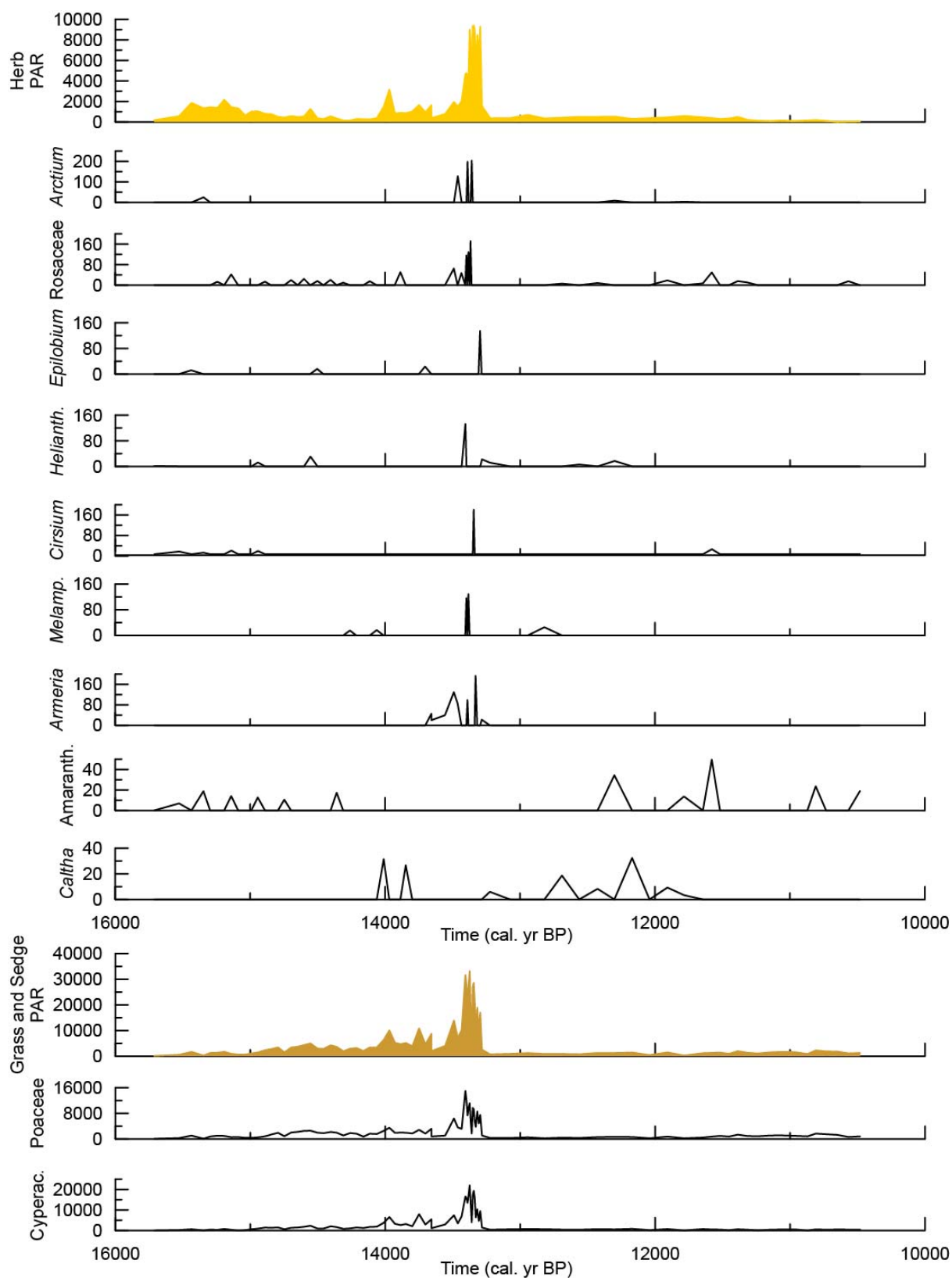
Detrended correspondence analysis of the plant taxonomic data at Dubh-Lochan shows overlap across the range of variation in herb, shrub and tree pollen influx (Appendix Fig8).



Appendix Fig8. Plot of species scores from detrended correspondence analysis of pollen accumulation rates for herbs (yellow), grass (brown), shrubs (orange) and trees (green) at Dubh Lochan.

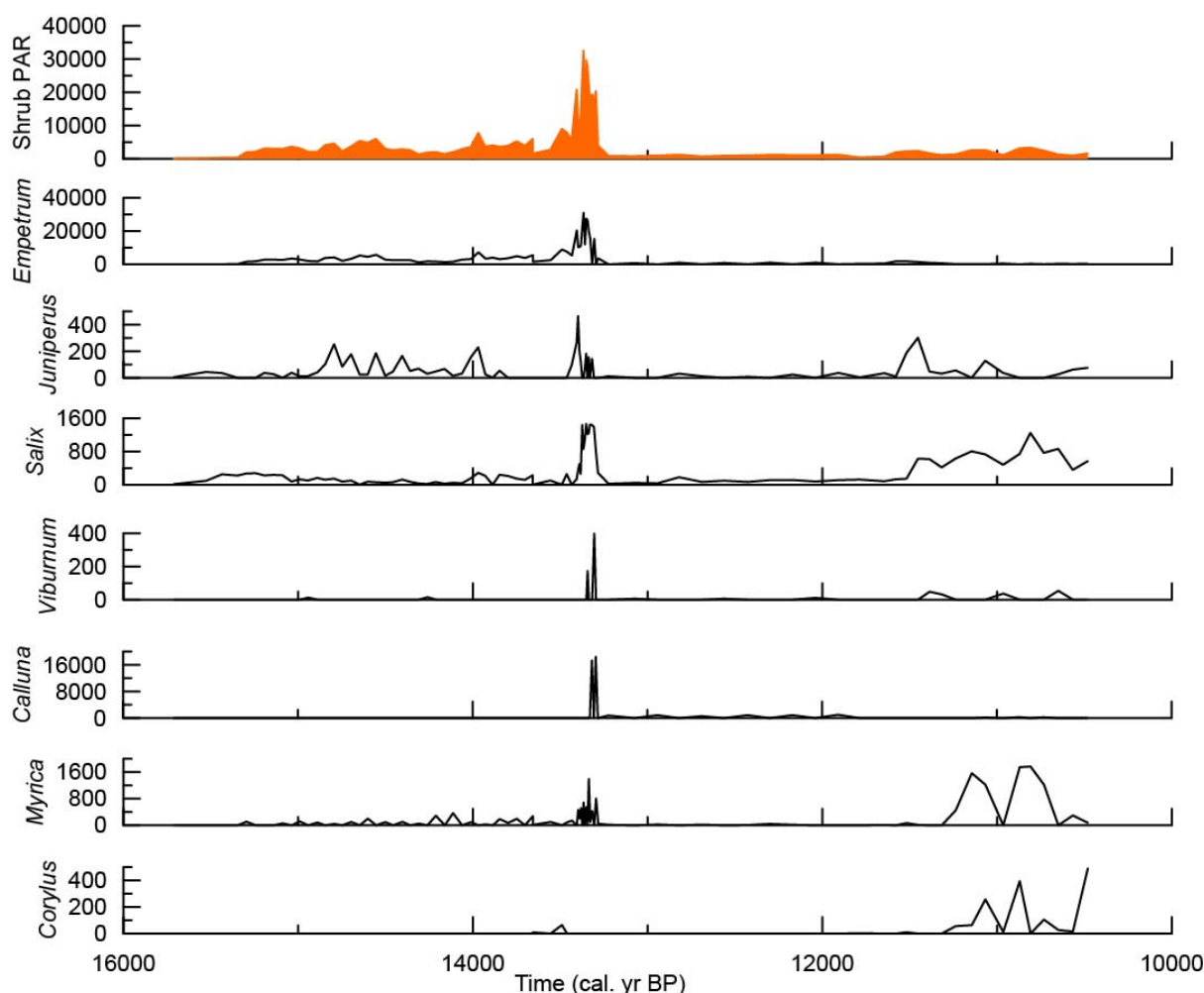
Lough Nadourcan. Lough Nadourcan, in the far north of Ireland, was an oligotrophic lake surrounded by blanket bog dominated by heathland plants at the Pleistocene – Holocene transition (Jeffers *et al.* 2012). Temperature dynamics in this part of Ireland were strongly influenced by the North Atlantic as indicated by strong similarities to patterns observed in Greenland during the Pleistocene – Holocene transition (Watson *et al.* 2010). Lough Nadourcan also had the most oceanic climate of all our study sites. Twenty-nine herb plant taxa are represented at Lough Nadourcan (Appendix Fig9) which were largely consistent with the dynamics of grasses and sedges. The six taxa not shown here include: *Brassicaceae*, *Centaurea*, *Dryas*, *Linum*, *Ononis*, and *Valeriana*. The initial rise in herb biomass was dominated by *Rumex*, *Plantago* and *Lamiaceae*. Peak values of herb biomass included these taxa as well as *Artemisia* and other *Compositae* taxa. All but a few herb taxa were present through the entire series.





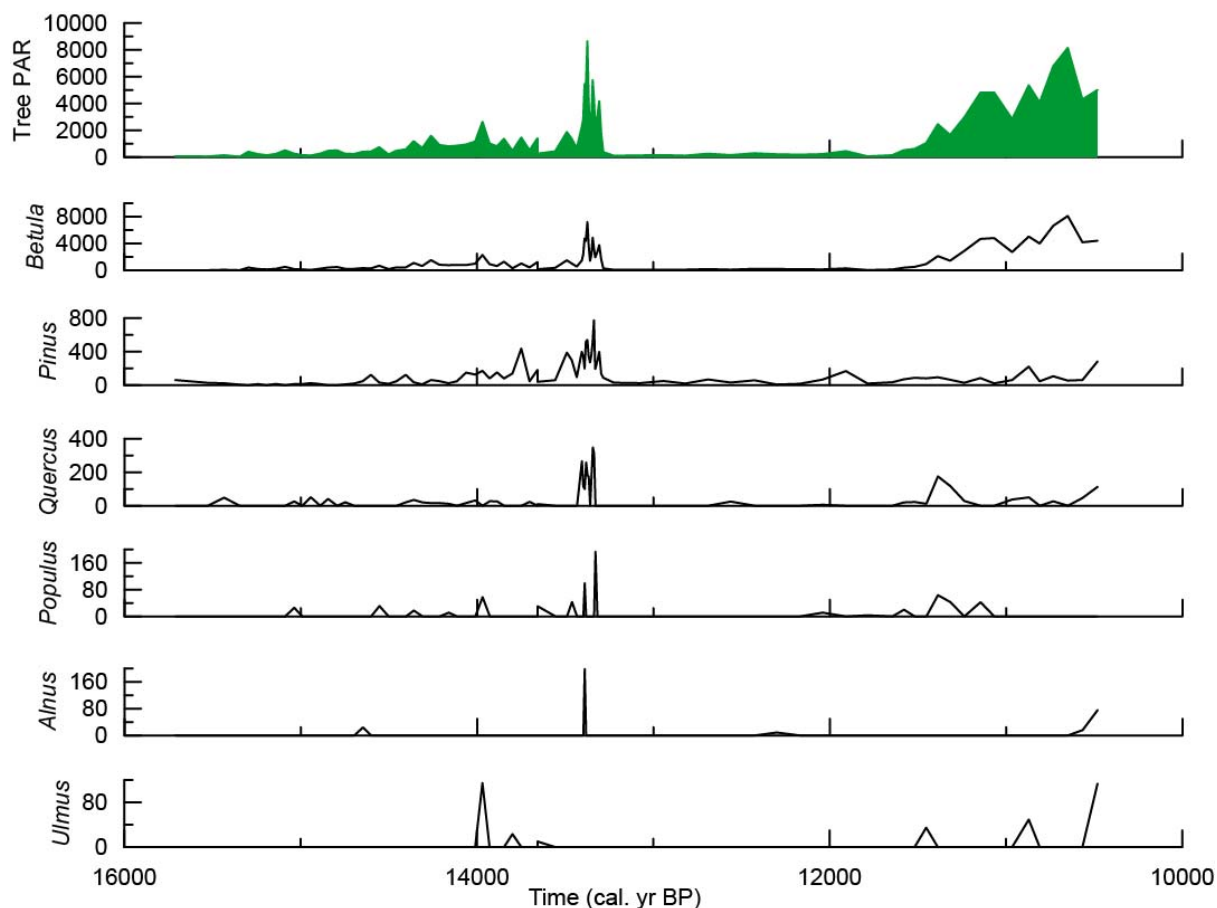
Appendix Fig9. Herb pollen accumulation rates (grains cm⁻² yr⁻¹) at Lough Nadourcan. The summary data for each growth form are presented in colour while the data for the component taxa within the group are presented in black. Note that the y-axis values vary between graphs.

There were nine shrub taxa at Lough Nadourcan (Appendix Fig10) although two of these were at insufficient quantities for plotting. Those not shown include: *Ephedra*, and *Hippophae*. *Empetrum* was the dominant shrub at Lough Nadourcan until the early Holocene when the Ericaceae shrubs were replaced by *Salix*, *Myrica* and *Corylus*.



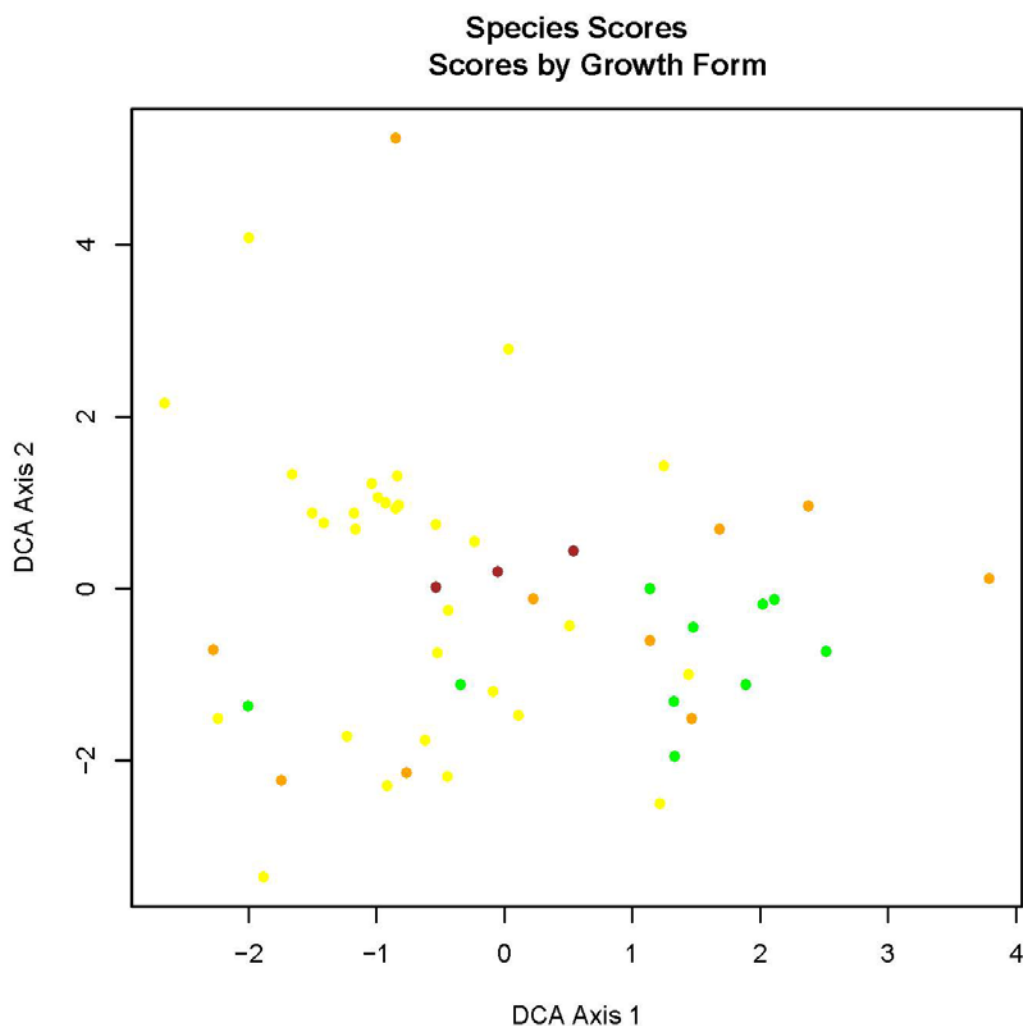
Appendix Fig10. Shrub pollen accumulation rates ($\text{grains cm}^{-2} \text{yr}^{-1}$) at Lough Nadourcan. The summary data for each growth form are presented in colour while the data for the component taxa within the group are presented in black. Note that the y-axis values vary between graphs.

Trees were present at low densities at Lough Nadourcan throughout the series, and only became dominant in the community in the early Holocene. There were nine genera of trees at Lough Nadourcan (Appendix Fig11) although three genera - *Abies*, *Carpinus* and *Fagus* - were not included in the graph due to insufficient quantities. *Betula* and (to a lesser extent) *Pinus* had the greatest densities of all genera.



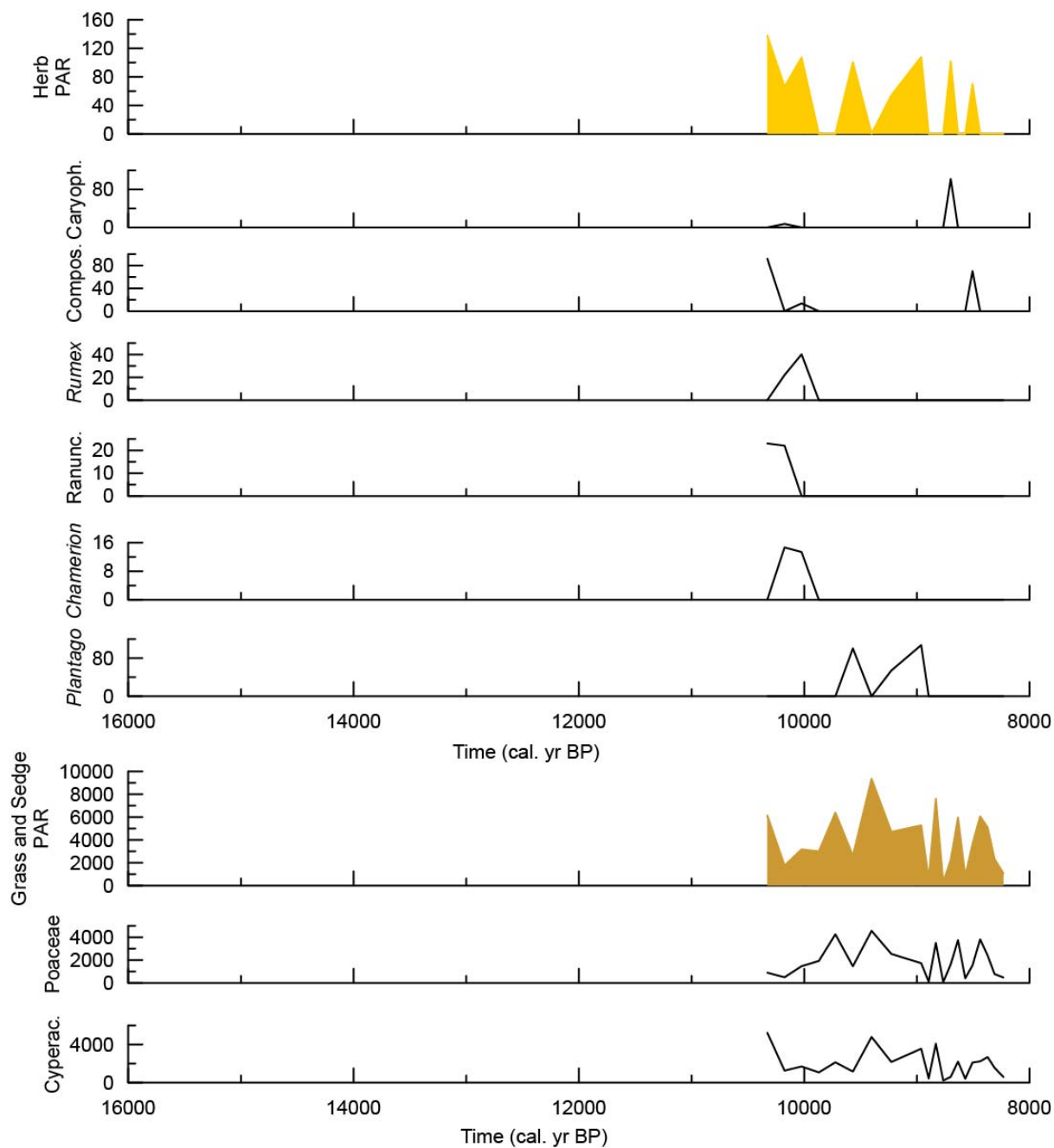
Appendix Fig11. Tree pollen accumulation rates ($\text{grains cm}^{-2} \text{yr}^{-1}$) at Lough Nadourcan. The summary data for each growth form are presented in colour while the data for the component taxa within the group are presented in black. Note that the y-axis values vary between graphs.

Detrended correspondence analysis of the individual plant taxa records at Lough Nadourcan show that herb pollen influx spans the breadth of the two primary axes of variation, while shrub and tree pollen influx have a relatively smaller range of variation (Appendix Fig12).



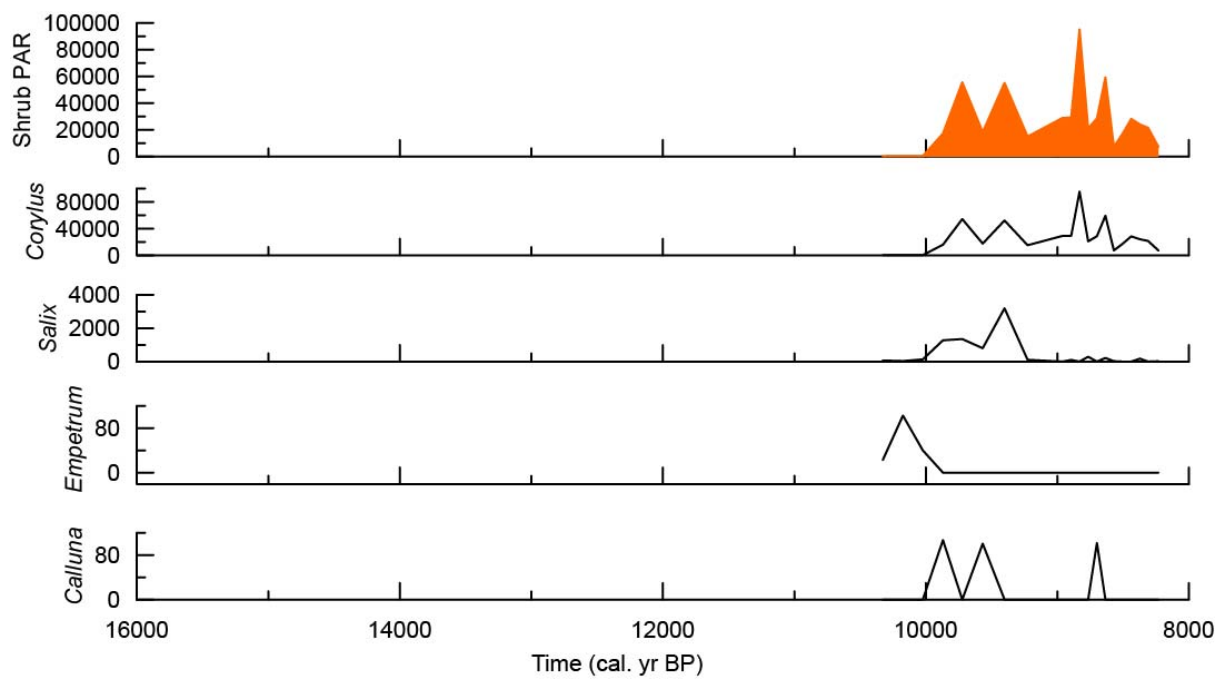
Appendix Fig12. Plot of species scores from detrended correspondence analysis of pollen accumulation rates for herbs (yellow), grass (brown), shrubs (orange) and trees (green) at Lough Nadourcan.

Ballynahatty. Ballynahatty is a fen peatland that was surrounded by grass and herbaceous plant taxa during the early Holocene period before deciduous shrubs and trees became established (Plunkett *et al.* 2008). Nine herb plant taxa are represented at Ballynahatty (Appendix Fig13), which were at much lower densities than the grasses and sedges. Three taxa were included in the summary herb pollen accumulation rate values but not shown here including: *Filipendula*, *Limonium*, and Rosaceae. The initial herb biomass peaks were primarily represented by Compositae, Ranunculaceae, *Rumex* and *Chamerion*. *Plantago* became the dominant herb taxon after the biomass of the initial taxa declined abruptly. Compositae and Caryophyllaceae were the remaining herb families represented in the final peaks in the series.



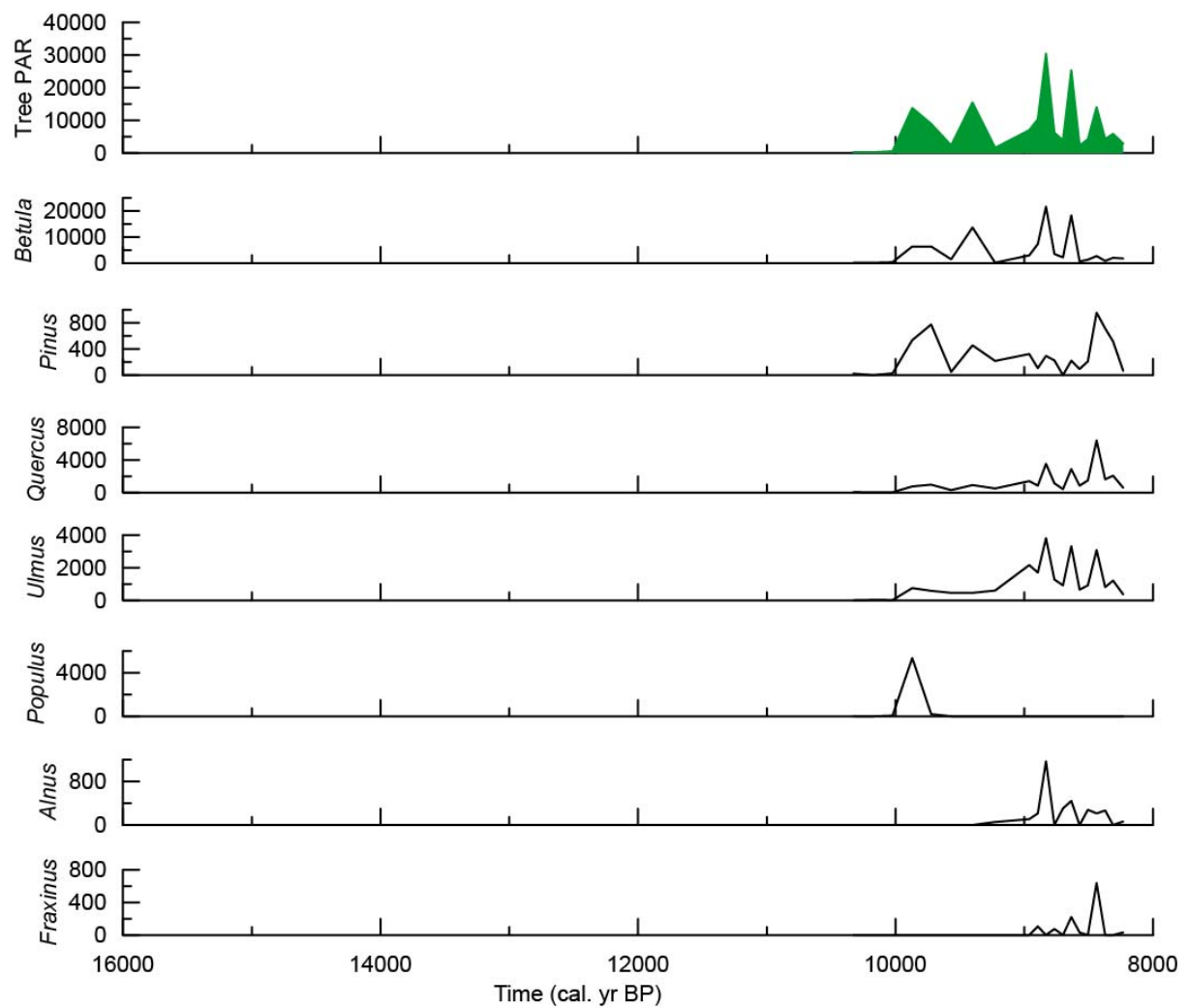
Appendix Fig13. Herb pollen accumulation rates (grains cm⁻² yr⁻¹) at Ballynahatty. The summary data for each growth form are presented in colour while the data for the component taxa within the group are presented in black. Note that the y-axis values vary between graphs.

There were six shrub taxa at Ballynahatty (Appendix Fig14) although two of these were at insufficient quantities for plotting. Those not shown include: *Hedera*, and *Juniperus*. *Corylus* was the dominant shrub genus at Ballynahatty throughout the series although *Empetrum*, *Calluna* and *Salix* also achieved relatively high densities early in the record.



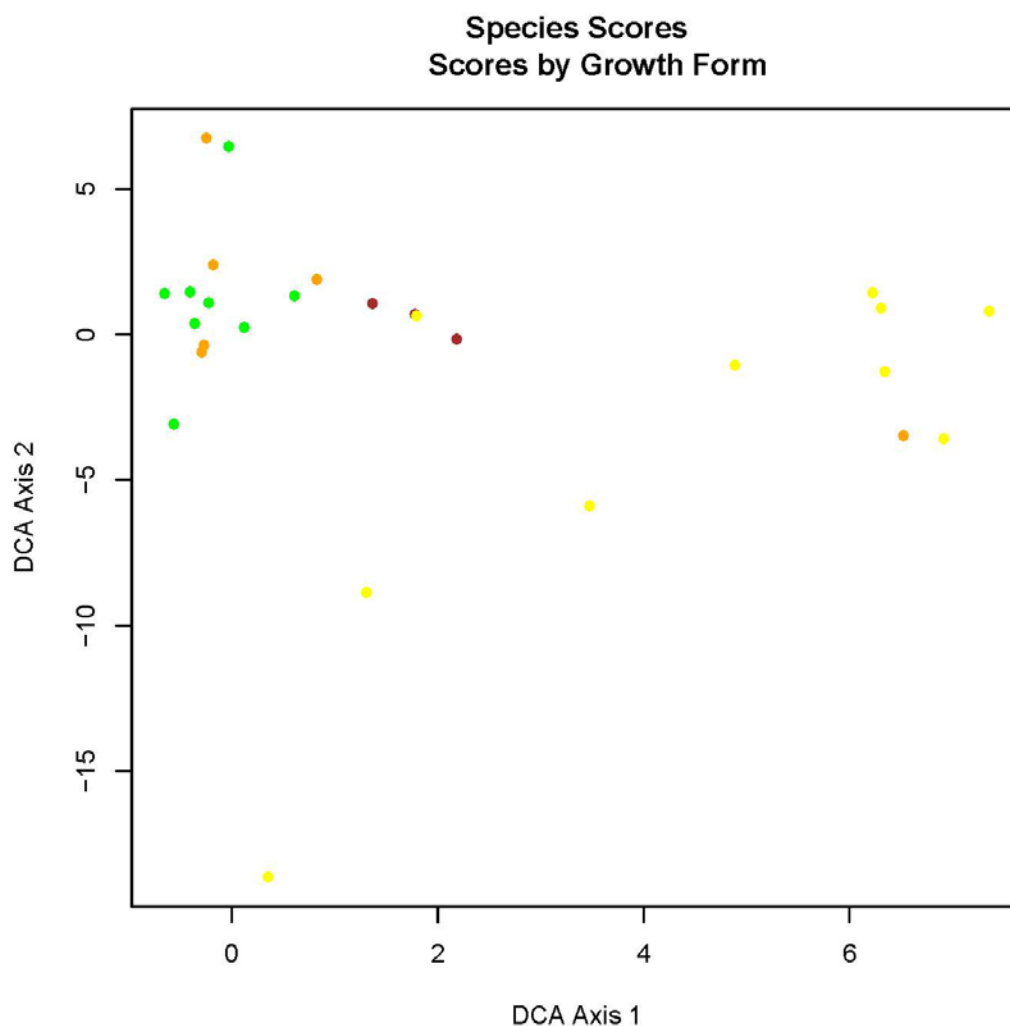
Appendix Fig14. Shrub pollen accumulation rates ($\text{grains cm}^{-2} \text{yr}^{-1}$) at Ballynahatty. The summary data for each growth form are presented in colour while the data for the component taxa within the group are presented in black. Note that the y-axis values vary between graphs.

There were seven genera of trees at Ballynahatty (Appendix Fig15). *Betula* was the dominant genera in the community throughout the series. *Quercus*, *Ulmus*, *Alnus* and *Fraxinus* biomass expanded after 9,000 cal. yrs BP.



Appendix Fig15. Tree pollen accumulation rates (grains cm⁻² yr⁻¹) at Ballynahatty. The summary data for each growth form are presented in colour while the data for the component taxa within the group are presented in black. Note that the y-axis values vary between graphs.

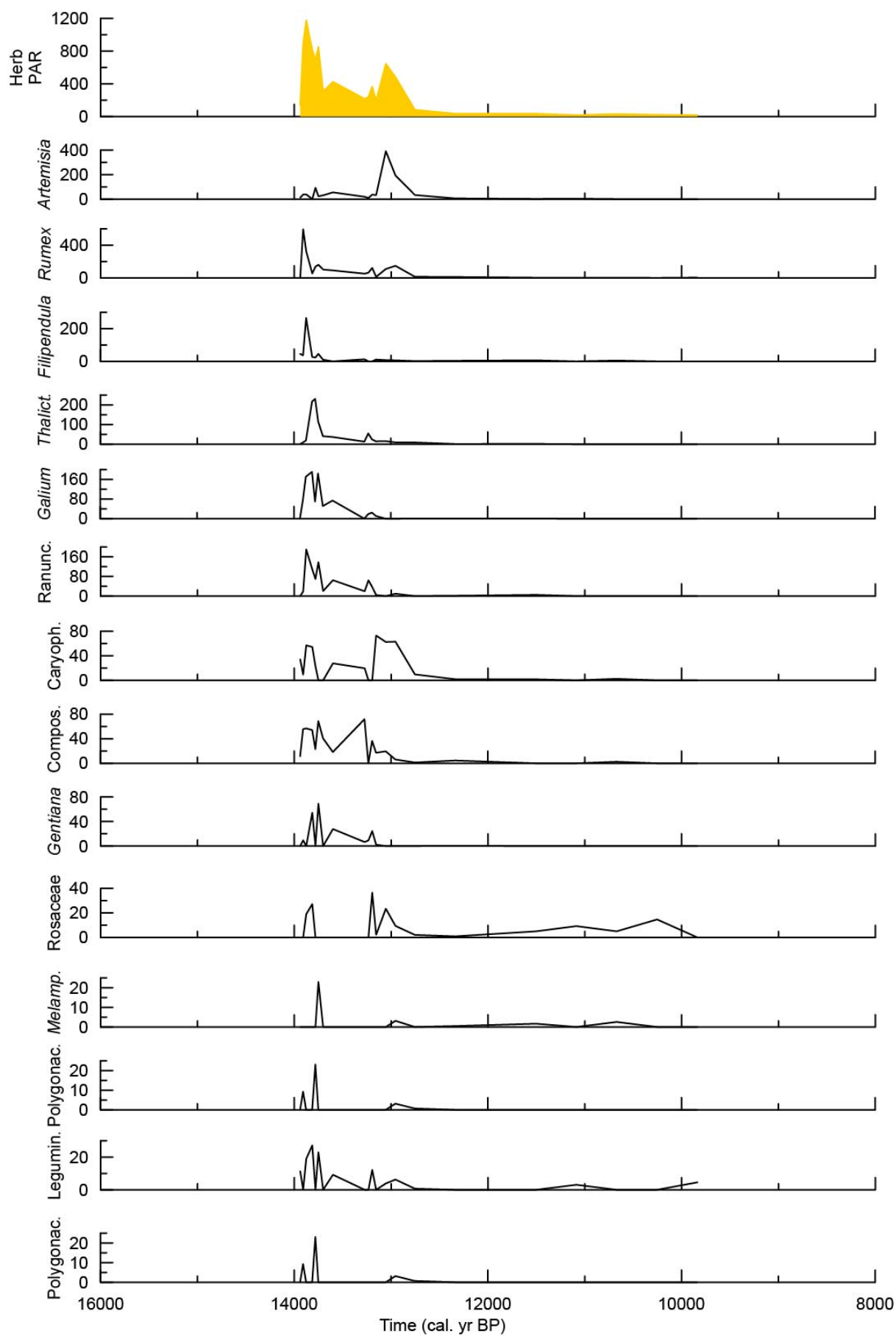
Detrended correspondence analysis of the individual plant taxa at Ballynahatty show a strong separation between herb pollen influx and shrub and tree influx (Appendix Fig16).

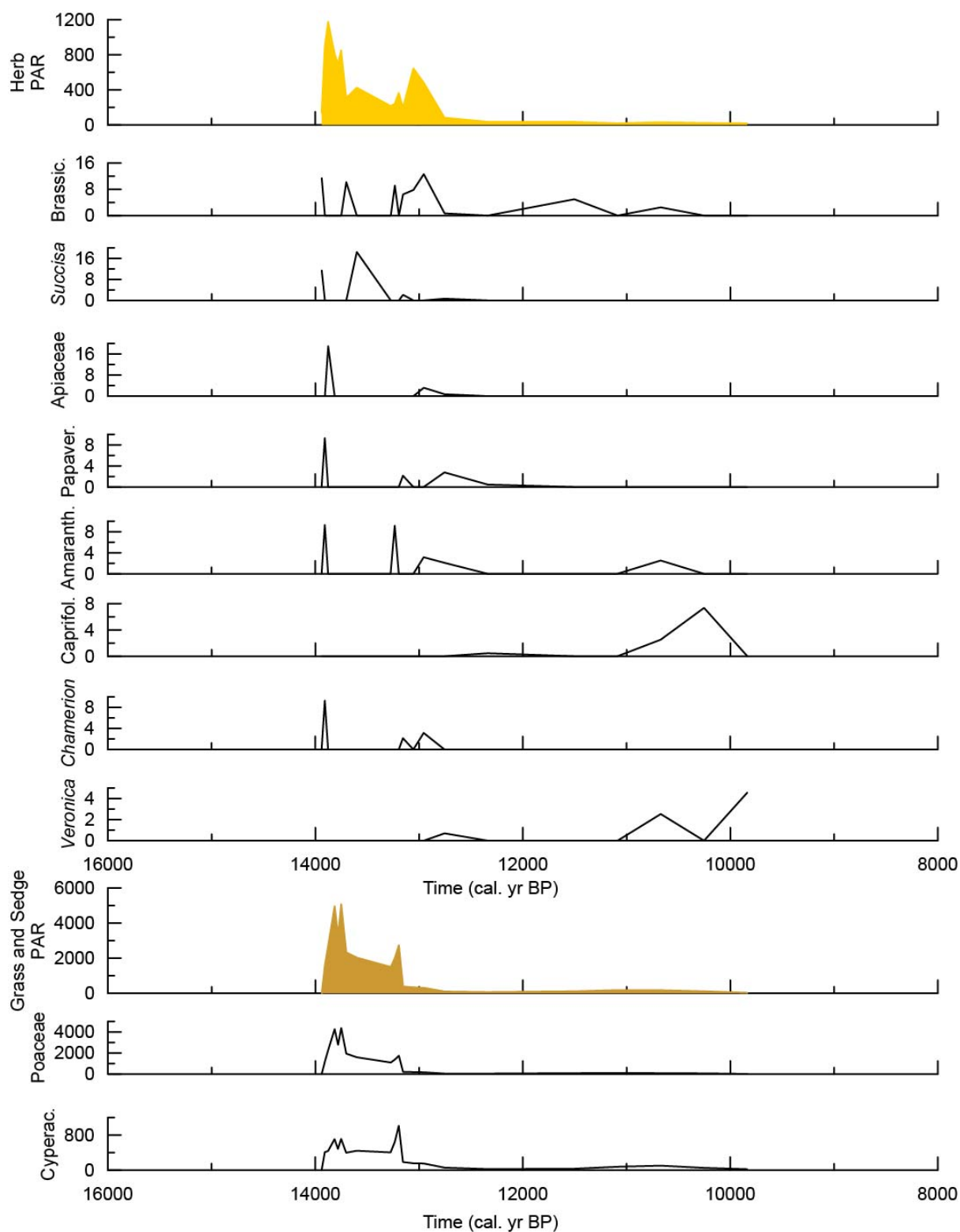


Appendix Fig16. Plot of species scores from detrended correspondence analysis of pollen accumulation rates for herbs (yellow), grass (brown), shrubs (orange) and trees (green) at Ballynahatty.

Long Lough. Long Lough is a small, inter-drumlin lake that comprised open water in the late glacial – early Holocene transition and was set within an area of open grassland until the arrival of woodland at the start of the Holocene. Twenty-seven herb plant taxa were represented at Long Lough (Appendix Fig17). Six taxa that were included in the summary herb pollen accumulation rate values but not shown here include: *Apiaceae*, *Armeria*, *Circea*, *Lamiaceae*, *Solanum*, and *Stachys*. The initial peak in herb biomass was dominated by *Rumex*, *Artemisia* and other *Compositae* taxa, as well as *Caryophyllaceae*; however all herb taxa were present throughout the record. The second peak also included *Ranunculaceae*, *Galium* and *Filipendula* (with other taxa at lower densities). Grasses and sedges were

relatively more abundant during the second peak (i.e. between 13,000 and 10,000 cal. yrs BP) than the first (14,000 to 13,200 cal. yrs BP).

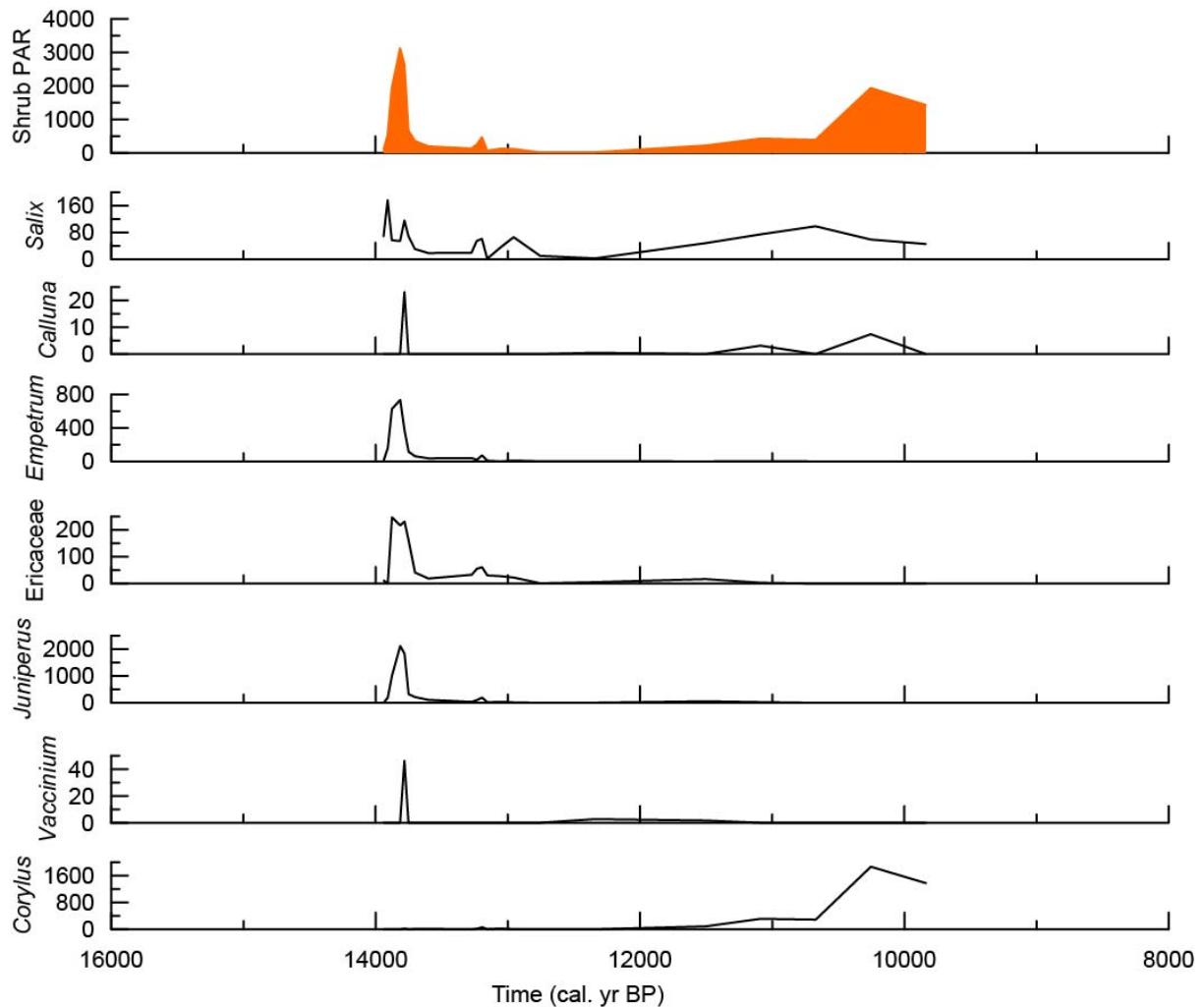




Appendix Fig17. Herb pollen accumulation rates (grains cm⁻² yr⁻¹) at Long Lough. The summary data for each growth form are presented in colour while the data for the component taxa within the group are presented in black. Note that the y-axis values vary between graphs.

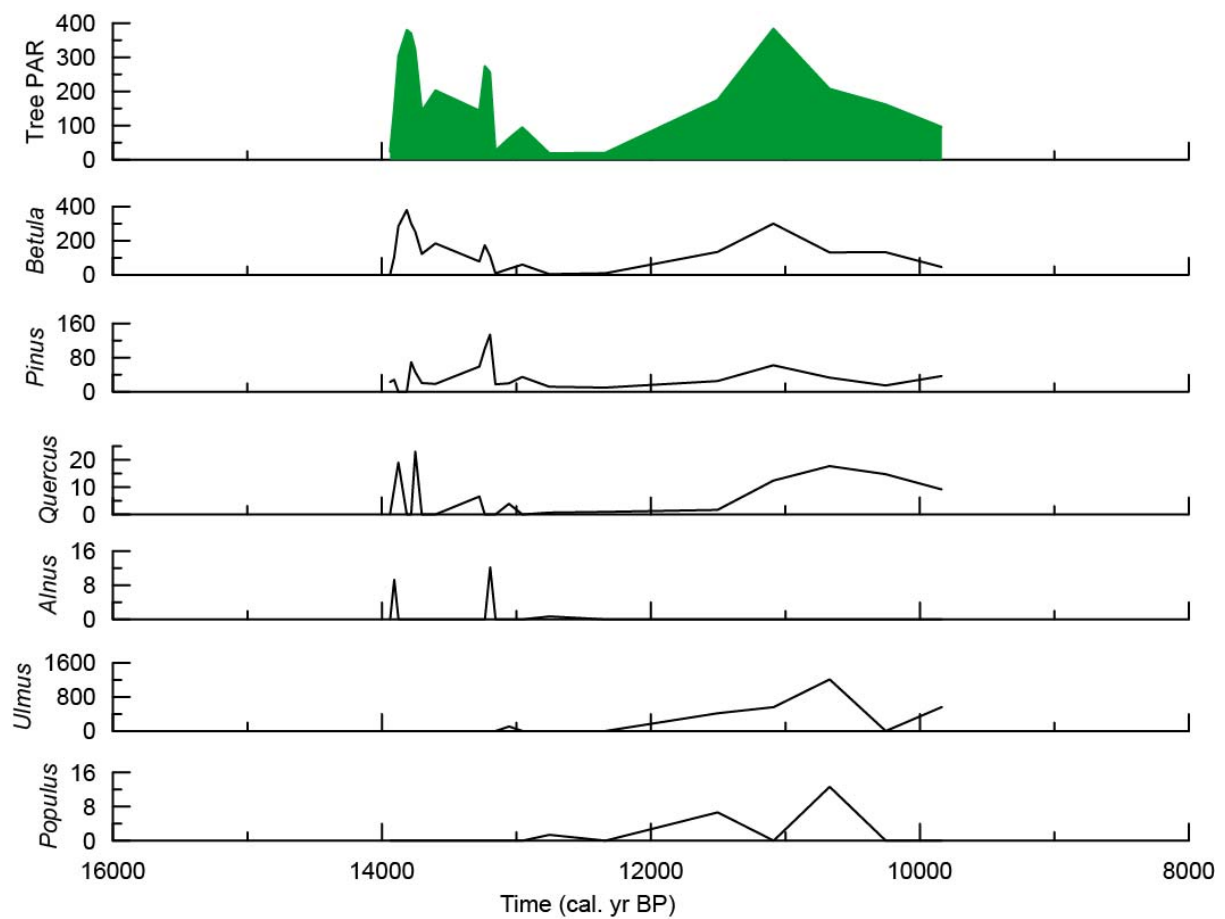
There were eight shrub taxa at Long Lough (Appendix Fig18); only *Hedera* is not shown due to insufficient quantities for plotting. *Corylus* was the dominant shrub taxon from the start of

the Long Lough series. *Juniperus* gradually increased alongside *Empetrum* and other Ericaceae taxa and *Salix* for the remainder of the record.



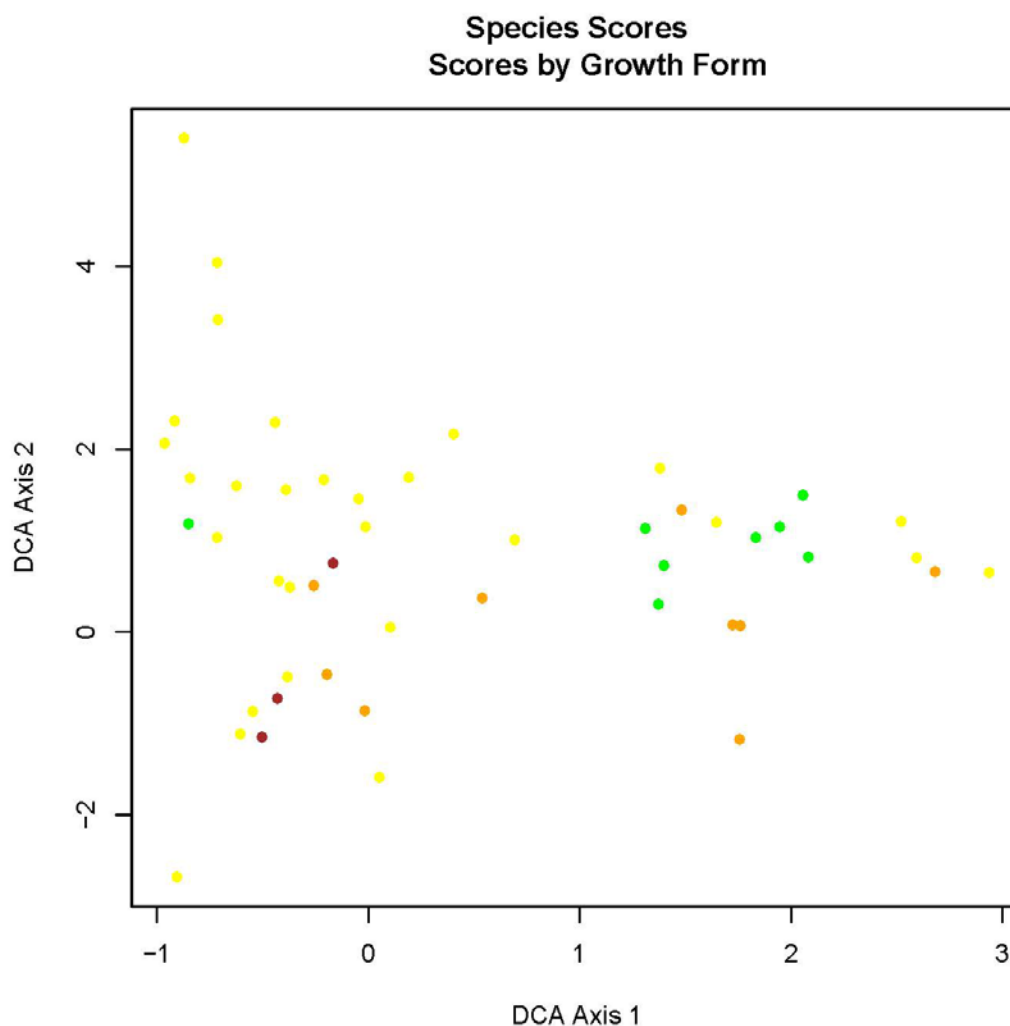
Appendix Fig18. Shrub pollen accumulation rates (grains cm⁻² yr⁻¹) at Long Lough. The summary data for each growth form are presented in colour while the data for the component taxa within the group are presented in black. Note that the y-axis values vary between graphs.

There were seven genera of trees at Long Lough (Appendix Fig19) and only *Taxus* was not included in the plot due to insufficient quantities. All tree genera were present throughout the series at Long Lough, although the densities were lower than for shrubs (Appendix Fig18).



Appendix Fig19. Tree pollen accumulation rates (grains cm⁻² yr⁻¹) at Long Lough. The summary data for each growth form are presented in colour while the data for the component taxa within the group are presented in black. Note that the y-axis values vary between graphs.

Detrended correspondence analysis of the individual plant taxa at Long Lough show that herb pollen influx spans the full extent of variation in the dataset, while shrub and tree influx is relatively more constrained (Appendix Fig20).



Appendix Fig20. Plot of species scores from detrended correspondence analysis of pollen accumulation rates for herbs (yellow), grass (brown), shrubs (orange) and trees (green) at Long Lough.

Appendix 1 References

- Brooks S.J. & Langdon P.G. (2014). Summer temperature gradients in northwest Europe during the Lateglacial to early Holocene transition (15–8 ka BP) inferred from chironomid assemblages. *Quaternary International*, 341, 80-90.
- Froyd C.A. (2002). Holocene pine (*Pinus sylvestris* L.) forest dynamics in the Scottish Highlands. In: *Selwyn College*. University of Cambridge Cambridge.
- Froyd C.A. & Bennett K.D. (2006). Long-term ecology of native pinewood communities in East Glen Affric, Scotland. *Forestry*, 79, 279-291.
- Jeffers E.S., Bonsall M.B., Brooks S.J. & Willis K.J. (2011). Abrupt environmental changes drive shifts in tree-grass interaction outcomes. *J. Ecol.*, 99, 1063-1070.

- Jeffers E.S., Bonsall M.B., Froyd C.A., Brooks S.J. & Willis K.J. (2015). The relative importance of biotic and abiotic processes for structuring plant communities through time. *J. Ecol.*, 103, 459-472.
- Jeffers E.S., Bonsall M.B., Watson J.E. & Willis K.J. (2012). Climate change impacts on ecosystem functioning: evidence from an *Empetrum* heathland. *New Phytologist*, 193, 150-164.
- Plunkett G., Carroll F., Hartwell B., Whitehouse N.J. & Reimer P.J. (2008). Vegetation history at the multi-period prehistoric complex at Ballynahatty, Co. Down, Northern Ireland. *Journal of Archaeological Science*, 35, 181-190.
- Watson J.E., Brooks S.J., Whitehouse N.J., Reimer P.J., Birks H.J.B. & Turney C. (2010). Chironomid-inferred late-glacial summer air temperatures from Lough Nadourcan, Co. Donegal, Ireland. *Journal of Quaternary Science*, 25, 1200-1210.

SUPPLEMENTARY INFORMATION

Plant controls on Late Quaternary whole ecosystem structure and function

E.S. Jeffers, N.J. Whitehouse, A. Lister, G. Plunkett, P. Barratt, E. Smyth, P. Lamb, M.W. Dee, S.J. Brooks, K.J. Willis, C.A. Froyd, J.E. Watson, M.B. Bonsall

Appendix 2 Sedimentary $\delta^{15}\text{N}$ as a proxy for nitrogen availability

Sedimentary $\delta^{15}\text{N}$ is an integrated indicator of the processes acting on reactive nitrogen across ecosystems via nitrogen isotope fractionation and mixing of the various nitrogen-containing pools (Robinson 2001). The occurrence of most transformations in the nitrogen cycle is determined by the balance between the amount (or availability) of reactive nitrogen supplied and the amount demanded by biota across the watershed, including processes within the lake (McLauchlan *et al.* 2013). This integrative interpretation of sedimentary $\delta^{15}\text{N}$ has been supported by empirical evidence that sedimentary $\delta^{15}\text{N}$ scales linearly with soil and foliar $\delta^{15}\text{N}$ and measures of nitrogen availability to plants in the catchment (McLauchlan *et al.* 2007), as well as mass balance models that suggest denitrification, a process that is strongly dependent on nitrogen availability, has the greatest fractionation effect on nitrogen molecules in soils (Houlton & Bai 2009).

Denitrification requires high concentrations of nitrate, organic carbon and a reduced environment (Groffman 2012). These conditions generally occur when the supply of reactive nitrogen is high relative to biotic demand. Denitrification preferentially transfers the light stable isotope of nitrogen (^{14}N) from the soil to the atmosphere, leaving the soil nitrogen pool relatively enriched (i.e. high values of soil $\delta^{15}\text{N}$). Therefore nitrogen input into lakes will be generally enriched in ^{15}N during times of relatively high rates of gaseous nitrogen loss from surrounding soils (Houlton & Bai 2009), and thus sedimentary $\delta^{15}\text{N}$ tracks long-term changes in nitrogen availability at the ecosystem scale (McLauchlan *et al.* 2013). Organisms alter the rate of nitrogen transformation in soils, and thus influence soil $\delta^{15}\text{N}$ values. There is very little fractionation during plant uptake of reactive nitrogen, particularly when soil nitrogen availability is low. Furthermore, there is generally little difference between root and leaf $\delta^{15}\text{N}$ values (Craine *et al.* 2015). Therefore, plant tissue $\delta^{15}\text{N}$ largely reflects the signature of

inorganic nitrogen available in the soil (Craine *et al.* 2015). Plants also influence soil $\delta^{15}\text{N}$ through uptake rates and preferences, since these factors will determine the likelihood of gaseous losses of the nitrogen molecules remaining in the soils (Craine *et al.* 2015).

In contrast, herbivores can contribute a relatively strong fractionation effect on nitrogen molecules through metabolic processes, conferring a fractionation effect of 3-5‰ on average relative to diet when the nitrogen is incorporated into animal tissues (Hogberg 1997). The decomposing bodies of large herbivores therefore provide surrounding soils with a pulse of nitrogen with relatively higher $\delta^{15}\text{N}$ values as compared with the plants they consumed (Hogberg 1997). Herbivores also influence $\delta^{15}\text{N}$ values in soils by redistributing nitrogen, creating sites of ammonia volatilization through urine deposition, thus leaving the residual soil N pool enriched in ^{15}N (ref. Hogberg 1997). Given these processes, we suggest that soil $\delta^{15}\text{N}$ values should be on average relatively higher in the presence of large herbivores as compared to times when they are absent. This should be recorded as relatively higher sediment $\delta^{15}\text{N}$ values in landscapes with abundant large herbivores as nitrogen molecules in soils are regularly transferred from the terrestrial environment into lakes through physical processes.

Appendix 2 References

- Craine J.M., Brookshire E.N.J., Cramer M.D., Hasselquist N.J., Koba K., Marin-Spiotta E. & Wang L. (2015). Ecological interpretations of nitrogen isotope ratios of terrestrial plants and soils. *Plant and Soil*, 396, 1-26.
- Groffman P.M. (2012). Terrestrial denitrification: challenges and opportunities. *Ecological Processes*, 1, 1-11.
- Hogberg P. (1997). Tansley Review No. 95 ^{15}N natural abundance in soil-plant systems. *New Phytologist*, 137, 179-203.
- Houlton B.Z. & Bai E. (2009). Imprint of denitrifying bacteria on the global terrestrial biosphere. *Proceedings of the National Academy of Sciences*, 106, 21713-21716.

- McLauchlan K.K., Craine J.M., Oswald W.W., Leavitt P.R. & Likens G.E. (2007). Changes in nitrogen cycling during the past century in a northern hardwood forest. *Proceedings of the National Academy of Sciences of the United States of America*, 104, 7466-7470.
- McLauchlan K.K., Williams J.J., Craine J.M. & Jeffers E.S. (2013). Changes in global nitrogen cycling during the Holocene epoch. *Nature*, 495, 352-355.
- Robinson D. (2001). $\delta^{15}\text{N}$ as an integrator of the nitrogen cycle. *Trends Ecol. Evol.*, 16, 153-162.

TableS5. Age determinations of sedimentary sequences. Radiocarbon dates were determined by accelerator mass spectrometry and are reported as conventional radiocarbon years BP (AD 1950). Dates were calibrated to calendar years at the 2 σ level and modelled in OxCal (version 4.2.3, Ramsey 1995). Model specifications are included in FileS5.

Site	Depth (cm)	14C Age (years BP)	Calendar Age, unmodelled (Cal. yr BP)	Calendar Age, modelled (Cal. yr BP)	Lab Identifier
Lough Nadourcan	822	12865 \pm 60	13656- 13201	13611- 13182	UB-7185
	806	12350 \pm 59	12786- 12151	12785- 12150	UB-7184
	797	10889 \pm 54	10922- 10741	10921- 10741	UB-7183
	782	10301 \pm 52	10438- 9886	10438- 9885	UB-7182
	768	12123 \pm 57	12196- 11839	12186- 11934	UB-7181
	760	12005 \pm 55	12081- 11788	12001- 11796	UBA-7975hm
	747	11648 \pm 57	11635- 11398	11644- 11511	UB-7180
	744	11639 \pm 55	11629- 11397	11608- 11475	UBA-7974hm
	734	11621 \pm 51	11616- 11386	11516- 11367	UBA-7973hm
	725	11636 \pm 56	11627- 11392	11627- 11391	UB-7179
	718	11512 \pm 49	11507- 11317	11452- 11308	UBA-7972hm
	708	11358 \pm 55	11354- 11139	11371- 11176	UB-7178
	690	10496 \pm 52	10657- 10190	10658- 10187	UB-7177
	686	10130 \pm 52	10076- 9459	10022- 9652	UB-7062
	684	10052 \pm 54	9971- 9363	9866- 9524	UB-7176
	674	9912 \pm 41	9647- 9274	9448- 9289	UBA-7978hm
	667	9706 \pm 41	9277- 8927	9260- 8865	UBA-7977hm
	665	9488 \pm 39	9120- 8641	9131- 8749	UBA-7979
	650	9122 \pm 41	8454- 8264	8461- 8266	UBA-7976hm
<i>Mean Resolution:</i>		61 years	<i>Median Resolution:</i>		52 years
Long Lough	473	12120 \pm 75	12218- 11818	12233- 11870	UBA-23722
	461	13047 \pm 70	13931- 13376	13932- 13376	UBA-23723
	455.5	12359 \pm 68	12844- 12144	12845- 12145	UBA-25212
	441	11920 \pm 52	12008- 11617	11791- 11606	UBA-23724
	425	11466 \pm 50	11486- 11246	11501- 11345	UBA-23725
	418	11273 \pm 53	11304- 11104	11304- 11103	UBA-23726
	408.2	11299 \pm 54	11319- 11118	11324- 11136	UBA-23727
	392	10873 \pm 50	10878- 10741	10842- 10737	UBA-23728
	387.5	10397 \pm 51	10572- 10108	10585- 10145	UBA-25213
	382	9835 \pm 66	9646- 9180	9654- 9218	UBA-25214
	379	9599 \pm 48	9207- 8807	9227- 8899	UBA-23729
	371	9346 \pm 41	8740- 8482	8731- 8474	UBA-23730
<i>Mean Resolution:</i>		205 years	<i>Median Resolution:</i>		100 years
Ballynahatty	384	9858 \pm 42	9401-9251	9383-9249	UBA-23731
	320.5	9249 \pm 57	8617-8312	8736- 8437	UBA-25215
	309	8831 \pm 56	8211-7745	8211- 7744	UBA-23732
	301	9463 \pm 41	9115-8627	9115- 8626	UBA-23733
	280.5	9653 \pm 45	9250- 8839	9250- 8838	UBA-25216
	250.5	8381 \pm 45	7543- 7342	7514- 7188	UBA-25217
	218.5	7428 \pm 44	6401- 6226	6393- 6224	UB-6604
	198.5	6523 \pm 42	5607- 5377	5612- 5391	UB-6605
	178	6036 \pm 20	4999- 4848	4998- 4853	UB-3885
	173.5	5962 \pm 40	4943- 4729	4908- 4740	UB-6603
	143.5	5009 \pm 41	3945- 3703	3940- 3706	UB-7121

Site	Depth (cm)	14C Age (years BP)	Calendar Age, unmodelled (Cal. yr BP)	Calendar Age, modelled (Cal. yr BP)	Lab Identifier
	128.5	4554 ± 38	3486- 3102	3497- 3121	UB-7120
	121.5	3482 ± 36	1897- 1693	1899- 1692	UB-7119
<i>Mean Resolution:</i>		110 years	<i>Median Resolution:</i>		67 years
Quidenham Mere	860	NA	14,125-13,925	14,105-13912	NA
	854	NA	14,005-13,805	14,013-13,820	NA
	837	10,927 ± 40	12,876-12,702	12,922-12,706	UB12013
	816	NA	12,765-12,565	12,750-12,565	NA
	764	NA	11,805-11,605	11,802-11,601	NA
	723	7376 ± 30	8,320-8,054	11,583-11,571	UB12015
<i>Mean Resolution:</i>		68 years	<i>Median Resolution:</i>		72 years
Dubh-Lochan	963	9715 ± 55	9294-8852	9293-9155	SRR 6581
	920	9330 ± 55	8751-8352	8712-8446	SRR 6580
	799	8105 ± 55	7310-6833	7312-6835	SRR 6579
	742	6800 ± 50	5776- 5623	5732- 5566	SRR 6578
	603	3550 ± 50	2024- 1751	2138- 1814	SRR 6577
	395	2075 ± 50	343-49	204- 53	SRR 6576
<i>Mean Resolution:</i>		334 years	<i>Median Resolution:</i>		261 years

S6 File. OxCal input to build chronologies for sedimentary sequences.

P_Sequence("Ballynahatty VI (v4)", 0.8, 2)

```
{
  Boundary("Bottom");
  R_Date("UBA-23731", 9858, 42)
  {
    z=384;
  };
  R_Date("UBA-25215", 9249, 57)
  {
    z=320.5;
  };
  R_Date("UBA-23732", 8831, 56)
  {
    outlier();
    color="red";
    z=309;
  };
  Boundary("sandy/silt- peat")
  {
    z=309;
  };
  R_Date("UBA-23733", 9463, 41)
  {
    outlier();
    color="red";
    z=301;
  };
  R_Date("UBA-25216", 9653, 45)
  {
    color="red";
    outlier();
    z=280.5;
  };
  R_Date("UBA-25217", 8381, 45)
  {
    z=250.5;
  };
  R_Date("UB-6604", 7428, 44)
  {
    z=218.5;
  };
  R_Date("UB-6605", 6523, 42)
  {
    z=198.5;
  };
  R_Date("UB-3885 Lairg A", 6036, 20)
  {
    z=178;
  };
  R_Date("UB-6603", 5962, 40)
  {
    z=173.5;
  };
};
```

```

R_Date("UB-7121", 5009, 41)
{
  z=143.5;
};
R_Date("UB-7120", 4554, 38)
{
  z=128.5;
};
R_Date("UB-7119", 3482, 36)
{
  outlier();
  color="red";
  z=121.5;
};
Boundary("Top");
};
P_Sequence("Dubh Lochan Version 2", 0.8, 1)
{
  Boundary("Bottom")
  {
  };
  R_Date("SRR 6581", 9715, 55)
  {
    z=963;
  };
  R_Date("SRR 6580", 9330, 55)
  {
    z=920;
  };
  R_Date("SRR 6579", 8105, 55)
  {
    outlier();
    color="red";
    z=799;
  };
  R_Date("SRR 6578", 6800, 50)
  {
    z=742;
  };
  Boundary("Detritus Mud")
  {
    z=636;
  };
  R_Date("SRR 6577", 3550, 50)
  {
    z=603;
  };
  R_Date("SRR 6576", 2075, 50)
  {
    z=395;
  };
  Boundary("top")
  {
  };
};

```



```

Plot()
{
  P_Sequence("Lough Nadourcan Humin", 0.8, 2)
  {
    Boundary("Bottom")
    {
      z=846;
    };
    R_Date("UB-7185 (c17)", 12865, 60)
    {
      z=822;
    };
    R_Date("UB-7184 (c17)", 12350, 59)
    {
      outlier();
      color="red";
      z=806;
    };
    R_Date("UB-7183 (c17)", 10889, 54)
    {
      outlier();
      color="red";
      z=797;
    };
    R_Date("UB-7182 (c17)", 10301, 52)
    {
      outlier();
      color="red";
      z=782;
    };
    R_Date("UB-7181 (c17)", 12123, 57)
    {
      z=768;
    };
    R_Date("UBA-7975hc (c17)", 11508, 52)
    {
      outlier();
      color="red";
      z=760;
    };
    R_Date("UBA-7975hm (c17)", 12005, 55)
    {
      z=760;
    };
    R_Date("UB-7180 (c17)", 11648, 57)
    {
      z=747;
    };
    R_Date("UBA-7974hc (c17)", 11062, 51)
    {
      outlier();
      color="red";
      z=744;
    };
    R_Date("UBA-7974hm (c17)", 11639, 55)
  }
}

```

```

{
  z=744;
};
Boundary("mud-rich mud")
{
  z=738;
};
R_Date("UBA-7973hc (c17)", 11204, 54)
{
  outlier();
  color="red";
  z=734;
};
R_Date("UBA-7973hm (c17)", 11621, 51)
{
  z=734;
};
R_Date("UB-7179 (c17)", 11636, 56)
{
  outlier();
  color="red";
  z=725;
};
R_Date("UBA-7972hc (c17)", 11187, 50)
{
  outlier();
  color="red";
  z=718;
};
R_Date("UBA-7972hm (c17)", 11512, 49)
{
  z=718;
};
Boundary("clay-mud")
{
  z=708.5;
};
R_Date("UB-7178 (c17)", 11358, 55)
{
  z=708;
};
R_Date("UB-7177 (c17)", 10496, 52)
{
  outlier();
  color="red";
  z=690;
};
R_Date("UB-7062 (c15)", 10130, 52)
{
  z=686;
};
Boundary("mud-clay")
{
  z=685;
};

```

```

R_Date("UB-7176 (c17)", 10052, 54)
{
  z=684;
};
R_Date("UBA-7978hc (c22)", 9689, 56)
{
  outlier();
  color="red";
  z=674;
};
R_Date("UBA-7978hm (c22)", 9912, 41)
{
  z=674;
};
R_Date("UBA-7977hc (c22)", 9233, 39)
{
  outlier();
  color="red";
  z=667;
};
R_Date("UBA-7977hm (c22)", 9706, 41)
{
  z=667;
};
R_Date("UBA-7979 (c15)", 9488, 39)
{
  z=665;
};
R_Date("UBA-7976hc (c22)", 8878, 39)
{
  outlier();
  color="red";
  z=650;
};
R_Date("UBA-7976hm (c22)", 9122, 41)
{
  z=650;
};
Boundary("Top")
{
};
};
P_Sequence("Long Lough version 4", 0.8, 2)
{
  Boundary("Bottom")
  {
  };
  R_Date("UBA-23722", 12120, 75)
  {
    z=473;
  };
  R_Date("UBA-23723", 13047, 70)
  {
    color="red";
  };
};

```

```
outlier();
z=461;
};
R_Date("UBA-25212", 12359, 68)
{
  color="red";
  outlier();
  z=455.5;
};
R_Date("UBA-23724", 11920, 52)
{
  z=441;
};
R_Date("UBA-23725", 11466, 50)
{
  z=425;
};
R_Date("UBA-23726", 11273, 53)
{
  outlier();
  color="red";
  z=418;
};
R_Date("UBA-23727", 11299, 54)
{
  z=408.2;
};
Boundary("clay-mud")
{
  z=408;
};
R_Date("UBA-23728", 10873, 50)
{
  z=392;
};
R_Date("UBA-25213", 10397, 51)
{
  z=387.5;
};
Boundary("clay-mud2")
{
  z=384;
};
R_Date("UBA-25214", 9835, 66)
{
  z=382;
};
R_Date("UBA-23729", 9599, 48)
{
  z=379;
};
R_Date("UBA-23730", 9346, 41)
{
  z=371;
};
```

```

Boundary("Top")
{
};
};
Plot("Quidenham Model 6")
{
  Outlier_Model("General",T(5),U(0,4),"t");
  P_Sequence("",0.4,1,U(-2,2))
  {
    Boundary("Bottom")
    {
      z=872;
    };
    Date("CM860", N(AD(2005)-14080,50))
    {
      z=860;
    };
    Date("CM854", N(AD(2005)-13960,50))
    {
      z=854;
    };
    R_Date("UB12013",10927,40)
    {
      Outlier(0.05);
      z=837;
    };
    Date("CM816", N(AD(2005)-12720,50))
    {
      z=816;
    };
    Date("CM764", N(AD(2005)-11760,50))
    {
      z=764;
    };
    R_Date("UB12015",7376,30)
    {
      Outlier(0.05);
      z=723;
    };
    Boundary("Top")
    {
      z=716;
    };
  };
};
};

```

S7 File. OxCal input to build chronologies for fossil bones.

```
Plot("England, Scotland & Ireland Fauna")
{
  Sequence("Alces alces Eng")
  {
    Boundary("Start Alces alces England");
    Phase("Alces alces England")
    {
      R_Date("OxA-11151", 11660, 60)
      {
        color="989898";
        latitude=53.847;
        longitude=-2.995;
      };
      R_Date("OxA-13075", 11715, 50)
      {
        color="989898";
        latitude=53.847;
        longitude=-2.995;
      };
      Sum("Alces alces England Sum (2)")
      {
        color="989898";
      };
    };
    Boundary("End Alces alces England");
  };
  Sequence("Bos primigenius Eng")
  {
    Boundary("Start Bos primigenius England");
    Phase("Bos primigenius England")
    {
      R_Date("OxA-3919", 8145, 90)
      {
        color="9999FF";
        latitude=51.521;
        longitude=-1.116;
      };
      R_Date("OxA-813", 11900, 140)
      {
        color="9999FF";
        latitude=51.282;
        longitude=-2.766;
      };
      R_Date("OxA-1203", 11880, 120)
      {
        color="9999FF";
        latitude=50.469;
        longitude=-3.503;
      };
      R_Date("OxA-7994", 12430, 80)
      {
        color="9999FF";
        latitude=50.469;
```

```

    longitude= -3.503;
};
R_Date("OxA-16339", 11555, 50)
{
    color="9999FF";
    latitude=54.087;
    longitude=-2.300;
};
R_Date("OxA-8095", 10775, 75)
{
    color="9999FF";
    latitude=54.124;
    longitude=-2.368;
};
R_Date("OxA-4495", 5010, 70)
{
    color="9999FF";
    latitude=50.494;
    longitude=-3.672;
};
R_Date("OxA-4493", 5060, 70)
{
    color="9999FF";
    latitude=50.494;
    longitude=-3.672;
};
R_Date("OxA-12143", 11600, 45)
{
    color="9999FF";
    latitude=54.128;
    longitude=-2.264;
};
Sum("Bos Primi England Sum (9)")
{
    color="9999FF";
};
};
Boundary("End Bos primigenius England");
};
Sequence("Cervus elaphus Eng")
{
    Boundary("Start Cervus elaphus England");
    Phase("Cervus elaphus England")
    {
        R_Date("OxA-1121", 12380, 130)
        {
            color="04B404";
            latitude=51.326;
            longitude=-2.754;
        };
        R_Date("OxA-17722", 12565, 50)
        {
            color="04B404";
            latitude=51.325;
            longitude=-2.754;
        };
    };
};

```

```
};
R_Date("OxA-801", 12100, 180)
{
  color="04B404";
  latitude=51.326;
  longitude=-2.754;
};
R_Date("OxA-17830", 10150, 40)
{
  color="04B404";
  latitude=51.287;
  longitude=-2.771;
};
R_Date("OxA-1783", 10910, 110)
{
  color="04B404";
  latitude=51.267;
  longitude=-2.739;
};
R_Date("OxA-811", 10600, 110)
{
  color="04B404";
  latitude=53.091;
  longitude=-1.860;
};
R_Date("OxA-18067", 12245, 55)
{
  color="04B404";
  latitude=51.282;
  longitude=-2.766;
};
R_Date("OxA-17845", 12500, 50)
{
  color="04B404";
  latitude=51.282;
  longitude=-2.766;
};
R_Date("OxA-16378", 12515, 50)
{
  color="04B404";
  latitude=51.282;
  longitude=-2.766;
};
R_Date("OxA-466", 12800, 170)
{
  color="04B404";
  latitude=51.282;
  longitude=-2.766;
};
R_Date("OxA-3412", 12490, 120)
{
  color="04B404";
  latitude=51.282;
  longitude=-2.765;
};
```



```
R_Date("OxA-6728", 10460, 90)
{
  color="04B404";
  latitude=51.227;
  longitude=-2.677;
};
R_Date("OxA-5700", 11320, 120)
{
  color="04B404";
  latitude=51.229;
  longitude=-2.672;
};
R_Date("OxA-1562", 12120, 120)
{
  color="04B404";
  latitude=51.835;
  longitude=-2.659;
};
R_Date("OxA-1563", 12210, 120)
{
  color="04B404";
  latitude=51.835;
  longitude=-2.659;
};
R_Date("OxA-6844", 12250, 100)
{
  color="04B404";
  latitude=51.838;
  longitude=-2.665;
};
R_Date("OxA-15215", 12310, 50)
{
  color="04B404";
  latitude=53.100;
  longitude=-1.860;
};
R_Date("OxA-5796", 12070, 90)
{
  color="04B404";
  latitude=50.596;
  longitude=-3.604;
};
R_Date("OxA-10808", 9505, 60)
{
  color="04B404";
  latitude=54.214;
  longitude=-0.423;
};
R_Date("OxA-10809", 9530, 55)
{
  color="04B404";
  latitude=54.214;
  longitude=-0.423;
};
R_Date("OxA-4578", 9590, 90)
```

```

{
  color="04B404";
  latitude=54.214;
  longitude=-0.423;
};
R_Date("OxA-4577", 9670, 100)
{
  color="04B404";
  latitude=54.214;
  longitude=-0.423;
};
R_Date("OxA-5191", 9510, 90)
{
  color="04B404";
  latitude=51.405;
  longitude=-1.265;
};
R_Date("OxA-4492", 6210, 75)
{
  color="04B404";
  latitude=50.494;
  longitude=-3.672;
};
R_Date("OxA-4491", 6330, 75)
{
  color="04B404";
  latitude=50.494;
  longitude=-3.672;
};
R_Date("OxA-4478", 10020, 80)
{
  color="04B404";
  latitude=50.494;
  longitude=-3.672;
};
R_Date("OxA-3891", 11980, 100)
{
  color="04B404";
  latitude=50.494;
  longitude=-3.672;
};
Sum("Cervus elaphus England Sum (27)")
{
  color="04B404";
};
};
Boundary("End Cervus elaphus England");
};
Sequence("Equus ferus Eng")
{
  Boundary("Start Equus ferus England");
  Phase("Equus ferus England")
  {
    R_Date("OxA-6671", 10220, 90)
    {

```

```
color="A901DB";
latitude=51.325;
longitude=-2.754;
};
R_Date("OxA-6632",10810,75)
{
color="A901DB";
latitude=51.235;
longitude=-2.681;
};
R_Date("OxA-1785",10370,110)
{
color="A901DB";
latitude=51.287;
longitude=-2.771;
};
R_Date("OxA-6637",10665,65)
{
color="A901DB";
latitude=51.287;
longitude=-2.771;
};
R_Date("OxA-5698",12280,110)
{
color="A901DB";
latitude=53.261;
longitude=-1.198;
};
R_Date("OxA-6327",11630,100)
{
color="A901DB";
latitude=53.355;
longitude=-1.219;
};
R_Date("OxA-6326",11800,100)
{
color="A901DB";
latitude=53.355;
longitude=-1.219;
};
R_Date("OxA-6329",9160,80)
{
color="A901DB";
latitude=53.442;
longitude=-2.382;
};
R_Date("OxA-6318",10090,90)
{
color="A901DB";
latitude=53.442;
longitude=-2.382;
};
R_Date("OxA-6319",10150,80)
{
color="A901DB";
```

```
latitude=53.442;
longitude=-2.382;
};
R_Date("OxA-6328",10150,90)
{
  color="A901DB";
  latitude=53.442;
  longitude=-2.382;
};
R_Date("OxA-6313",10770,90)
{
  color="A901DB";
  latitude=53.193;
  longitude=-1.854;
};
R_Date("OxA-6312",10980,100)
{
  color="A901DB";
  latitude=53.193;
  longitude=-1.854;
};
R_Date("OxA-6310",11920,130)
{
  color="A901DB";
  latitude=53.193;
  longitude=-1.854;
};
R_Date("OxA-6311",12030,90)
{
  color="A901DB";
  latitude=53.193;
  longitude=-1.854;
};
R_Date("BM-2185R",12200,250)
{
  color="A901DB";
  latitude=51.282;
  longitude=-2.766;
};
R_Date("BM-2184R",12250,160)
{
  color="A901DB";
  latitude=51.282;
  longitude=-2.766;
};
R_Date("OxA-591",12260,160)
{
  color="A901DB";
  latitude=51.282;
  longitude=-2.766;
};
R_Date("BM-2187R",12300,200)
{
  color="A901DB";
  latitude=51.282;
```

```
longitude=-2.766;
};
R_Date("OxA-589",12340,150)
{
  color="A901DB";
  latitude=51.282;
  longitude=-2.766;
};
R_Date("BM-2183R",12350,160)
{
  color="A901DB";
  latitude=51.282;
  longitude=-2.766;
};
R_Date("OxA-465",12360,170)
{
  color="A901DB";
  latitude=51.282;
  longitude=-2.766;
};
R_Date("OxA-590",12370,150)
{
  color="A901DB";
  latitude=51.282;
  longitude=-2.766;
};
R_Date("BM-2188R",12380,230)
{
  color="A901DB";
  latitude=51.282;
  longitude=-2.766;
};
R_Date("OxA-3452",12400,110)
{
  color="A901DB";
  latitude=51.282;
  longitude=-2.766;
};
R_Date("OxA-17832",12415,50)
{
  color="A901DB";
  latitude=51.282;
  longitude=-2.766;
};
R_Date("BM-2186R",12470,240)
{
  color="A901DB";
  latitude=51.282;
  longitude=-2.766;
};
R_Date("OxA-464",12470,160)
{
  color="A901DB";
  latitude=51.282;
  longitude=-2.766;
```

```
};  
R_Date("OxA-18065",12490,55)  
{  
  color="A901DB";  
  latitude=51.282;  
  longitude=-2.766;  
};  
R_Date("OxA-12104",12495,50)  
{  
  color="A901DB";  
  latitude=51.282;  
  longitude=-2.766;  
};  
R_Date("OxA-592",12500,160)  
{  
  color="A901DB";  
  latitude=51.282;  
  longitude=-2.766;  
};  
R_Date("OxA-18068",12520,55)  
{  
  color="A901DB";  
  latitude=51.282;  
  longitude=-2.766;  
};  
R_Date("OxA-17833",12570,45)  
{  
  color="A901DB";  
  latitude=51.282;  
  longitude=-2.766;  
};  
R_Date("OxA-16292",12585,55)  
{  
  color="A901DB";  
  latitude=51.282;  
  longitude=-2.766;  
};  
R_Date("OxA-4106",12670,120)  
{  
  color="A901DB";  
  latitude=51.282;  
  longitude=-2.766;  
};  
R_Date("OxA-3413",12940,140)  
{  
  color="A901DB";  
  latitude=51.282;  
  longitude=-2.766;  
};  
R_Date("OxA-11241",12710,90)  
{  
  color="A901DB";  
  latitude=51.282;  
  longitude=-2.766;  
};
```

```
R_Date("OxA-587",12530,150)
{
  color="A901DB";
  latitude=51.282;
  longitude=-2.766;
};
R_Date("OxA-8003",11800,180)
{
  color="A901DB";
  latitude=50.469;
  longitude=-3.503;
};
R_Date("OxA-8002",12240,100)
{
  color="A901DB";
  latitude=50.469;
  longitude=-3.503;
};
R_Date("OxA-5692",12250,110)
{
  color="A901DB";
  latitude=50.469;
  longitude=-3.503;
};
R_Date("OxA-6669",12330,90)
{
  color="A901DB";
  latitude=50.469;
  longitude=-3.503;
};
R_Date("OxA-6631",12000,80)
{
  color="A901DB";
  latitude=51.838;
  longitude=-2.662;
};
R_Date("OxA-6732",12150,100)
{
  color="A901DB";
  latitude=51.838;
  longitude=-2.662;
};
R_Date("OxA-6733",12230,100)
{
  color="A901DB";
  latitude=51.838;
  longitude=-2.662;
};
R_Date("OxA-17725",12610,55)
{
  color="A901DB";
  latitude=51.838;
  longitude=-2.662;
};
R_Date("OxA-6734",13320,130)
```

```
{
  color="A901DB";
  latitude=51.838;
  longitude=-2.662;
};
R_Date("OxA-8739",11270,80)
{
  color="A901DB";
  latitude=53.261;
  longitude=-1.918;
};
R_Date("OxA-6735",11910,110)
{
  color="A901DB";
  latitude=53.261;
  longitude=-1.918;
};
R_Date("OxA-8738",11970,75)
{
  color="A901DB";
  latitude=53.261;
  longitude=-1.918;
};
R_Date("OxA-6666",12040,80)
{
  color="A901DB";
  latitude=53.261;
  longitude=-1.918;
};
R_Date("OxA-3398",12280,110)
{
  color="A901DB";
  latitude=53.261;
  longitude=-1.918;
};
R_Date("OxA-3400",12340,110)
{
  color="A901DB";
  latitude=53.261;
  longitude=-1.918;
};
R_Date("OxA-4102",12540,140)
{
  color="A901DB";
  latitude=53.261;
  longitude=-1.918;
};
R_Date("OxA-6321",11070,100)
{
  color="A901DB";
  latitude=54.148;
  longitude=-2.331;
};
R_Date("OxA-6670",10420,75)
{
```



```
color="A901DB";
latitude=50.434;
longitude=-3.557;
};
R_Date("OxA-6316",10920,90)
{
color="A901DB";
latitude=53.091;
longitude=-1.854;
};
R_Date("OxA-14068",12585,60)
{
color="A901DB";
latitude=50.597;
longitude=-3.605;
};
R_Date("OxA-6323",10460,90)
{
color="A901DB";
latitude=53.263;
longitude=-1.201;
};
R_Date("OxA-6324",12210,100)
{
color="A901DB";
latitude=53.263;
longitude=-1.201;
};
R_Date("BM-2350",9790,180)
{
color="A901DB";
latitude=54.239;
longitude=-0.441;
};
R_Date("OxA-6636",10715,75)
{
color="A901DB";
latitude=54.124;
longitude=-2.368;
};
R_Date("OxA-16389",10810,50)
{
color="A901DB";
latitude=54.124;
longitude=-2.368;
};
R_Date("OxA-6315",10290,100)
{
color="A901DB";
latitude=52.056;
longitude=1.112;
};
R_Date("Birm-820",10280,200)
{
color="A901DB";
```

```
latitude=51.284;
longitude=-2.766;
};
R_Date("Birm-821",10470,190)
{
  color="A901DB";
  latitude=51.284;
  longitude=-2.766;
};
R_Date("OxA-4986",11530,120)
{
  color="A901DB";
  latitude=51.284;
  longitude=-2.766;
};
R_Date("OxA-18705",12490,45)
{
  color="A901DB";
  latitude=51.284;
  longitude=-2.766;
};
R_Date("OxA-14477",12540,75)
{
  color="A901DB";
  latitude=51.284;
  longitude=-2.766;
};
R_Date("OxA-14438",12545,55)
{
  color="A901DB";
  latitude=51.284;
  longitude=-2.766;
};
R_Date("OxA-14476",12610,90)
{
  color="A901DB";
  latitude=51.284;
  longitude=-2.766;
};
R_Date("OxA-1499",11970,150)
{
  color="A901DB";
  latitude=50.494;
  longitude=-3.672;
};
R_Date("OxA-3890",12150,110)
{
  color="A901DB";
  latitude=50.494;
  longitude=-3.672;
};
R_Date("OxA-4494",12220,110)
{
  color="A901DB";
  latitude=50.494;
```

```

longitude=-3.672;
};
R_Date("OxA-1902",10010,120)
{
color="A901DB";
latitude=51.600;
longitude=-0.500;
};
R_Date("OxA-1788",10270,100)
{
color="A901DB";
latitude=51.600;
longitude=-0.500;
};
R_Date("OxA-15078",12325,50)
{
color="A901DB";
latitude=54.128;
longitude=-2.264;
};
R_Date("OxA-6633",10125,70)
{
color="A901DB";
latitude=54.267;
longitude=-2.084;
};
Sum("Equus England Sum (78)")
{
color="A901DB";
};
};
Boundary("End Equus ferus England");
};
Sequence("Mammuthus primigenius Eng")
{
Boundary("Start Mammuthus primigenius England");
Phase("Mammuthus primigenius England")
{
R_Date("OxA-20129",12230,50)
{
color="3366CC";
latitude=52.648;
longitude=-2.750;
};
R_Date("OxA-19903",12375,50)
{
color="3366CC";
latitude=52.648;
longitude=-2.750;
};
R_Date("OxA-17846",12470,55)
{
color="3366CC";
latitude=51.282;
longitude=-2.766;
};
};

```

```

};
R_Date("OxA-1890",12470,55)
{
  color="3366CC";
  latitude=51.282;
  longitude=-2.766;
};
R_Date("OxA-1204",12460,160)
{
  color="3366CC";
  latitude=53.262;
  longitude=-1.201;
};
R_Date("OxA-1462",12320,120)
{
  color="3366CC";
  latitude=53.263;
  longitude=-1.201;
};
Sum("Mammuthus primigenius England Sum (6)")
{
  color="3366CC";
};
};
Boundary("End Mammuthus primigenius England");
};
Sequence("Megaloceros giganteus Eng")
{
  Boundary("Start Megaloceros giganteus England");
  Phase("Megaloceros giganteus England")
  {
    R_Date("BIRM-55",12850,250)
    {
      color="F781F3";
      latitude=53.912;
      longitude=-0.301;
    };
    R_Date("OxA-11645",12210,80)
    {
      color="F781F3";
      latitude=54.123;
      longitude=-2.766;
    };
    R_Date("GrN-6204",12180,100)
    {
      color="F781F3";
      latitude=50.469;
      longitude=-3.503;
    };
    Sum("Megaloceros giganteus England Sum (3)")
    {
      color="F781F3";
    };
  };
};
Boundary("End Megaloceros giganteus England");

```

```

};
Sequence("Rangifer tarandus Eng")
{
  Boundary("Start Rangifer tarandus England");
  Phase("Rangifer tarandus England")
  {
    R_Date("OxA-1122",12480,130)
    {
      color="FFFF00";
      latitude=51.326;
      longitude=-2.754;
    };
    R_Date("OxA-1782",10140,100)
    {
      color="FFFF00";
      latitude=51.267;
      longitude=-2.739;
    };
    R_Date("OxA-1784",10230,110)
    {
      color="FFFF00";
      latitude=51.267;
      longitude=-2.739;
    };
    R_Date("OxA-1781",10600,200)
    {
      color="FFFF00";
      latitude=51.267;
      longitude=-2.739;
    };
    R_Date("OxA-14827",10145,55)
    {
      color="FFFF00";
      latitude=51.287;
      longitude=-2.771;
    };
    R_Date("OxA-17829",10150,40)
    {
      color="FFFF00";
      latitude=51.287;
      longitude=-2.771;
    };
    R_Date("OxA-17831",10480,45)
    {
      color="FFFF00";
      latitude=51.287;
      longitude=-2.771;
    };
    R_Date("OxA-17828",10655,45)
    {
      color="FFFF00";
      latitude=51.287;
      longitude=-2.771;
    };
    R_Date("OxA-5804",10020,80)
  }
}

```

```
{
  color="FFFF00";
  latitude=53.355;
  longitude=-1.218;
};
R_Date("OxA-15214",10125,45)
{
  color="FFFF00";
  latitude=53.355;
  longitude=-1.218;
};
R_Date("OxA-18064",12535,55)
{
  color="FFFF00";
  latitude=51.282;
  longitude=-2.766;
};
R_Date("OxA-1120",10190,120)
{
  color="FFFF00";
  latitude=51.282;
  longitude=-2.766;
};
R_Date("OxA-14826",14395,60)
{
  color="FFFF00";
  latitude=50.469;
  longitude=-3.503;
};
R_Date("OxA-2456",11270,110)
{
  color="FFFF00";
  latitude=54.087;
  longitude=-2.300;
};
R_Date("OxA-11154",11465,75)
{
  color="FFFF00";
  latitude=54.087;
  longitude=-2.300;
};
R_Date("OxA-632",10600,140)
{
  color="FFFF00";
  latitude=53.091;
  longitude=-1.854;
};
R_Date("OxA-631",10780,160)
{
  color="FFFF00";
  latitude=53.091;
  longitude=-1.854;
};
R_Date("OxA-17160",14550,55)
{
```

```

    color="FFFF00";
    latitude=50.366;
    longitude=-4.128;
};
R_Date("OxA-8096",10740,65)
{
    color="FFFF00";
    latitude=54.124;
    longitude=-2.368;
};
R_Date("OxA-3894",11130,100)
{
    color="FFFF00";
    latitude=50.490;
    longitude=-3.665;
};
R_Date("OxA-2453",10220,110)
{
    color="FFFF00";
    latitude=54.128;
    longitude=-2.264;
};
R_Date("OxA-2454",10970,120)
{
    color="FFFF00";
    latitude=54.128;
    longitude=-2.264;
};
R_Date("OxA-15170",11290,55)
{
    color="FFFF00";
    latitude=54.128;
    longitude=-2.264;
};
R_Date("OxA-2457",11590,130)
{
    color="FFFF00";
    latitude=54.128;
    longitude=-2.264;
};
R_Date("OxA-2455",11750,120)
{
    color="FFFF00";
    latitude=54.128;
    longitude=-2.264;
};
Sum("Rangifer tarandus England Sum (25)")
{
    color="FFFF00";
};
};
Boundary("End Rangifer tarandus England");
};
Sequence("Saiga tatarica Eng")
{

```

```

Boundary("Start Saiga tatarica England");
Phase("Saiga tatarica England")
{
  R_Date("OxA-463", 12380, 160)
  {
    color="333366";
    latitude=51.282;
    longitude=-2.766;
  };
  Sum("Saiga tatarica England Sum (1)")
  {
    color="333366";
  };
};
Boundary("End Saiga tartaric England");
};
Sequence("Bos taurus Ire")
{
  Boundary("Start Bos taurus Ireland");
  Phase("Bos taurus Ireland")
  {
    R_Date("OxA-3869",5510,70)
    {
      color="A9D0F5";
      latitude=52.174;
      longitude=-10.445;
    };
    R_Date("OxA-4269",5190,80)
    {
      color="A9D0F5";
      latitude=52.083;
      longitude=-7.733;
    };
    R_Date("OxA-3691",6660,80)
    {
      color="A9D0F5";
      latitude=53.384;
      longitude=-6.117;
    };
  };
  Sum("Bos taurus Ireland Sum (3)")
  {
    color="A9D0F5";
  };
};
Boundary("End Bos taurus Ireland");
};
Sequence("Cervus elaphus Ire")
{
  Boundary("Start Cervus elaphus Ireland");
  Phase("Cervus elaphus Ireland")
  {
    R_Date("OxA-3693",11790,120)
    {
      color="04B404";
      latitude=54.059;
    };
  };
};

```



```

    longitude=-8.450;
};
R_Date("OxA-6110",3760,50)
{
    color="04B404";
    latitude=54.470;
    longitude=-6.260;
};
R_Date("OxA-3712",4190,65)
{
    color="04B404";
    latitude=53.604;
    longitude=-7.035;
};
R_Date("OxA-3711",3985,60)
{
    color="04B404";
    latitude=52.134;
    longitude=-10.367;
};
Sum("Cervus elaphus Ireland Sum (4)")
{
    color="04B404";
};
};
Boundary("End Cervus elaphus Ireland");
};
Sequence("Megaloceros giganteus Ire")
{
    Boundary("Start Megaloceros giantess Ireland");
    Phase("Megaloceros giganteus Ireland")
    {
        R_Date("UB-2699",10610,495)
        {
            color="F781F3";
            latitude=53.220;
            longitude=-6.210;
        };
        R_Date("Unspecified 1",15170,160)
        {
            color="F781F3";
            latitude=53.220;
            longitude=-6.210;
        };
        R_Date("OxA-4249",11110,110)
        {
            color="F781F3";
            latitude=52.100;
            longitude=-7.717;
        };
        R_Date("OxA-3723",11750,90)
        {
            color="F781F3";
            latitude=52.670;
            longitude=-9.000;
        };
    };
};

```

```

};
R_Date("OxA-4270",11820,120)
{
  color="F781F3";
  latitude=51.867;
  longitude=-8.517;
};
R_Date("OxA-4241",10960,110)
{
  color="F781F3";
  latitude=52.083;
  longitude=-7.733;
};
R_Date("OxA-4605",11510,100)
{
  color="F781F3";
  latitude=52.590;
  longitude=-8.317;
};
R_Date("OxA-11684",11730,70)
{
  color="F781F3";
  latitude=54.817;
  longitude=-5.767;
};
R_Date("OxA-12016",10985,45)
{
  color="F781F3";
  latitude=54.600;
  longitude=-5.900;
};
R_Date("BM-1840",10920,250)
{
  color="F781F3";
};
R_Date("BM-1904",11380,280)
{
  color="F781F3";
};
Sum("Megaloceros giganteus Ireland Sum (11)")
{
  color="F781F3";
};
};
Boundary("End Megaloceros giganteus Ireland");
};
Sequence("Rangifer tarandus Ire")
{
  Boundary("Start Rangifer tarandus Ireland");
  Phase("Rangifer tarandus Ireland")
  {
    R_Date("OxA-3602",12480,130)
    {
      color="FFFF00";
      latitude=52.220;

```

```

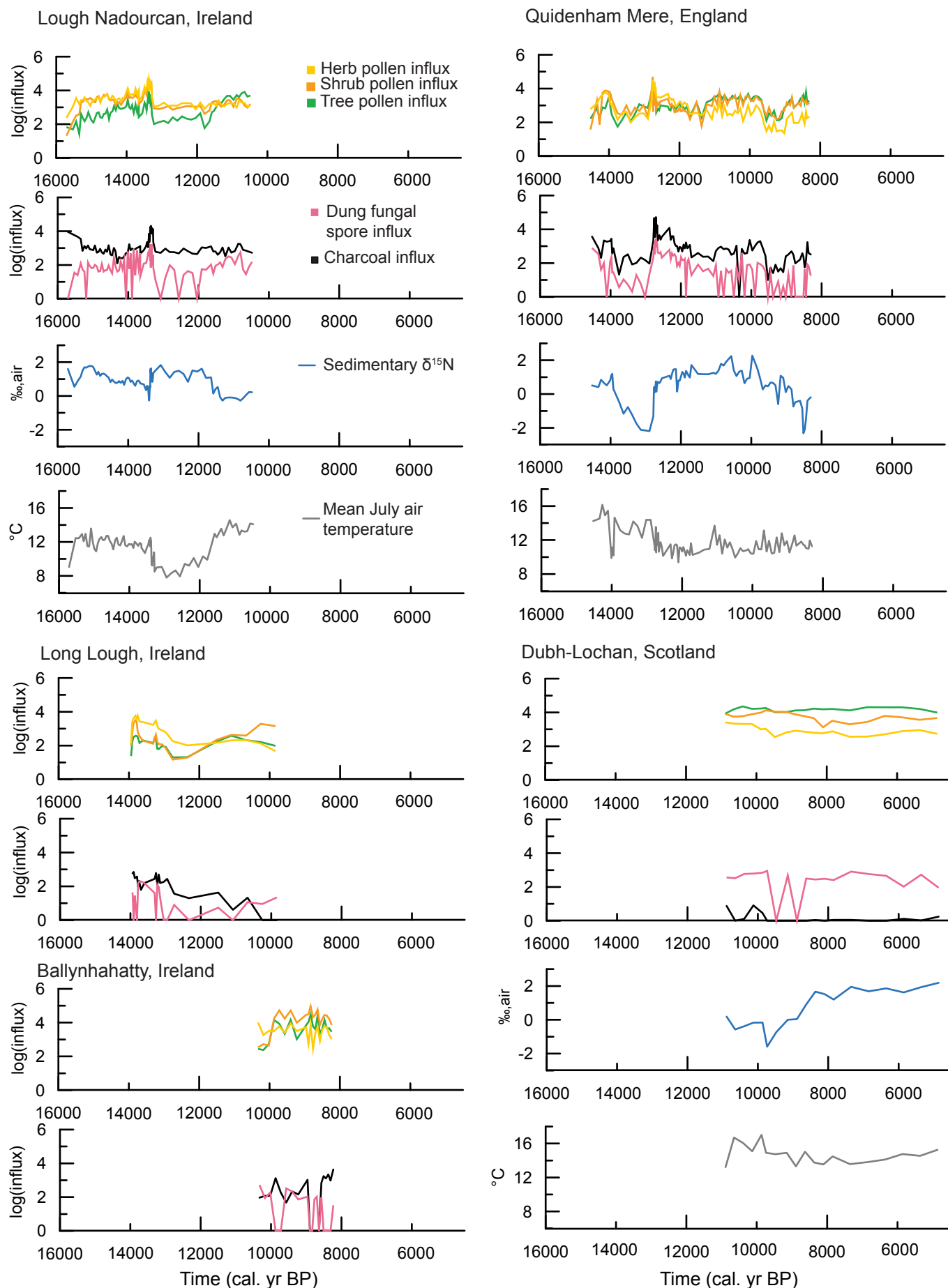
    longitude=-8.580;
};
R_Date("OxA-3701",10850,80)
{
    color="FFFF00";
    latitude=52.670;
    longitude=-9.000;
};
R_Date("OxA-4240",10990,120)
{
    color="FFFF00";
    latitude=52.083;
    longitude=-7.733;
};
R_Date("Unspecified 2",10250,350)
{
    color="FFFF00";
    latitude=54.510;
    longitude=-5.470;
};
Sum("Rangifer tarandus Ireland Sum (25)")
{
    color="FFFF00";
};
};
Boundary("End Rangifer tarandus Ireland");
};
Sequence("Equus ferus Sco")
{
    Boundary("Start Equus ferus Scotland");
    Phase("Equus ferus Scotland")
    {
        R_Date("AA-18506", 10165, 125)
        {
            color="A901DB";
            latitude=55.891;
            longitude=-3.236;
        };
        Sum("Equus ferus Scotland Sum (1)")
        {
            color="A901DB";
        };
    };
    Boundary("End Equus ferus Scotland");
};
Sequence("Megaloceros giganteus Sco")
{
    Boundary("Start Megaloceros giganteus Scotland");
    Phase("Megaloceros giganteus Scotland")
    {
        R_Date("OxA-9040",11985,70)
        {
            color="F781F3";
            latitude=55.788;
            longitude=-6.203;
        };
    };
};

```

```

};
R_Date("AA-51350",10257,75)
{
  color="F781F3";
  latitude=54.920;
  longitude=-4.420;
};
R_Date("OxA-11498",10585,65)
{
  color="F781F3";
  latitude=54.920;
  longitude=-4.420;
};
Sum("Megaloceros giganteus  Scotland Sum (3)")
{
  color="F781F3";
};
};
Boundary("End Megaloceros giganteus  Ireland");
};
Sequence("Rangifer tarandus Sco")
{
  Boundary("Start Rangifer tarandus Scotland");
  Phase("Rangifer tarandus Scotland")
  {
    R_Date("SRR-1788", 10080, 70)
    {
      color="FFFF00";
      latitude=58.108;
      longitude=-4.942;
    };
    Sum("Rangifer tarandus Scotland Sum (1)")
    {
      color="FFFF00";
    };
  };
  Boundary("End Rangifer tarandus Scotland");
};
};

```



FigS8. Log-transformed time series data used in the generalised additive models. The pollen, dung spore and charcoal influx data were log-transformed prior to statistical modelling to minimize the effect of extreme values from periods of high sedimentation rates on model results ($n=241$). Sedimentary $\delta^{15}\text{N}$ and mean July air temperature, which are not measured with respect to sediment accumulation rates, were not transformed and are the same as presented in Fig. 2 ($n=199$).

TableS9. Correlation coefficients for each dataset. Pearson's product moment correlation coefficients were calculated in R using the *cor* function and significance values were obtained using a t-test with the *cor.test* function.

3-site Dataset	<i>Sporormiella</i> influx	Charcoal influx	Herb pollen influx	Shrub pollen influx	Tree pollen influx	Temperature	Time
Sedimentary $\delta^{15}\text{N}$	0.115 (p=0.1065)	0.124 (p=0.0804)	0.192 (p=0.0066)	0.037 (p=0.6033)	-0.139 (p=0.0495)	-0.34 (p=8.64e-07)	0.125 (p=0.0786)
Herb pollen	0.61 (p \leq 2.2e-16)	0.549 (p \leq 2.2e-16)	-	0.632 (p \leq 2.2e-16)	0.165 (p=0.01956)	-0.09 (p=0.2056)	0.588 (p \leq 2.2e-16)
Shrub pollen	0.43 (p=2.502e-10)	0.107 (p=0.1325)	0.632 (p \leq 2.2e-16)	-	0.61 (p \leq 2.2e-16)	0.07 (p=0.3236)	0.041 (p=0.539)
Tree pollen	0.376 (p=4.441e-08)	-0.292 (p=2.938e-05)	0.165 (p=0.01956)	0.61 (p \leq 2.2e-16)	-	0.36 (p=1.675e-07)	-0.545 (p \leq 2.2e-16)
5-site Dataset	<i>Sporormiella</i> influx	Charcoal influx	Herb pollen influx	Shrub pollen influx	Tree pollen influx	Temperature	Time
Herb pollen	0.505 (p \leq 2.2e-16)	0.506 (p \leq 2.2e-16)	-	0.565 (p \leq 2.2e-16)	0.236 (p=0.01956)	NA	0.473 (p=7.55e-15)
Shrub pollen	0.258 (p=4.952e-05)	0.051 (p=0.4306)	0.565 (p \leq 2.2e-16)	-	0.717 (p \leq 2.2e-16)	NA	-0.163 (p=0.0115)
Tree pollen	0.266 (p=2.949e-05)	-0.190 (p=0.0031)	0.236 (p=0.01956)	0.717 (p \leq 2.2e-16)	-	NA	-0.555 (p \leq 2.2e-16)

SUPPLEMENTARY INFORMATION

Plant controls on Late Quaternary whole ecosystem structure and function

E.S. Jeffers, N.J. Whitehouse, A. Lister, G. Plunkett, P. Barratt, E. Smyth, P. Lamb, M.W. Dee, S.J. Brooks, K.J. Willis, C.A. Froyd, J.E. Watson, M.B. Bonsall

Appendix 3 Statistical Modelling

Temporal autocorrelation. We tested for an effect of temporal autocorrelation on our GAM results by comparing the goodness of fit between our original model and a model that accounted for a lag of one period (AR-1) and two periods (AR-2). We found no difference in model selection metrics between original model and AR-1 or AR-2 (Appendix Table21). This is likely due to the relatively long-time intervals between observations, such that the observations are essentially independent and therefore any temporal autocorrelation had at most a weak effect on the model.

Appendix Table 21. Goodness of fit for models with temporally autocorrelated errors

Model	Dev. Exp.	Adj. R ²	AIC
$\delta^{15}\text{N}$ without temporal auto-correlation	57.20%	0.505	407.8037
$\delta^{15}\text{N}$ with AR-1 correlation between residuals	57.20%	0.505	407.8037
$\delta^{15}\text{N}$ with AR-2 correlation between residuals	57.20%	0.505	407.8037
Herbs (3-sites) without temporal auto-correlation	91.40%	0.891	15.98281
Herbs (3-sites) with AR-1 correlation between residuals	91.40%	0.891	15.98281
Herbs (3-sites) with AR-2 correlation between residuals	91.40%	0.891	15.98281
Shrubs (3-sites) without temporal auto-correlation	85.10%	0.818	33.31709
Shrubs (3-sites) with AR-1 correlation between residuals	85.10%	0.818	33.31709
Shrubs (3-sites) with AR-2 correlation between residuals	85.10%	0.818	33.31709
Trees (3-sites) without temporal auto-correlation	78.60%	0.757	124.1384
Trees (3-sites) with AR-1 correlation between residuals	78.60%	0.757	124.1384
Trees (3-sites) with AR-2 correlation between residuals	78.60%	0.757	124.1384
Herbs (5-sites) without temporal auto-correlation	91.70%	0.886	28.8873
Herbs (5-sites) with AR-1 correlation between residuals	91.70%	0.886	28.8873
Herbs (5-sites) with AR-2 correlation between residuals	91.70%	0.886	28.8873
Shrubs (5-sites) without temporal auto-correlation	89.60%	0.871	44.73457
Shrubs (5-sites) with AR-1 correlation between residuals	89.60%	0.871	44.73457
Shrubs (5-sites) with AR-2 correlation between residuals	89.60%	0.871	44.73457
Trees (5-sites) without temporal auto-correlation	82.40%	0.802	143.24
Trees (5-sites) with AR-1 correlation between residuals	82.40%	0.802	143.24
Trees (5-sites) with AR-2 correlation between residuals	82.40%	0.802	143.24

Concurvity. We showed in TableS9 that there were no consistent patterns of correlation between the variables. To determine if there is any evidence of non-linear correlation between the variables (i.e. concurvity), we applied the concurvity function in the *mgcv* package in R to each model. Results are reported in Appendix Tables22-28. Overall, high concurvity effects (where concurvity ≥ 0.8) were only evident in the three sites that had

relatively few observations (i.e. $n=19, 20$ or 21). Typically smoother terms affected by concurvity were excluded or estimated to have low significance and therefore did not effect the main results of our study. For the model predicting sedimentary $\delta^{15}\text{N}$ (Appendix Table 22), there were high concurvity values involving pairs with tree and herb pollen influx, but these terms were excluded from the model or had low significance (respectively).

Appendix Table22. Estimated pairwise concavity values between smoother terms in the model predicting sedimentary $\delta^{15}\text{N}$.

Estimated:	para	s(dung-Dubh)	s(dung-Quid)	s(dung-Nad)	s(temp)	s(char)	s(herb-Dubh)	s(herb-Quid)	s(herb-Nad)	s(shrub-Dubh)	s(shrub-Quid)	s(shrub-Nad)	s(tree-Dubh)	s(tree-Quid)	s(tree-Nad)
para	1.0	0.0	0.1	0.0	0.0	0.0	0.0	0.1	0.1	0.0	0.1	0.1	0.1	0.1	0.1
s(dung-D)	1.0	1.0	0.1	0.1	0.1	0.1	0.6	0.1	0.1	0.6	0.1	0.1	0.9	0.1	0.1
s(dung-Q)	0.5	0.0	1.0	0.0	0.1	0.1	0.0	0.4	0.0	0.0	0.2	0.0	0.0	0.3	0.0
s(dung-N)	0.4	0.0	0.0	1.0	0.1	0.1	0.0	0.0	0.3	0.0	0.0	0.3	0.0	0.0	0.3
s(temp)	0.0	0.1	0.0	0.1	1.0	0.1	0.2	0.0	0.1	0.2	0.0	0.1	0.3	0.1	0.1
s(char)	0.0	0.2	0.2	0.0	0.1	1.0	0.4	0.2	0.1	0.2	0.2	0.2	0.6	0.1	0.1
s(herb-D)	0.1	0.8	0.0	0.0	0.1	0.1	1.0	0.0	0.0	0.7	0.0	0.0	0.9	0.0	0.0
s(herb-Q)	0.5	0.0	0.3	0.0	0.1	0.2	0.0	1.0	0.0	0.0	0.3	0.0	0.0	0.3	0.0
s(herb-N)	0.4	0.0	0.0	0.2	0.1	0.1	0.0	0.0	1.0	0.0	0.0	0.5	0.0	0.0	0.3
s(shrub-D)	0.2	0.6	0.1	0.0	0.1	0.1	0.6	0.0	0.0	1.0	0.0	0.0	0.9	0.0	0.0
s(shrub-Q)	0.5	0.0	0.3	0.0	0.1	0.1	0.0	0.3	0.0	0.0	1.0	0.0	0.0	0.4	0.0
s(shrub-N)	0.4	0.0	0.0	0.2	0.2	0.2	0.0	0.0	0.5	0.0	0.0	1.0	0.0	0.0	0.3
s(tree-D)	0.2	0.7	0.1	0.0	0.1	0.1	0.6	0.1	0.0	0.6	0.0	0.0	1.0	0.0	0.0
s(tree-Q)	0.5	0.0	0.3	0.0	0.1	0.1	0.0	0.3	0.0	0.0	0.5	0.0	0.0	1.0	0.0
s(tree-N)	0.4	0.0	0.0	0.2	0.1	0.1	0.0	0.0	0.4	0.0	0.0	0.3	0.0	0.0	1.0

Appendix Table23. Estimated pairwise concavity values between smoother terms in the model predicting herb pollen influx (3-sites).

Estimated:	para	s(dung-D)	s(dung-Q)	s(dung-N)	s(temp)	s(char)	s(shrub-D)	s(shrub-Q)	s(shrub-N)	s(tree-D)	s(tree-Q)	s(tree-N)
para	1.0	0.0	0.1	0.0	0.0	0.0	0.0	0.1	0.1	0.1	0.1	0.1
s(dung-D)	1.0	1.0	0.1	0.1	0.1	0.1	0.6	0.1	0.1	0.9	0.1	0.1
s(dung-Q)	0.5	0.0	1.0	0.0	0.1	0.1	0.0	0.2	0.0	0.0	0.3	0.0
s(dung-N)	0.4	0.0	0.0	1.0	0.1	0.1	0.0	0.0	0.3	0.0	0.0	0.3
s(temp)	0.0	0.2	0.2	0.0	1.0	0.1	0.2	0.2	0.2	0.6	0.1	0.1
s(char)	0.0	0.1	0.0	0.1	0.1	1.0	0.2	0.0	0.1	0.3	0.1	0.1
s(shrub-D)	0.1	0.7	0.0	0.0	0.1	0.1	1.0	0.0	0.0	0.9	0.0	0.0
s(shrub-Q)	0.5	0.0	0.3	0.0	0.1	0.1	0.0	1.0	0.0	0.0	0.4	0.0
s(shrub-N)	0.4	0.0	0.0	0.2	0.2	0.2	0.0	0.0	1.0	0.0	0.0	0.3
s(tree-D)	0.2	0.7	0.1	0.0	0.1	0.1	0.6	0.0	0.0	1.0	0.0	0.0
s(tree-Q)	0.5	0.0	0.3	0.0	0.1	0.1	0.0	0.5	0.0	0.0	1.0	0.0
s(tree-N)	0.4	0.0	0.0	0.2	0.1	0.1	0.0	0.0	0.3	0.0	0.0	1.0

Appendix Table24. Estimated pairwise concavity values between smoother terms in the model predicting herb pollen influx (5-sites).

Estimated:	para	s(dung-Dubh)	s(dung-Quid)	s(dung-Nad)	s(dung-Bally)	s(dung-Long)	s(char)	s(shrub-Dubh)	s(shrub-Quid)	s(shrub-Nad)	s(shrub-Bally)	s(shrub-Long)	s(tree-Dubh)	s(tree-Quid)	s(tree-Nad)	s(tree-Bally)	s(tree-Long)
para	1.0	0.0	0.0	0.0	0.0	0.0	0.0	0.0	0.1	0.1	0.0	0.0	0.1	0.1	0.0	0.0	0.0
s(dung-D)	1.0	1.0	0.0	0.0	0.0	0.0	0.1	0.6	0.1	0.1	0.0	0.0	1.0	0.1	0.0	0.0	0.0
s(dung-Q)	0.4	0.0	1.0	0.0	0.0	0.0	0.1	0.0	0.2	0.0	0.0	0.0	0.0	0.3	0.0	0.0	0.0
s(dung-N)	0.4	0.0	0.0	1.0	0.0	0.0	0.1	0.0	0.0	0.3	0.0	0.0	0.0	0.0	0.3	0.0	0.0
s(dung-B)	0.1	0.0	0.0	0.0	1.0	0.0	0.0	0.0	0.0	0.0	0.9	0.0	0.0	0.0	0.0	0.6	0.0
s(dung-L)	0.1	0.0	0.0	0.0	0.0	1.0	0.0	0.1	0.0	0.0	0.0	0.5	0.0	0.0	0.0	0.0	0.5
s(char)	0.0	0.2	0.1	0.0	0.1	0.1	1.0	0.2	0.1	0.2	0.1	0.1	0.5	0.1	0.1	0.0	0.0
s(shrub-D)	0.1	0.6	0.1	0.0	0.0	0.0	0.1	1.0	0.0	0.0	0.0	0.0	1.0	0.0	0.0	0.0	0.0
s(shrub-Q)	0.4	0.0	0.3	0.0	0.0	0.0	0.0	0.0	1.0	0.0	0.0	0.0	0.0	0.4	0.0	0.0	0.0
s(shrub-N)	0.4	0.0	0.0	0.2	0.0	0.0	0.2	0.0	0.0	1.0	0.0	0.0	0.0	0.0	0.3	0.0	0.0
s(shrub-B)	0.2	0.0	0.0	0.0	0.6	0.0	0.0	0.0	0.0	0.0	1.0	0.1	0.0	0.0	0.0	0.6	0.0
s(shrub-L)	0.2	0.1	0.0	0.0	0.0	0.4	0.1	0.1	0.0	0.0	0.0	1.0	0.1	0.0	0.0	0.0	0.7
s(tree-D)	0.2	0.6	0.1	0.0	0.0	0.0	0.1	0.6	0.0	0.0	0.0	0.0	1.0	0.0	0.0	0.0	0.0
s(tree-Q)	0.4	0.0	0.3	0.0	0.0	0.0	0.1	0.0	0.4	0.0	0.0	0.0	0.0	1.0	0.0	0.0	0.0
s(tree-N)	0.4	0.0	0.0	0.2	0.0	0.0	0.1	0.0	0.0	0.3	0.0	0.0	0.0	0.0	1.0	0.0	0.0
s(tree-B)	0.1	0.0	0.0	0.0	0.7	0.0	0.0	0.0	0.0	0.0	0.9	0.0	0.0	0.0	0.0	1.0	0.0
s(tree-L)	0.1	0.1	0.0	0.0	0.0	0.4	0.0	0.2	0.0	0.0	0.0	0.6	0.1	0.0	0.0	0.0	1.0

Appendix Table25. Estimated pairwise concavity values between smoother terms in the model predicting shrub pollen influx (3-sites)

Estimated:	para	s(dung-D)	s(dung-Q)	s(dung-N)	s(temp)	s(char)	s(herb-D)	s(herb-Q)	s(herb-N)	s(tree-D)	s(tree-Q)	s(tree-N)
para	1.0	0.0	0.1	0.0	0.0	0.0	0.0	0.1	0.1	0.1	0.1	0.1
s(dung-D)	1.0	1.0	0.1	0.1	0.1	0.1	0.6	0.1	0.1	0.9	0.1	0.1
s(dung-Q)	0.5	0.0	1.0	0.0	0.1	0.1	0.0	0.4	0.0	0.0	0.3	0.0
s(dung-N)	0.4	0.0	0.0	1.0	0.1	0.1	0.0	0.0	0.3	0.0	0.0	0.3
s(temp)	0.0	0.2	0.2	0.0	1.0	0.1	0.4	0.2	0.1	0.6	0.1	0.1
s(char)	0.0	0.1	0.0	0.1	0.1	1.0	0.2	0.0	0.1	0.3	0.1	0.1
s(herb-D)	0.1	0.8	0.0	0.0	0.1	0.1	1.0	0.0	0.0	0.9	0.0	0.0
s(herb-Q)	0.5	0.0	0.3	0.0	0.2	0.1	0.0	1.0	0.0	0.0	0.3	0.0
s(herb-N)	0.4	0.0	0.0	0.2	0.1	0.1	0.0	0.0	1.0	0.0	0.0	0.3
s(tree-D)	0.2	0.7	0.1	0.0	0.1	0.1	0.6	0.0	0.0	1.0	0.0	0.0
s(tree-Q)	0.5	0.0	0.3	0.0	0.1	0.1	0.0	0.3	0.0	0.0	1.0	0.0
s(tree-N)	0.4	0.0	0.0	0.2	0.1	0.1	0.0	0.0	0.4	0.0	0.0	1.0

Appendix Table26. Estimated pairwise concavity values between smoother terms in the model predicting shrub pollen influx (5-sites).

Estimated:	para	s(dung-Dubh)	s(dung-Quid)	s(dung-Nad)	s(dung-Bally)	s(dung-Long)	s(char)	s(herb-Dubh)	s(herb-Quid)	s(herb-Nad)	s(herb-Bally)	s(herb-Long)	s(tree-Dubh)	s(tree-Quid)	s(tree-Nad)	s(tree-Bally)	s(tree-Long)
para	1.0	0.0	0.0	0.0	0.0	0.0	0.0	0.0	0.1	0.1	0.0	0.0	0.1	0.1	0.0	0.0	0.0
s(dung-D)	1.0	1.0	0.0	0.0	0.0	0.0	0.1	0.7	0.1	0.1	0.0	0.0	1.0	0.1	0.0	0.0	0.0
s(dung-Q)	0.4	0.0	1.0	0.0	0.0	0.0	0.1	0.0	0.4	0.0	0.0	0.0	0.0	0.3	0.0	0.0	0.0
s(dung-N)	0.4	0.0	0.0	1.0	0.0	0.0	0.1	0.0	0.0	0.3	0.0	0.0	0.0	0.0	0.3	0.0	0.0
s(dung-B)	0.1	0.0	0.0	0.0	1.0	0.0	0.0	0.0	0.0	0.0	0.6	0.0	0.0	0.0	0.0	0.6	0.0
s(dung-L)	0.1	0.0	0.0	0.0	0.0	1.0	0.0	0.0	0.0	0.0	0.0	0.6	0.0	0.0	0.0	0.0	0.5
s(char)	0.0	0.2	0.1	0.0	0.1	0.1	1.0	0.3	0.2	0.1	0.0	0.1	0.5	0.1	0.1	0.0	0.0
s(herb-D)	0.1	0.8	0.0	0.0	0.0	0.0	0.1	1.0	0.0	0.0	0.0	0.0	1.0	0.0	0.0	0.0	0.0
s(herb-Q)	0.4	0.0	0.3	0.0	0.0	0.0	0.1	0.0	1.0	0.0	0.0	0.0	0.0	0.4	0.0	0.0	0.0
s(herb-N)	0.4	0.0	0.0	0.2	0.0	0.0	0.1	0.0	0.0	1.0	0.0	0.0	0.0	0.0	0.3	0.0	0.0
s(herb-B)	0.1	0.0	0.0	0.0	0.7	0.0	0.0	0.0	0.0	0.0	1.0	0.0	0.0	0.0	0.0	0.6	0.0
s(herb-L)	0.1	0.0	0.0	0.0	0.0	0.6	0.0	0.0	0.0	0.0	0.0	1.0	0.0	0.0	0.0	0.0	0.8
s(tree-D)	0.2	0.6	0.1	0.0	0.0	0.0	0.1	0.6	0.0	0.0	0.0	0.0	1.0	0.0	0.0	0.0	0.0
s(tree-Q)	0.4	0.0	0.3	0.0	0.0	0.0	0.1	0.0	0.3	0.0	0.0	0.0	0.0	1.0	0.0	0.0	0.0
s(tree-N)	0.4	0.0	0.0	0.2	0.0	0.0	0.1	0.0	0.0	0.4	0.0	0.0	0.0	0.0	1.0	0.0	0.0
s(tree-B)	0.1	0.0	0.0	0.0	0.7	0.0	0.0	0.0	0.0	0.0	0.6	0.0	0.0	0.0	0.0	1.0	0.0
s(tree-L)	0.2	0.1	0.0	0.0	0.0	0.4	0.0	0.2	0.0	0.0	0.0	0.5	0.1	0.0	0.0	0.0	1.0

Appendix Table27. Estimated pairwise concavity values between smoother terms in the model predicting tree pollen influx (3-sites)

Estimated:	para	s(dung-D)	s(dung-Q)	s(dung-N)	s(temp)	s(char)	s(herb-D)	s(herb-Q)	s(herb-N)	s(shrub-D)	s(shrub-Q)	s(shrub-N)
para	1.0	0.0	0.1	0.0	0.0	0.0	0.0	0.1	0.1	0.0	0.1	0.1
s(dung-D)	1.0	1.0	0.1	0.1	0.1	0.1	0.6	0.1	0.1	0.6	0.1	0.1
s(dung-Q)	0.5	0.0	1.0	0.0	0.1	0.1	0.0	0.4	0.0	0.0	0.2	0.0
s(dung-N)	0.4	0.0	0.0	1.0	0.1	0.1	0.0	0.0	0.3	0.0	0.0	0.3
s(temp)	0.0	0.2	0.2	0.0	1.0	0.1	0.4	0.2	0.1	0.2	0.2	0.2
s(char)	0.0	0.1	0.0	0.1	0.1	1.0	0.2	0.0	0.1	0.2	0.0	0.1
s(herb-D)	0.1	0.8	0.0	0.0	0.1	0.1	1.0	0.0	0.0	0.7	0.0	0.0
s(herb-Q)	0.5	0.0	0.3	0.0	0.2	0.1	0.0	1.0	0.0	0.0	0.3	0.0
s(herb-N)	0.4	0.0	0.0	0.2	0.1	0.1	0.0	0.0	1.0	0.0	0.0	0.5
s(shrub-D)	0.1	0.7	0.0	0.0	0.1	0.1	0.6	0.0	0.0	1.0	0.0	0.0
s(shrub-Q)	0.5	0.0	0.3	0.0	0.1	0.1	0.0	0.3	0.0	0.0	1.0	0.0
s(shrub-N)	0.4	0.0	0.0	0.2	0.2	0.2	0.0	0.0	0.5	0.0	0.0	1.0

Appendix Table28. Estimated pairwise concavity values between smoother terms in the model predicting tree pollen influx (5-sites).

Estimated:	para	s(dung-Dubh)	s(dung-Quid)	s(dung-Nad)	s(dung-Bally)	s(dung-Long)	s(char)	s(herb-Dubh)	s(herb-Quid)	s(herb-Nad)	s(herb-Bally)	s(herb-Long)	s(shrub-Dubh)	s(shrub-Quid)	s(shrub-Nad)	s(shrub-Bally)	s(shrub-Long)
para	1.0	0.0	0.0	0.0	0.0	0.0	0.0	0.0	0.1	0.1	0.0	0.0	0.0	0.1	0.1	0.0	0.0
s(dung-D)	1.0	1.0	0.0	0.0	0.0	0.0	0.1	0.7	0.1	0.1	0.0	0.0	0.6	0.1	0.1	0.0	0.0
s(dung-Q)	0.4	0.0	1.0	0.0	0.0	0.0	0.1	0.0	0.4	0.0	0.0	0.0	0.0	0.2	0.0	0.0	0.0
s(dung-N)	0.4	0.0	0.0	1.0	0.0	0.0	0.1	0.0	0.0	0.3	0.0	0.0	0.0	0.0	0.3	0.0	0.0
s(dung-B)	0.1	0.0	0.0	0.0	1.0	0.0	0.0	0.0	0.0	0.0	0.6	0.0	0.0	0.0	0.0	0.9	0.0
s(dung-L)	0.1	0.0	0.0	0.0	0.0	1.0	0.0	0.0	0.0	0.0	0.0	0.6	0.1	0.0	0.0	0.0	0.5
s(char)	0.0	0.2	0.1	0.0	0.1	0.1	1.0	0.3	0.2	0.1	0.0	0.1	0.2	0.1	0.2	0.1	0.1
s(herb-D)	0.1	0.8	0.0	0.0	0.0	0.0	0.1	1.0	0.0	0.0	0.0	0.0	0.7	0.0	0.0	0.0	0.0
s(herb-Q)	0.4	0.0	0.3	0.0	0.0	0.0	0.1	0.0	1.0	0.0	0.0	0.0	0.0	0.3	0.0	0.0	0.0
s(herb-N)	0.4	0.0	0.0	0.2	0.0	0.0	0.1	0.0	0.0	1.0	0.0	0.0	0.0	0.0	0.5	0.0	0.0
s(herb-B)	0.1	0.0	0.0	0.0	0.7	0.0	0.0	0.0	0.0	0.0	1.0	0.0	0.0	0.0	0.0	0.9	0.0
s(herb-L)	0.1	0.0	0.0	0.0	0.0	0.6	0.0	0.0	0.0	0.0	0.0	1.0	0.0	0.0	0.0	0.0	0.8
s(shrub-D)	0.1	0.6	0.1	0.0	0.0	0.0	0.1	0.7	0.0	0.0	0.0	0.0	1.0	0.0	0.0	0.0	0.0
s(shrub-Q)	0.4	0.0	0.3	0.0	0.0	0.0	0.0	0.0	0.3	0.0	0.0	0.0	0.0	1.0	0.0	0.0	0.0
s(shrub-N)	0.4	0.0	0.0	0.2	0.0	0.0	0.2	0.0	0.0	0.5	0.0	0.0	0.0	0.0	1.0	0.0	0.0
s(shrub-B)	0.2	0.0	0.0	0.0	0.6	0.0	0.1	0.1	0.0	0.0	0.6	0.0	0.1	0.0	0.0	1.0	0.0
s(shrub-L)	0.1	0.0	0.0	0.0	0.0	0.4	0.0	0.0	0.0	0.0	0.0	0.6	0.0	0.0	0.0	0.0	1.0

In the model predicting herb pollen influx, high concurrency effects involved *Sporormiella* (dung), shrub and tree pollen influx at Dubh-Lochan (Appendix Tables23-24). These terms all had moderate (*Sporormiella* and tree) or high (shrubs) levels of estimated significance, but also extremely wide confidence intervals, particularly at lower values of *Sporormiella* and shrub influx. At Ballynahatty, there were high levels of concurrency between *Sporormiella* and shrub influx, and tree and shrub influx (Appendix Table24). Of these terms, only shrub influx was highly significant and all terms have wide confidence intervals. At Long Lough, there was high concurrency between shrub and tree influx, but neither of these terms was highly significant (Appendix Table24).

For the model predicting shrub pollen influx, high concurrency was evident for *Sporormiella* and herb pollen influx, *Sporormiella* and tree pollen influx, and tree and herb pollen influx at Dubh-Lochan (Appendix Tables25-26); however none of these terms were significant. At Ballynahatty, concurrency affected *Sporormiella* and herb pollen influx, and *Sporormiella* and tree pollen influx (Appendix Table26); yet, the *Sporormiella* term was excluded from the model and herb pollen influx had a low level of significance. At Long Lough, there was high concurrency between herb and tree pollen influx (Appendix Table26); herb pollen influx had a low estimated significance level.

Concurrency in the model predicting tree pollen influx was limited to terms that were excluded (*Sporormiella* and shrub pollen influx at Dubh-Lochan, Appendix Table27-28; herb pollen influx at Ballynahatty, Appendix Table28) or had low (*Sporormiella* influx at Ballynahatty, Appendix Table28) or moderate significance (herb pollen influx at Long Lough, Appendix Table28).

Alternative model configurations. To determine if our grouping of herbs and grasses had an effect on our modelling results, we re-ran the models for each response variable using separate predictor terms for herbs and grasses. Model selection metrics show that this resulted in slight increases in the deviance explained and adjusted r^2 relative to the original model (Appendix Table29). As expected, there are differences in the parameters for each

smooth term for the models predicting changes in sedimentary $\delta^{15}\text{N}$ and shrub and tree pollen influx. (Appendix Tables30-36); however the patterns of significance remain largely consistent with those predicted by the original model. Herb and grass pollen influx were modelled separately and the estimated smoother terms are shown in Appendix Fig37. Not surprisingly, there are also differences in the smooth term statistics relative to the original model. For the most part, the smooth functions were relatively similar between herbs and grasses (Appendix Fig37) but there were differences in the significance of the smoother terms at each site. Yet there were no consistent patterns in the changes in smoother term significance relative to the original model (Appendix Table38). For example, the *Sporormiella* smoother term was more significant for explaining herb pollen influx at Dubh-Lochan and Ballynahatty than in the original model, but less significant at Lough Nadourcan and Long Long (and no difference at Quidenham Mere). When predicting grass pollen influx, the *Sporormiella* smoother term had a higher level of significance at Lough Nadourcan relative to the original model, but less significance at Dubh-Lochan and Ballynahatty (and no difference at Quidenham Mere and Long Lough). Overall, *Sporormiella* was highly significant for predicting changes in herbs at three sites, compared to two sites for grasses (and the combination of these variables). Ballynahatty shows the greatest change, although there is a lot of variability in the smoother term (Appendix F37), making it difficult to interpret. In general, the smoother terms predicting herb pollen influx also had wider confidence intervals than for grass pollen influx (or the original model where these variables are combined).

We also re-ran the models for each predictor term without the two sites that only include observations in the Holocene. While our *Sporormiella* data suggest that mega-herbivores persisted during the Holocene (Fig. 2), these are at relatively lower levels than during the preceding Pleistocene observations. We therefore evaluated the impact of removing the Holocene-only sites on the modelling results. All three model selection metrics show that dropping Dubh-Lochan and Ballynahatty resulted in poorer model fit.

Appendix Table29. Goodness of fit for the original Generalised Additive Model and two alternative models.

Models predicting Sedimentary $\delta^{15}\text{N}$		
Model	Dev. Exp.	Adj. R²
Original	57.20%	0.505
Separate herb and grass predictor variables	69.50%	0.62
Without Dubh-Lochan	47.20%	0.41
Models predicting Herb Pollen Influx (3-sites)		
Model	Dev. Exp.	Adj. R²
Original	91.40%	0.891
Separate herb and grass predictor variables	NA	NA
Without Dubh-Lochan	89.40%	0.879
Models predicting Shrub Pollen Influx (3-sites)		
Model	Dev. Exp.	Adj. R²
Original	85.10%	0.818
Separate herb and grass predictor variables	89.60%	0.861
Without Dubh-Lochan	84.80%	0.816
Models predicting Tree Pollen Influx (3-sites)		
Model	Dev. Exp.	Adj. R²
Original	78.60%	0.757
Separate herb and grass predictor variables	89.90%	0.873
Without Dubh-Lochan	78.60%	0.757
Models predicting Herb Pollen Influx (5-sites)		
Model	Dev. Exp.	Adj. R²
Original	91.70%	0.886
Separate herb and grass predictor variables	NA	NA
Without Dubh-Lochan and Ballynahatty	84.40%	0.821
Models predicting Shrub Pollen Influx (5-sites)		
Model	Dev. Exp.	Adj. R²
Original	89.60%	0.871
Separate herb and grass predictor variables	91.90%	0.895
Without Dubh-Lochan and Ballynahatty	79.90%	0.772
Models predicting Tree Pollen Influx (3-sites)		
Model	Dev. Exp.	Adj. R²
Original	82.40%	0.802
Separate herb and grass predictor variables	91.60%	0.896
Without Dubh-Lochan and Ballynahatty	78.20%	0.754

Furthermore, while the parameter estimates vary from the original model, the overall patterns once again remain consistent with the original findings. Importantly, excluding the Holocene-only had little to no effect on the significance of the *Sporormiella* smoother terms.

Appendix Table30. Parameters for original and alternative models for Sedimentary $\delta^{15}\text{N}$ and changes relative to original model.

	Original Model		Separate herb and grass predictor terms			Without Dubh-Lochan		
Smooth	edf	p-value	edf	p-value		edf	p-value	
s(dung-Dubh)	0.849	0.014783*	0.581	0.04610*	-			
s(dung-Quid)	7.058	0.006006**	6.916	0.00013***	↑	7.092	0.01000**	-
s(dung-Nad)	4.25e-07	0.811955 (excluded)	2.46e-10	0.86449 (excluded)	-	5.86e-11	0.75722 (excluded)	-
s(herb-Dubh)			0.589	0.10112 (excluded)	NA			
s(herb-Quid)			7.526	2.72e-08***	NA			
s(herb-Nad)			0.504	0.13763 (excluded)	NA			
s(grass-Dubh)			2.116	0.00483**	NA			
s(grass-Quid)			2.629	0.00012***	NA			
s(grass-Nad)			1.600	0.03674*	NA			
s(herbandgrass-Dubh)	1.614	0.051202						
s(herbandgrass-Quid)	2.255	0.073181				1.845	0.10922	-
s(herbandgrass-Nad)	5.47e-07	0.759954 (excluded)				1.04e-10	0.80597 (excluded)	-
s(shrub-Dubh)	1.702	0.000179***	2.027	1.18e-07***	-			
s(shrub-Quid)	0.360	0.142071	0.700	0.22514 (excluded)	↓	6.22e-06	0.19895 (excluded)	↓
s(shrub-Nad)	0.711	0.112197	0.949	0.05015 (excluded)	↓	1.37e-10	0.70003 (excluded)	↓
s(tree-Dubh)	4.42e-06	0.334729 (excluded)	2.32e-10	0.45492 (excluded)	-			
s(tree-Quid)	3.864	0.052212	4.203	0.00039***	↑	3.820	0.01916	-
s(tree-Nad)	1.467	8.37e-05***	0.786	0.00137**	↓	1.649	0.00215	↓
s(charcoal)	5.127	1.66e-05***	5.255	5.59e-05***	-	1.924	4.96e-10***	-
s(temperature)	1.628	2.43e-07***	2.972	8.62e-11***	-	4.727	1.49e-07***	-

Appendix Table31. Parameters for original and alternative models for Herb Pollen Influx (3-site) and changes relative to original model.

	Original Model		Separate herb and grass predictor terms			Without Dubh-Lochan		
Smooth	edf	p-value	edf	p-value		edf	p-value	
s(dung-Dubh)	6.372	0.00924**	NA	NA	NA			
s(dung-Quid)	2.326	2.71e-14***	NA	NA	NA	1.773	2.74e-14***	-
s(dung-Nad)	6.084	0.02465*	NA	NA	NA	5.975	0.04060*	-
s(shrub-Dubh)	5.933	0.00370**	NA	NA	NA			
s(shrub-Quid)	4.750	1.25e-06***	NA	NA	NA	5.537	5.38e-06***	-
s(shrub-Nad)	1.550	2.07e-17***	NA	NA	NA	1.591	1.22e-17***	-
s(tree-Dubh)	2.718	0.00119**	NA	NA	NA			
s(tree-Quid)	0.662	0.12054	NA	NA	NA	0.343	0.15471	-
s(tree-Nad)	3.214	0.01276*	NA	NA	NA	2.081	0.01072*	-
s(charcoal)	5.272	3.98e-23***	NA	NA	NA	4.184	8.90e-25***	-
s(temperature)	3.771	0.00014***	NA	NA	NA	3.573	1.36e-05***	-

Appendix Table32. Parameters for original and alternative models for Shrub Pollen Influx (3-site) and changes relative to original model.

	Original Model		Separate herb and grass predictor terms			Without Dubh-Lochan		
Smooth	edf	p-value	edf	p-value		edf	p-value	
s(dung-Dubh)	0.853	0.05985	0.906	0.01761*	↑			
s(dung-Quid)				0.99932 (excluded)	↓	2.884	0.03700*	↑
s(dung-Nad)	1.964	0.25815	1.663	0.22161	-	2.059	0.29380	-
s(herb-Dubh)			1.892	0.05410	NA			
s(herb-Quid)			7.646	1.40e-07***	NA			
s(herb-Nad)			1.789	5.29e-05***	NA			
s(grass-Dubh)				0.53213 (excluded)	NA			
s(grass-Quid)			4.207	8.32e-06***	NA			
s(grass-Nad)			4.953	1.88e-06***	NA			
s(herbandgrass-Dubh)	0.016	0.29597						
s(herbandgrass-Quid)	3.646	0.00093***				3.702	0.00117**	↓
s(herbandgrass-Nad)	5.446	2.19e-21***				6.518	3.02e-20***	-
s(tree-Dubh)	1.939	0.01878*	0.598	0.15254	↓			
s(tree-Quid)	6.544	9.78e-31***	6.610	3.00e-30***	-	5.870	9.70e-32***	-
s(tree-Nad)	3.112	0.00067***	3.524	0.00374**	↓	3.109	0.00093***	-
s(charcoal)	8.683	1.17e-05***	7.620	2.50e-05***	-	8.758	1.10e-05***	-
s(temperature)	1.082	0.16506	8.497	0.01640*	↑	0.824	0.17115	-

Appendix Table33. Parameters for original and alternative models for Tree Pollen Influx (3-site) and changes relative to original model.

	Original Model		Separate herb and grass predictor terms			Without Dubh-Lochan		
Smooth	edf	p-value	edf	p-value		edf	p-value	
s(dung-Dubh)		0.50222 (excluded)		0.14081 (excluded)	-			
s(dung-Quid)	2.763	0.00444**	2.795	0.01651*	↓	2.710	0.00480**	-
s(dung-Nad)	2.508	0.00045***	1.923	0.04023**	↓	2.469	0.00026***	-
s(herb-Dubh)				0.99824 (excluded)	NA			
s(herb-Quid)			4.54e-10	0.01386*	NA			
s(herb-Nad)			5.698	4.31e-33***	NA			
s(grass-Dubh)			4.055	0.00374**	NA			
s(grass-Quid)			3.269	0.00227**	NA			
s(grass-Nad)			0.862	5.36e-07***	NA			
s(herbandgrass-Dubh)	9.07e-07	0.48265 (excluded)						
s(herbandgrass-Quid)	5.782	0.00039***				5.764	0.00039***	-
s(herbandgrass-Nad)	0.167	0.28475				0.389	0.18471	-
s(shrub-Dubh)	4.15e-07	0.65366 (excluded)	0.315	0.21818	↑			
s(shrub-Quid)	1.941	1.44e-22***	1.091	3.64e-16***	-	1.996	1.36e-22***	-
s(shrub-Nad)	6.787	8.22e-19***	0.828	8.72e-06***	-	6.732	8.71e-16***	-
s(charcoal)	1.675	0.10182	5.483	4.15e-06***	↑	1.616	0.11653	-
s(temperature)	1.969	0.00020***	7.454	0.06429	↓	2.198	0.00023***	-

Appendix Table34. Parameters for original and alternative models for Herb Pollen Influx (5-site) and changes relative to original model.

Smooth	Original Model		Separate herb and grass predictor terms			Without Dubh-Lochan and Ballynahatty		
	edf	p-value	edf	p-value		edf	p-value	
s(dung-Dubh)	6.153	0.00373**	NA	NA	NA			
s(dung-Quid)	1.657	8.33e-14***	NA	NA	NA	3.063	1.43e-16***	-
s(dung-Nad)	6.286	0.02790*	NA	NA	NA	9.08e-09	0.44327 (excluded)	↓
s(dung-Bal)	2.456	0.01978*	NA	NA	NA			
s(dung-Long)	6.131	0.00020***	NA	NA	NA	6.117	0.00130**	↓
s(shrub-Dubh)	6.024	0.00034***	NA	NA	NA			
s(shrub-Quid)	5.009	5.13e-08***	NA	NA	NA	8.141	6.45e-05***	-
s(shrub-Nad)	1.477	5.34e-22***	NA	NA	NA	2.481	5.09e-25***	-
s(shrub- Bal)	2.431	5.47e-07***	NA	NA	NA			
s(shrub- Long)	5.062	0.00228**	NA	NA	NA	4.243	0.04672*	↓
s(tree-Dubh)	1.699	0.00279**	NA	NA	NA			
s(tree-Quid)	7.947	0.00374**	NA	NA	NA	0.204	0.21019	↓
s(tree-Nad)	1.616	0.01131*	NA	NA	NA	0.340	0.29034	↓
s(tree- Bal)	2.976	0.00104**	NA	NA	NA			
s(tree- Long)	0.896	0.01913*	NA	NA	NA	0.680	0.04243*	-
s(charcoal)	6.255	1.62e-33***	NA	NA	NA	4.812	2.52e-19***	-

Appendix Table35. Parameters for original and alternative models for Shrub Pollen Influx (5-site) and changes relative to original model.

Smooth	Original Model		Separate herb and grass predictor terms			Without Dubh-Lochan and Ballynahatty		
	edf	p-value	edf	p-value		edf	p-value	
s(dung-Dubh)	0.823	0.06619	0.800	0.05993	-			
s(dung-Quid)	1.988	0.24381	1.21e-06	0.58224 (excluded)	↓	2.689	0.03949*	↑
s(dung-Nad)	3.85e-08	0.59113 (excluded)	3.68e-06	0.51392 (excluded)	-	3.03e-09	0.70995 (excluded)	-
s(dung-Bal)	2.55e-08	0.78638 (excluded)	2.10e-06	0.58081 (excluded)	-			
s(dung-Long)	2.289	0.00102**	1.955	0.00032***	↑	1.279	0.00180**	-
s(herb-Dubh)			1.977	0.01940*	NA			
s(herb-Quid)			7.386	2.08e-07***	NA			
s(herb-Nad)			1.907	1.16e-05***	NA			
s(herb- Bal)			1.818	0.04886*	NA			
s(herb-Long)			1.364	0.00083***	NA			
s(grass-Dubh)			4.65e-06	0.21407 (excluded)	NA			
s(grass-Quid)			6.800	1.68e-08***	NA			
s(grass-Nad)			6.269	1.03e-07***	NA			
s(grass-Bal)			1.248	0.00054***	NA			
s(grass-Long)			1.562	0.00940**	NA			
s(herbandgrass-Dubh)	1.045	0.06746						
s(herbandgrass-Quid)	6.435	0.00027***				3.116	0.00825**	↓
s(herbandgrass-Nad)	4.386	1.49e-25***				3.601	2.46e-19***	-
s(herbandgrass-Bal)	0.470	0.03570*						
s(herbandgrass-Long)	2.387	0.01568*				0.613	0.12020	↓
s(tree-Dubh)	2.169	0.21184	0.784	0.02549*	↑			
s(tree-Quid)	6.112	9.91e-43***	6.199	1.57e-25***	-	4.538	6.47e-18***	-
s(tree-Nad)	3.491	0.00116**	1.327	3.21e-05***	↑	1.854	0.00526**	-
s(tree- Bal)	5.623	3.47e-19***	3.910	2.94e-15***	-			
s(tree- Long)	3.688	2.86e-12***	3.377	1.22e-12***	-	3.655	1.83e-37***	-
s(charcoal)	6.961	0.00017***	6.328	0.00100***	-	7.115	3.48e-06***	-

Appendix Table36. Parameters for original and alternative models for Tree Pollen Influx (5-site) and changes relative to original model.

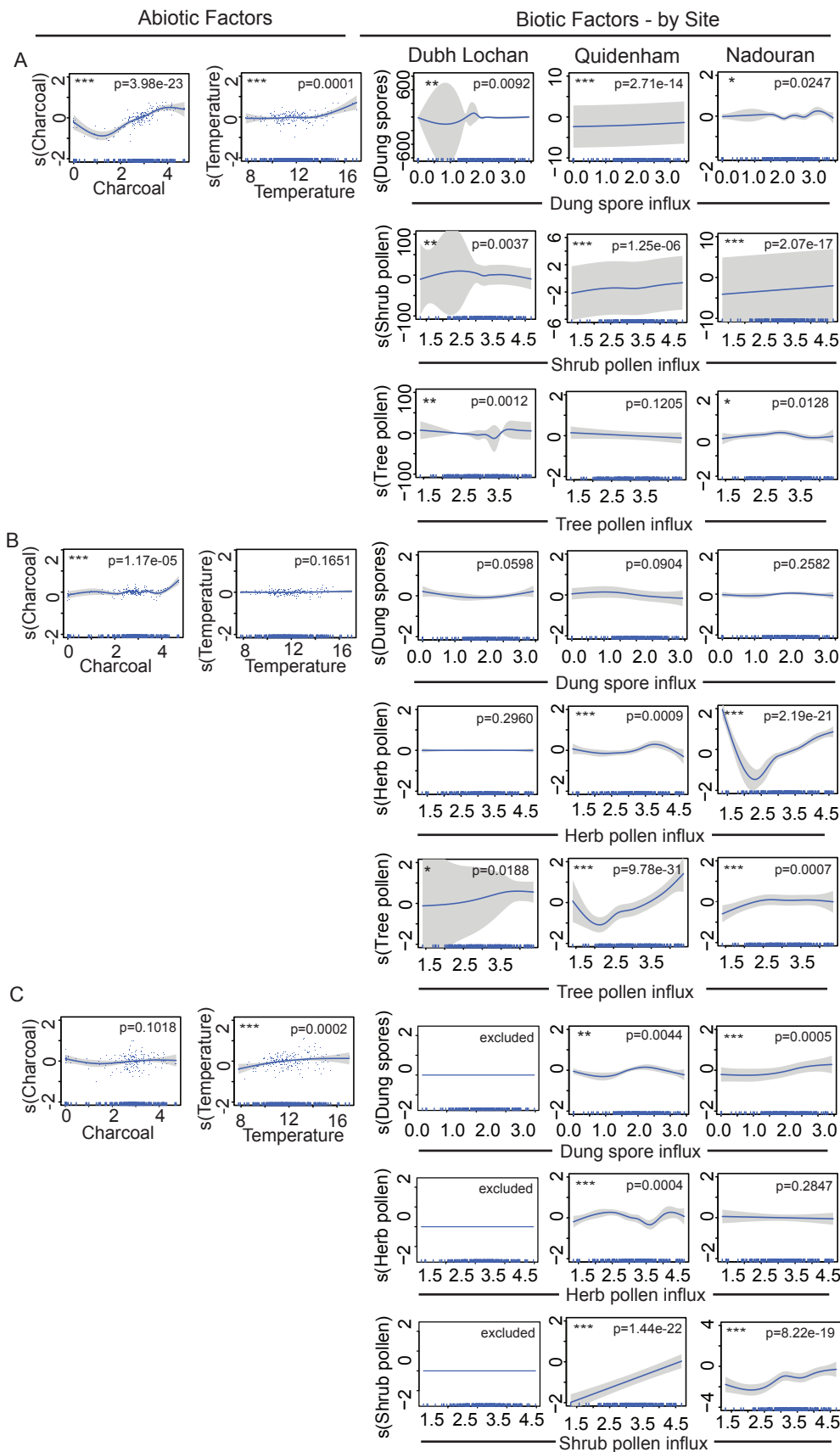
	Original Model		Separate herb and grass predictor terms			Without Dubh-Lochan and Ballynahatty		
Smooth	edf	p-value	edf	p-value		edf	p-value	
s(dung-Dubh)	3.84e-10	0.58362 (excluded)	0.009	0.32095	↑			
s(dung-Quid)	2.649	0.00495**	2.844	0.00296**	-	2.592	0.00913**	-
s(dung-Nad)	3.428	1.44e-06***	2.144	0.02348*	↓	3.052	6.14e-05***	-
s(dung-Bal)	0.466	0.04532*	6.48e-07	0.28697 (excluded)	↓			
s(dung-Long)	4.56e-10	0.56415 (excluded)	7.23e-07	0.59279 (excluded)	-	6.06e-10	0.98420 (excluded)	-
s(herb-Dubh)			3.78e-07	0.96684 (excluded)	NA			
s(herb-Quid)			5.680	0.01497*	NA			
s(herb-Nad)			5.772	2.39e-45***	NA			
s(herb- Bal)			0.556	0.02110*	NA			
s(herb-Long)			6.628	1.49e-12***	NA			
s(grass-Dubh)			2.000	9.12e-11***	NA			
s(grass-Quid)			5.451	0.00012***	NA			
s(grass-Nad)			1.002	2.50e-07***	NA			
s(grass-Bal)			6.06e-07	0.47587 (excluded)	NA			
s(grass-Long)			3.940	5.37e-05***	NA			
s(herbandgrass-Dubh)	1.848	1.22e-20***						
s(herbandgrass-Quid)	6.058	5.41e-05***				5.646	0.00044***	-
s(herbandgrass-Nad)	2.82e-10	0.51181 (excluded)				2.67e-09	0.33203 (excluded)	-
s(herbandgrass-Bal)	2.56e-10	0.58222 (excluded)						
s(herbandgrass-Long)	0.906	0.00392**				0.895	0.00088***	↑
s(shrub-Dubh)	3.60e-10	0.52156 (excluded)	3.65e-07	1 (excluded)	-			
s(shrub-Quid)	1.866	7.83e-19***	1.926	9.46e-20***	-	1.860	1.17e-22***	-
s(shrub-Nad)	6.396	1.91e-14***	0.953	1.05e-07***	-	7.087	1.95e-14***	-
s(shrub- Bal)	1.780	3.42e-18***	1.836	2.67e-15***	-			
s(shrub- Long)	1.644	1.26e-07***	0.661	0.11740	↓	2.551	1.37e-05***	-
s(charcoal)	0.333	0.09637	3.567	1.24e-06***	↑	2.954	1.10e-09***	↑

Appendix Table38. Significance (p-value) of smoother terms for predicting herb and grass pollen influx and changes relative to the original model. Statistics were estimated using the 5-site dataset except for the temperature smooth term, which was estimated from the 3-site dataset.

Smooth	Herbs and grasses	Herbs only	Change	Grasses only	Change
s(dung-Dubh)	0.00373**	1.45e-05***	↑	0.0556	↓
s(dung-Quid)	8.33e-14***	5.21e-06***	-	4.76e-12***	-
s(dung-Nad)	0.02790*	0.1794	↓	0.0095**	↑
s(dung-Bal)	0.01978*	3.25e-11***	↑	0.4240 excluded	↓
s(dung-Long)	0.00020***	0.1973	↓	3.41e-13***	-
s(shrub-Dubh)	0.00034***	0.0004***	-	0.0045**	↓
s(shrub-Quid)	5.13e-08***	6.61e-05***	-	3.37e-07***	-
s(shrub-Nad)	5.34e-22***	7.29e-12***	-	1.32e-14***	-
s(shrub- Bal)	5.47e-07***	0.3753 excluded	↓	3.49e-11***	-
s(shrub- Long)	0.00228**	0.0367*	↓	0.0142*	↓
s(tree-Dubh)	0.00279**	1.22e-06***	↑	1 excluded	↓
s(tree-Quid)	0.00374**	0.0458*	↓	0.0255 *	↓
s(tree-Nad)	0.01131*	3.75e-10***	↑	0.0004***	↑
s(tree- Bal)	0.00104**	5.21e-10***	↑	4.20e-05***	↑
s(tree- Long)	0.01913*	0.1944	↓	0.0192*	-
s(charcoal)	1.62e-33***	2.88e-23***	-	8.28e-26***	-
s(temperature)	0.00014***	0.0125*	↓	1.65e-05***	-

TableS10. Model statistics for individual smooth terms describing changes in sedimentary $\delta^{15}\text{N}$ at Dubh-Lochan, Quidenham Mere and Lough Nadourcan. Generalized additive models were fit to the data using the *mgcv* package in R. Statistics for each GAM smooth term were determined using the *summary* function in *mgcv*, which applies a Wald test to approximate p-values.

Model: $\delta^{15}\text{N} \sim \log(\text{Dung spores}_{i,j} \text{ for all sites } j) + \text{Temp.} + \log(\text{Charcoal}) + \log(\text{Herb pollen}_{i,j} \text{ for all sites } j) + \log(\text{Shrub pollen}_{i,j} \text{ for all sites } j) + \log(\text{Tree pollen}_{i,j} \text{ for all sites } j)$				
Parameter:	Estimate	Std Error	t-value	Pr(> t)
Intercept	0.5454	0.1756	3.105	0.00223**
	edf	Ref.df	F	p-value
log(Dung spores Dubh-Lochan)	0.849	8	0.475	0.014783*
log(Dung spores Quidenham)	7.058	10	1.887	0.006006**
log(Dung spores Nadourcan)	4.25E-07	10	9.84E-09	0.811955 (excluded)
log(Herb pollen Dubh-Lochan)	1.614	9	0.395	0.051202
log(Herb pollen Quidenham)	2.255	10	0.475	0.073181
log(Herb pollen Nadourcan)	5.47E-07	10	1.07E-08	0.759954 (excluded)
log(Shrub pollen Dubh-Lochan)	1.702	9	1.385	0.000179***
log(Shrub pollen Quidenham)	0.360	9	0.061	0.142071
log(Shrub pollen Nadourcan)	0.711	6	0.224	0.112197
log(Tree pollen Dubh-Lochan)	4.42E-06	3	5.70E-07	0.334729 (excluded)
log(Tree pollen Quidenham)	3.864	10	0.754	0.052212
log(Tree pollen Nadourcan)	1.467	6	2.091	8.37e-05***
log(Charcoal)	5.127	9	3.027	1.66e-05***
Mean July air temperature (°C)	1.628	9	2.667	2.43e-07***



FigS11. Modelled effects of biotic and abiotic factors on plant biomass using 3-site dataset. Plots of GAM smooth functions from the best-fitting model for describing the influx of herb (A), shrub (B) and tree (C) pollen at the three sites for which climate data are available ($n=199$). Asterisks indicate significance levels: * = p-value ≤ 0.05 ; ** = p-value ≤ 0.01 ; *** = p-value ≤ 0.001 . Gray areas represent two standard errors around the estimated effect. Tick marks along the x-axis indicate data points. The model included site-specific effects of the biotic factors on each response variable. Models were fit using the *mgcv* package in R with cross-validation and term selection. Flat lines indicate where a term has been dropped from the model. Note that some y-axes are shown on a different scale due to large error bars.

TableS12. Model statistics for individual smooth terms describing changes in plant biomass at Dubh-Lochan, Quidenham Mere and Lough Nadourcan. Generalized additive models were fit to the data using the *mgcv* package in R. Statistics for each GAM smooth term were determined using the *summary* function in *mgcv*, which applies a Wald test to approximate p-values.

Model predicting Herb Pollen Influx				
Model: log(Herb pollen) ~ log(Dung spores _i for all sites <i>i</i>) + Temp. + log(Charcoal) + log(Shrub pollen _i for all sites <i>i</i>) + log(Tree pollen _i for all sites <i>i</i>)				
Parameter:	Estimate	Std Error	t-value	Pr(> t)
Intercept	6.25	4.491	1.392	0.166
	edf	Ref.df	F	p-value
log(Dung spores Dubh-Lochan)	6.372	8	2.217	0.00924**
log(Dung spores Quidenham)	2.326	10	6.216	2.71e-14***
log(Dung spores Nadourcan)	6.084	9	1.565	0.02465*
log(Shrub pollen Dubh-Lochan)	5.933	8	2.346	0.00370**
log(Shrub pollen Quidenham)	4.750	10	3.117	1.25e-06***
log(Shrub pollen Nadourcan)	1.550	5	15.008	2.07e-17***
log(Tree pollen Dubh-Lochan)	2.718	6	2.092	0.00119**
log(Tree pollen Quidenham)	0.662	8	0.191	0.12054
log(Tree pollen Nadourcan)	3.214	10	0.983	0.01276*
log(Charcoal)	5.272	9	13.084	3.98e-23***
Mean July air temperature (°C)	3.771	9	2.209	0.00014***
Model predicting Shrub Pollen Influx				
Model: log(Shrub pollen) ~ log(Dung spores _i for all sites <i>i</i>) + Temp. + log(Charcoal) + log(Herb pollen _i for all sites <i>i</i>) + log(Tree pollen _i for all sites <i>i</i>)				
Parameter:	Estimate	Std Error	t-value	Pr(> t)
Intercept	3.3098	0.1251	26.25	<2e-16***
	edf	Ref.df	F	p-value
log(Dung spores Dubh-Lochan)	0.853	8	0.337	0.05985
log(Dung spores Quidenham)	2.601	10	0.488	0.09004
log(Dung spores Nadourcan)	1.964	10	0.248	0.25815
log(Herb pollen Dubh-Lochan)	0.016	8	0.002	0.29597
log(Herb pollen Quidenham)	3.646	10	1.514	0.00093***
log(Herb pollen Nadourcan)	5.446	10	11.280	2.19e-21***
log(Tree pollen Dubh-Lochan)	1.939	3	2.129	0.01878*
log(Tree pollen Quidenham)	6.544	10	15.815	9.78e-31***
log(Tree pollen Nadourcan)	3.112	10	1.444	0.00067***
log(Charcoal)	8.683	9	4.250	1.17e-05***
Mean July air temperature (°C)	1.082	9	0.191	0.16506
Model predicting Tree Pollen Influx				
Model: log(Tree pollen) ~ log(Dung spores _i for all sites <i>i</i>) + Temp. + log(Charcoal) + log(Herb pollen _i for all sites <i>i</i>) + log(Shrub pollen _i for all sites <i>i</i>)				
Parameter:	Estimate	Std Error	t-value	Pr(> t)
Intercept	3.963	0.131	30.25	<2e-16***
	edf	Ref.df	F	p-value
log(Dung spores Dubh-Lochan)	7.38e-07	8	4.86e-08	0.50222 (excluded)
log(Dung spores Quidenham)	2.763	9	1.232	0.00444**
log(Dung spores Nadourcan)	2.508	10	1.463	0.00045***
log(Herb pollen Dubh-Lochan)	9.07e-07	8	5.29e-08	0.48265 (excluded)
log(Herb pollen Quidenham)	5.782	10	2.180	0.00039***
log(Herb pollen Nadourcan)	0.167	7	0.025	0.28475
log(Shrub pollen Dubh-Lochan)	4.15e-07	8	1.13e-08	0.65366 (excluded)
log(Shrub pollen Quidenham)	1.941	6	17.733	1.44e-22***
log(Shrub pollen Nadourcan)	6.787	10	9.321	8.22e-19***
log(Charcoal)	1.675	9	0.362	0.10182
Mean July air temperature (°C)	1.969	9	1.522	0.00020***

TableS13. Model statistics for individual smooth terms describing changes in plant biomass at all five study sites. Generalized additive models were fit to the data using the *mgcv* package in R. Statistics for each GAM smooth term were determined using the *summary* function in *mgcv*, which applies a Wald test to approximate p-values.

Model predicting Herb Pollen Influx				
Model: log(Herb pollen) ~ log(Dung spores _i for all sites <i>i</i>) + log(Charcoal) + log(Shrub pollen _i for all sites <i>i</i>) + log(Tree pollen _i for all sites <i>i</i>)				
Parameter:	Estimate	Std Error	t-value	Pr(> t)
Intercept	3.3286	0.1946	16.89	<2e-16***
	edf	Ref.df	F	p-value
log(Dung spores Dubh-Lochan)	6.153	8	2.331	0.00373**
log(Dung spores Quidenham)	1.657	9	6.208	8.33e-14***
log(Dung spores Nadourcan)	6.286	10	1.412	0.02790*
log(Dung spores Ballynahatty)	2.456	10	0.649	0.01978*
log(Dung spores Long Lough)	6.131	8	3.000	0.00020***
log(Shrub pollen Dubh-Lochan)	6.024	9	2.655	0.00034***
log(Shrub pollen Quidenham)	5.009	10	3.773	5.13e-08***
log(Shrub pollen Nadourcan)	1.477	7	12.980	5.34e-22***
log(Shrub pollen Ballynahatty)	2.431	8	2.831	5.47e-07***
log(Shrub pollen Long Lough)	5.062	9	1.720	0.00228**
log(Tree pollen Dubh-Lochan)	1.699	5	1.639	0.00279**
log(Tree pollen Quidenham)	7.947	10	2.050	0.00374**
log(Tree pollen Nadourcan)	1.616	10	0.611	0.01131*
log(Tree pollen Ballynahatty)	2.976	9	1.453	0.00104**
log(Tree pollen Long Lough)	0.896	7	0.516	0.01913*
log(Charcoal)	6.255	9	19.038	1.62e-33***
Model predicting Shrub Pollen Influx				
Model: Shrub pollen ~ log(Dung spores _i for all sites <i>i</i>) + log(Charcoal) + log(Herb pollen _i for all sites <i>i</i>) + log(Tree pollen _i for all sites <i>i</i>)				
Parameter:	Estimate	Std Error	t-value	Pr(> t)
Intercept	3.8848	0.1292	30.08	<2e-16***
	edf	Ref.df	F	p-value
log(Dung spores Dubh-Lochan)	0.823	9	0.269	0.06619
log(Dung spores Quidenham)	1.988	9	0.285	0.24381
log(Dung spores Nadourcan)	3.85e-08	10	1.40e-09	0.59113 (excluded)
log(Dung spores Ballynahatty)	2.55e-08	10	2.43e-10	0.78638 (excluded)
log(Dung spores Long Lough)	2.289	9	1.400	0.00102**
log(Herb pollen Dubh-Lochan)	1.045	9	0.303	0.06746
log(Herb pollen Quidenham)	6.435	9	2.706	0.00027***
log(Herb pollen Nadourcan)	4.386	10	12.408	1.49e-25***
log(Herb pollen Ballynahatty)	0.470	4	0.365	0.03570*
log(Herb pollen Long Lough)	2.387	10	0.765	0.01568*
log(Tree pollen Dubh-Lochan)	2.169	4	0.521	0.21184
log(Tree pollen Quidenham)	6.112	10	20.868	9.91e-43***
log(Tree pollen Nadourcan)	3.491	10	1.419	0.00116**
log(Tree pollen Ballynahatty)	5.623	9	11.724	3.47e-19***
log(Tree pollen Long Lough)	3.688	6	9.327	2.86e-12***
log(Charcoal)	6.961	9	2.957	0.00017***
Model predicting Tree Pollen Influx				
Model: log(Tree pollen) ~ log(Dung spores _i for all sites <i>i</i>) + log(Charcoal) + log(Herb pollen _i for all sites <i>i</i>) + log(Shrub pollen _i for all sites <i>i</i>)				
Parameter:	Estimate	Std Error	t-value	Pr(> t)
Intercept	2.731	0.13	21.01	<2e-16***
	edf	Ref.df	F	p-value
log(Dung spores Dubh-Lochan)	3.84e-10	10	1.61e-11	0.58362 (excluded)
log(Dung spores Quidenham)	2.649	10	1.071	0.00495**
log(Dung spores Nadourcan)	3.428	10	2.748	1.44e-06***
log(Dung spores Ballynahatty)	0.466	4	0.417	0.04532*
log(Dung spores Long Lough)	4.56e-10	10	1.62e-11	0.56415 (excluded)
log(Herb pollen Dubh-Lochan)	1.848	4	21.359	1.22e-20***
log(Herb pollen Quidenham)	6.058	8	3.471	5.41e-05***
log(Herb pollen Nadourcan)	2.82e-10	10	1.41e-11	0.51181 (excluded)
log(Herb pollen Ballynahatty)	2.56e-10	10	8.92e-12	0.58222 (excluded)
log(Herb pollen Long Lough)	0.906	5	1.064	0.00392**
log(Shrub pollen Dubh-Lochan)	3.60e-10	10	1.46e-11	0.52156 (excluded)
log(Shrub pollen Quidenham)	1.866	6	13.927	7.83e-19***
log(Shrub pollen Nadourcan)	6.396	10	7.479	1.91e-14***
log(Shrub pollen Ballynahatty)	1.780	7	8.386	3.42e-18***
log(Shrub pollen Long Lough)	1.644	8	2.736	1.26e-07***
log(Charcoal)	0.333	8	0.092	0.09637